ABSTRACT

THE TEMPER ANNEALING OF METASTABLE

AUSTENITIC STAINLESS STEEL

by

Rein R. Mutso

Department of Metallurgical Engineering
McGill University
Montreal, Canada

Master of Engineering in
Metallurgical Engineering

The mechanical properties of temper rolled (work hardened) austenitic stainless steel AISI 301 were examined and compared with those of temper annealed (partially annealed from a fully cold worked structure) material.

At most strength levels, the temper annealed material possessed superior ductility over that of temper rolled material. The improvement was modest, but possibly commercially significant. This steel showed extremely rapid strain hardening. This rapid hardening was primarily due to the formation of strain induced martensite. Temper annealing produced gross carbide precipitation, causing loss of corrosion resistance and obliteration of microstructure. X-ray diffraction techniques were used extensively to follow structural changes in both types of materials.

A model describing temper annealing behavior was examined. The present experimental results did not agree very well with the model. This disagreement was believed to be a result of the extremely complex processes encountered, rather than to any deficiency in the model.

Short Title

" TEMPER ANNEALING OF AUSTENITIC STAINLESS STEEL"

THE TEMPER ANNEALING OF

METASTABLE AUSTENITIC STAINLESS STEEL

by

Rein R. Mutso

A thesis submitted to the Faculty of Graduate Studies and Research in partial fulfilment of the requirements for the degree of Master of Engineering in Metallurgical Engineering.

McGill University
Montreal, Canada

April, 1970

THE TEMPER ANNEALING OF

METASTABLE AUSTENITIC STAINLESS STEEL

by

Rein R. Mutso

A thesis submitted to the Faculty of Graduate Studies and Research in partial fulfilment of the requirements for the degree of Master of Engineering in Metallurgical Engineering.

McGill University
Montreal, Canada

April, 1970

ACKNOWLEDGEMENTS

This writer wishes to express his gratitude to Dr. W.M. Williams, Director of this Research for his assistance and advice. Thanks are due to Atlas Steels Company for supplying the material and to Mr. P. Thomas, Mr. W.T. Yen, and Mr. M. Knoepfel for their technical assistance. The work was supported by a grant from the National Research Council of Canada.

TABLE OF CONTENTS

LIST OF FIGURES

LIST OF TABLES

Section I

INTRODUCTION

I INTRODUCTION

Some of the most important semi-finished metal products in modern industry are derived from sheet or strip. The products may be fabricated directly from the flat sheet or else the sheet can be processed further by drawing or spinning in order to achieve some desired shape required prior to final assembly. By varying the production parameters such as rolling reduction, annealing time and temperature, etc., sheet may be produced for varying product requirements with different mechanical properties, i.e. tempers from "dead soft" to "extra hard".

There are two basic processing methods used to obtain sheet with a desired combination of mechanical properties:

(1) Temper Rolling, also called " rolling to temper", is the method used almost exclusively at the present time.

(11) Temper Annealing, also called " partial annealing", is a method rarely used on an industrial scale, at present, because of difficulties encountered in controlled annealing. These difficulties will be discussed below.

A. Temper Rolling

It is well known (1,2,3,4) that cold work increases the yield point and tensile strength of metals, while at the same time decreasing their ductility. A wide range of mechanical properties can be achieved by varying the amount of cold work. A temper rolling schedule is a carefully regulated series of cold rolling and annealing steps, the final reduction bringing the metal to both the desired gauge and temper.

The larger the final reduction, the stronger will be the metal product. Table I shows a typical industrial rolling schedule for the production of ¼-hard tough pitch copper (1,5).

B. Temper Annealing

The alternative method of producing sheet to a desired temper first involves the production of a heavily cold worked product. This product is then partially recrystallized to the point where the desired mechanical properties are obtained. The full range of tempers can be obtained by varying the degree of partial recrystallization, which in turn, is controlled by the time and temperature of annealing.

The rate of softening of a metal is influenced by the complete history of the metal (6). This history includes variations in composition, casting technique, the number of intermediate anneals, etc. Because of the influence of these processing variables on the recrystallization behavior, closer control of the starting sheet material is required for temper annealing than is required for temper rolling.

As can be seen from Table I, a temper rolling schedule has more interruptions for intermediate anneals than a comparable temper annealing schedule. During temper rolling, the final reduction is less than the full capacity of the rolling mill. When employing temper annealing, on the other hand, plant capacity is used more effectively.

Another advantage of a partially annealed product is that a more economic stock of starting material of standard thickness can be stored. All the stored material can be of a similar hard temper, and can be subsequently partially annealed, as required, to meet customer orders for softer tempers.

The temperature sensitivity of partial annealing is its chief drawback. Fritz (5) has shown that a temperature variation of 1.5°C affects the tensile strength of tough pitch copper sheet by 1,000 psi. Industrially, this fine temperature control would be difficult to achieve.

C. Comparison of the Mechanical Properties of Temper Annealed and Temper Rolled Materials.

From previous work in this field (1,2,3,5) it is clear that partially annealed metals have greater ductility and lower yield strengths than the corresponding temper rolled materials of the same tensile strengths.

The increased ductility is a distinct advantage in fabrication processes involving drawing, folding, bending. The degree of improvement varies, however, from material to material. Sometimes these improvements are significant, sometimes temper annealing brings about only minor benefits.

Some typical mechanical property comparisons are given in Fig. 1 (p.6), Fig. 2, Fig. 3, and Fig.4.

D. Objective of the Present Research

The objective of this work was to study the temper annealing of a metastable austenitic stainless steel and, specifically, to compare the mechanical properties of the material produced by temper annealing with those of material produced by temper rolling.

Austenitic stainless steels are used extensively in applications requireing deep drawing or heavy deformation, eg. automobile hub caps, deep drawn domestic articles such as sinks, utensils and equipment in the dairy and food industries, etc.

In the annealed state, the tensile strength of austenitic stainless steel varies from 75,000 psi to 120,000 psi and the total elongation varies from 45% to 75% (7). The metastable austenitic stainless steels are unique in that very high tensile strengths, up to 300,000 psi can be achieved by cold working, with a corresponding reduction in the total elongation to about 3%.

It was hoped that by using temper annealing techniques, a substantial part of the very high strength of the cold worked steel could be maintained, while, at the same time, achieving a substantial increase in ductility, beyond the 3% level. High strength austenitic stainless steel could thus be made more workable and deep drawing would not be confined to fully annealed material.

TABLE I

COMPARISON OF PRODUCTION SCHEDULE FOR 1/4 HARD MATERIAL BY

(a) TEMPER ROLLING

(b) TEMPER ANNEALING

Starting Material - Hot Rolled Slab - 0.420 in. Thick

(a) Temper Rolling Steps		(b) Temper Annealing Steps	
1. Cold Roll to	0.128 in.	1. Cold Roll to	0.160 in.
2. Anneal		2. Anneal	
3. Cold Roll to	0.088 in.	3. Cold Roll to	0.040 in.
4. Anneal		4. Temper Anneal	
5. Cold Roll to	0.045 in.		
6. Anneal			
7. Cold Roll to	0.040 in.		

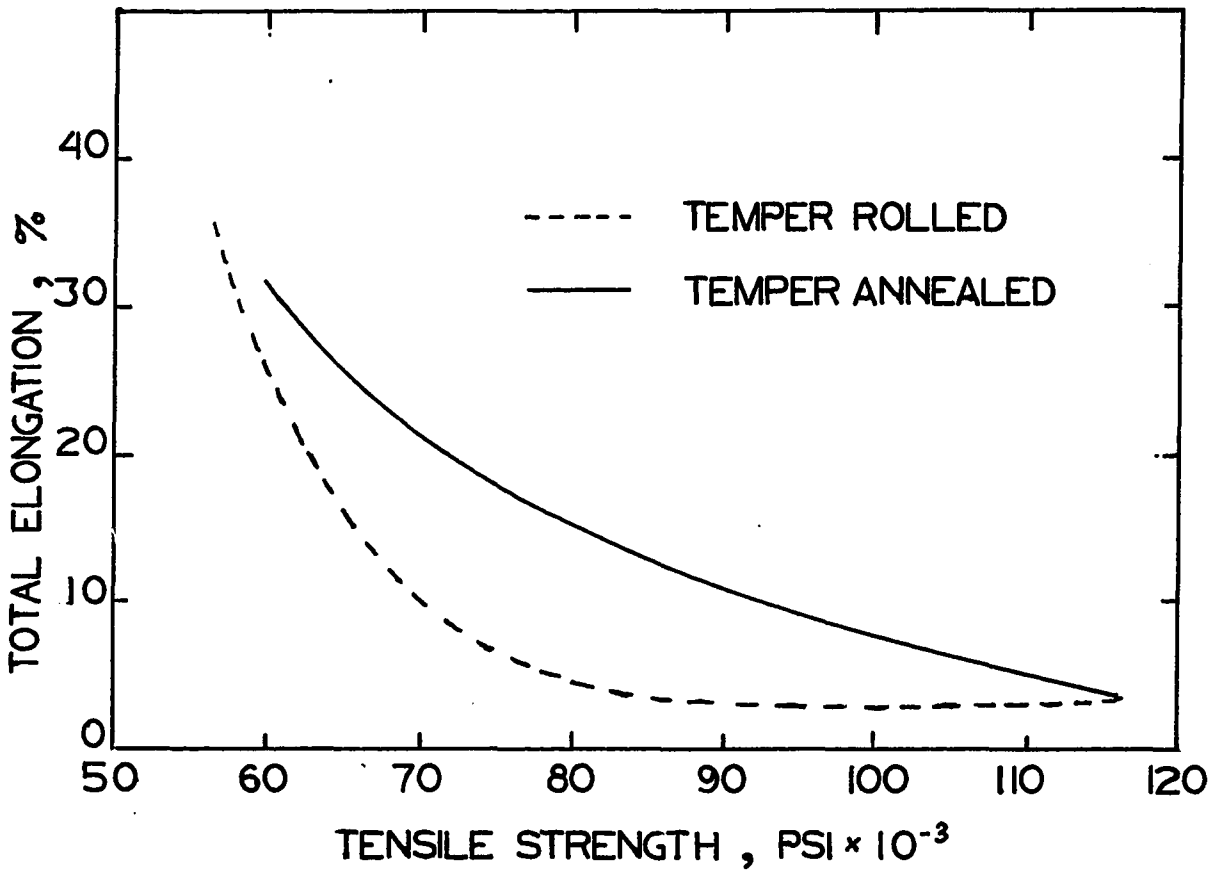

Fig. 1. Comparison of percentage total elongation for temper annealed and temper rolled mild steel (3)

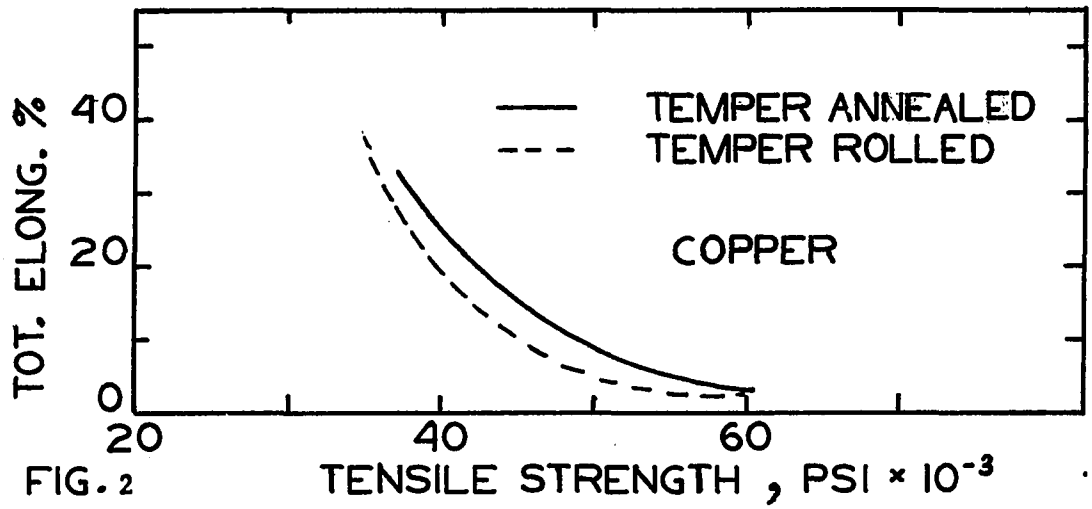

FIG. 2

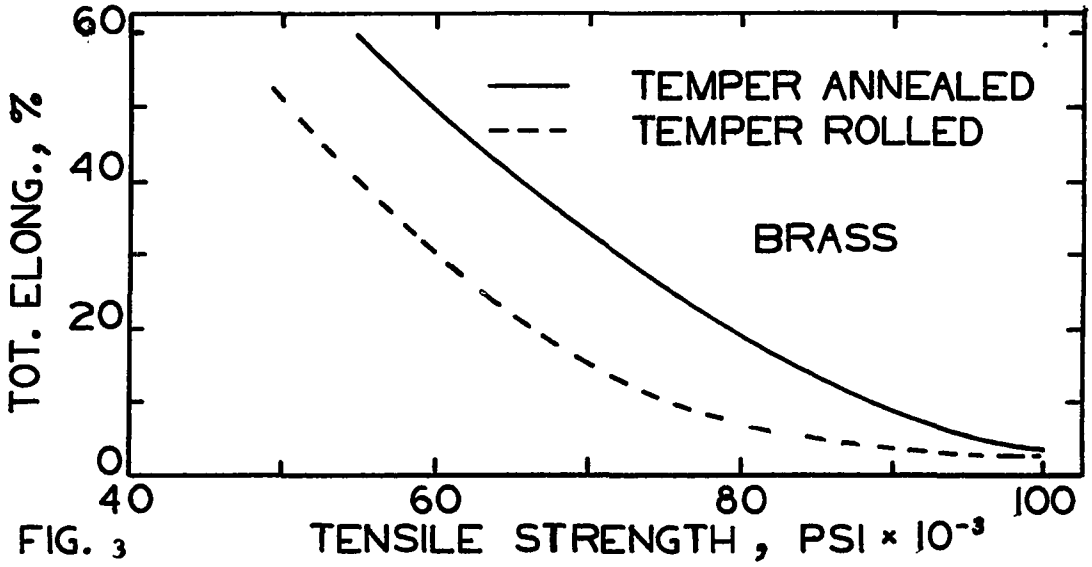

FIG. 3

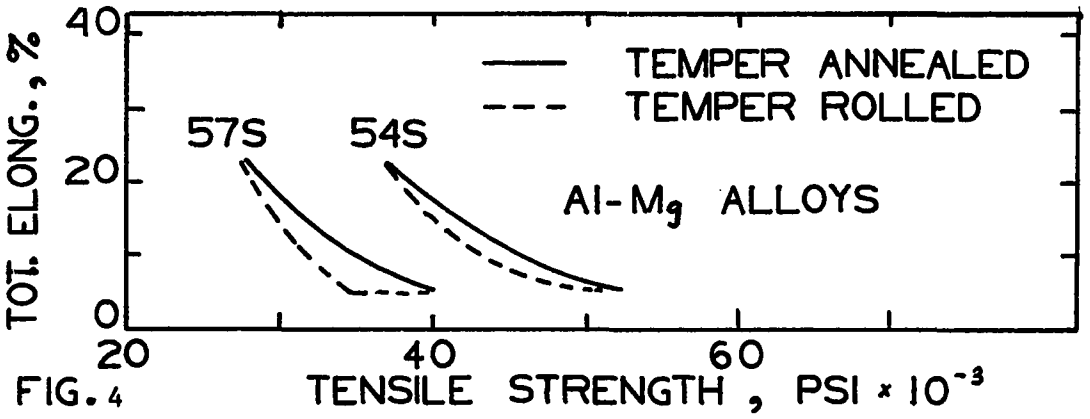

FIG. 4

Comparison of percentage elongation for temper annealed and temper rolled -
Fig. 2 Copper, Fig. 3 Brass, Fig. 4 Aluminum Alloys

Section II

THEORETICAL BACKGROUND

II THEORETICAL BACKGROUND

Theories of work hardening and annealing have been described clearly in previous work reported from McGill University (1,2,3). For this reason, as well as the fact that adequate summaries are readily available in may text books, (8,9,10) , only a resumé of these topics will be included in the present thesis.

A. Theory of Work Hardening

Grain distortion produced by plastic deformation at a temperature lower than about half the melting temperature, (measured on the absolute scale), may be termed cold work(5 p.175). Increased cold work causes the metal to become stronger and harder, a process called strain hardening.

The various strain hardening theories have been reviewed by Weidersich (11). Recent work has supported the following ideas about strain hardening. In unstrained material the dislocation density is comparatively low, about 10 dislocation lines per square cm. in ferrite. An applied stress causes the dislocation lines to move and interact with each other, thus increasing the resistance to deformation. Higher and higher stresses are therefore required to bring about further dislocation movement. As dislocations become locked, new dislocations are generated by the applied stress to permit further plastic flow in the material. The number of lattice vacancies is also increased.

As moving dislocations become tangled, they begin to form a cellular structure of about a 3 micron cell size. The cell walls are dense networks of dislocations, surrounding areas of lower dislocation density. In ferrite, for example, after about 10% strain, the cell size decreases to one micron and then remains approximately constant, further strain only increasing the dislocation density in the cell walls.

The perfection of this cellular structure decreases with increased solute (or impurity) content. Lattice misorientation between cells is about 2°. This misorientation is additive and thus, lattice misorientations of up to 20° can occur within any one grain.

As dislocations represent regions of lattice strain, increased dislocation density indicates a higher strain energy in the metal. This strain energy is approximately proportional to the square root of the dislocation density (12). Thus, in ferrite, where cold work increases the dislocation density from 10^{7} to 10^{12} dislocation lines per square cm. (3), a substantial increase in the strain energy is induced and consequently an increase in hardness and strength is also achieved.

B. Theory of Annealing

When a metal is annealed, radical changes take place in the structure of the metal. The driving force for these changes, which will be discussed below, is the strain energy of the cold worked material. The three steps normally encountered during annealing are:

(1) Recovery (2) Recrystallization (3) Grain Growth

(1) Recovery: The physical and mechanical properties of cold worked materials tend to return towards their original values before new strain free grains are formed. This phenomenon is termed recovery. The three stages of recovery occurring in 3% silicon-iron-crystals are discussed by Hu (13). These basic stages should exist, in modified form, in other metal crystals and probably in commercial steels.

a) 150°C to 190°C Range Vacancies are annealed out. Crystal density recovers but X-ray diffraction lines do not sharpen.

b) 200°C - 500°C Range Rearrangement and annihilation of dislocations occurs. X-ray lines sharpen and hardness begins to decrease.

c) 500°C - 660°C Range Well defined subgrains form. The recovery of mechanical properties is nearly complete.

After the third stage of recovery, the dislocation network is well defined. The cells are nearly dislocation free and are now termed subgrains. It is the initial growth of these subgrains to a critical nucleus size that constitutes the incubation period of recrystallization.

The rate of recovery is temperature dependant and also dependent on the amount of cold work. Higher temperatures produce greater dislocation mobility. Increased cold work provides greater free energy for transformation as well as more vacancies which , in turn, facilitate dislocation climb and therefore, dislocation mobility.

The third stage of recovery and the start of recrystallization may overlap, there being no distinct line of separation between the two processes (14). This is illustrated in Fig. 5 .

(2) Recrystallization

Primary recrystallization is defined as the nucleation and growth of new strain free grains and the gradual consumption of the cold worked matrix (3 p.23). Recrystallization is a growth controlled process, the subgrains growing until high angle boundaries are formed between them and the cold worked matrix (15). This is illustrated in Fig. 6 .

Nucleation of a strain free grain may be occur at:

a) The interior of the deformed grain
b) At a high angle boundary
c) At inclusions or a second phase material.

Inclusions are preferred sites for nucleation. They also hinder grain boundary movement. The general result of inclusion is, therefore, a fine grain size.

The newly nucleated strain free grains grow by outward migration of their high angle boundaries, until all the cold worked structure is consumed. The kinetics of this growth has been discussed in detail by Burke and Turnbull (16).

For heavily cold reduced metals, recovery and recrystallization are believed to occur simultaneously.

(3) Grain Growth: This phenomenon is defined as the increase in average grain size upon further annealing, after the cold worked structure has already been consumed by recrystallization of strain free grains. When recrystallization is complete, the retained energy of deformation is already spent, but the grain structure is not yet stable. The material still contains many high energy grain boundaries. When average grain size increases, the grain boundary area decreases, and consequently, the total energy of the system also decreases. Certain grains grow in size at the expense of other grains, which eventually disappear. The ultimate effect, theoretically, could be the production of one single large grain. Grain growth is a function of time and temperature and not of cold work (9p.199).

Grain growth may be restricted by a finely dispersed second phase, eg. carbides, non-metallic inclusions, or possibly by preferred orientation of the initial set of grains (8 p.434). These restrictive influences are overcome at high temperatures. There may exist a critical temperature. Significant rate of growth is only possible above this temperature. The rate of this growth is very temperature dependent.

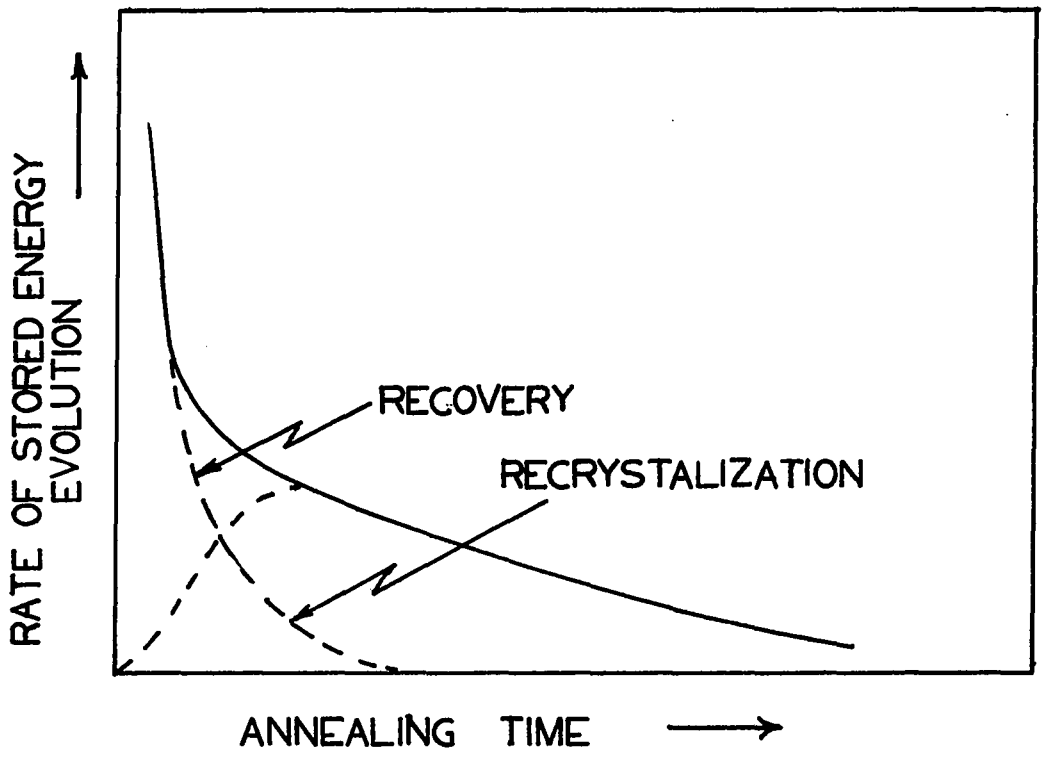

Fig. 5. Schematic illustration of the overlapping of recovery and recrystallization on the rate of stored energy evolution versus annealing time (3)

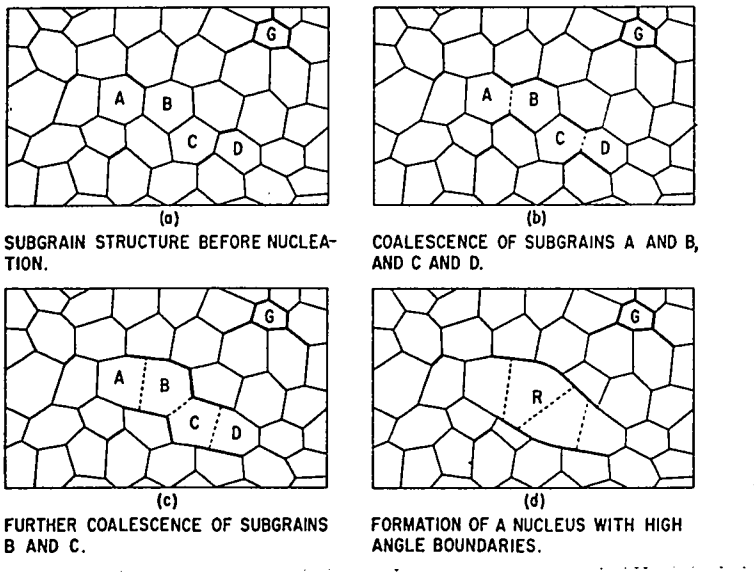

Fig. 6 (13)

Schematic representation for the formation of a recrystallized grain by the coalescence of subgrains

C. Theory of the Martensitic Transformation

In the temper annealing of pure metals or simple solid solutions, and also in relatively simple structures such as low carbon steel, temper annealing involves only partial recrystallization of a cold worked matrix, i.e., cold worked ferrite, for example, gradually transforms to recrystallized ferrite (17). In austenitic stainless steel, however, both the cold working process and the subsequent annealing process bring about more complicated changes in the material. In particular, cold working partly transforms the metastable austenite to martensite; in subsequent annealing, this martensite is tempered and there is also a partial transformation back to austenite. The effects of this martensitic transformation process are superimposed on the recrystallization process. The martensitic transformation is discussed in more detail in the following paragraphs.

The two main criteria for what is termed the Martensitic phase transformation are the following: (18 p.228, 19)

1) There is no change in composition during the phase change. The atomic readjustment is not more than about one atomic spacing, and hence it is often referred to as Diffusionless or Allotropic Transformation.

2) The transformation is accompanied by a change in shape corresponding, macroscopically, to a homogeneous deformation. The positions of the atoms in the martensitic product are crystallographically related to the atoms in the parent phase (austenite). The habit or interface plane, between the austenitic and martensitic phases is an undistorted plane, which remains unrotated, even though there is a shape deformation.

This phase change has also been called (Military Transformation" (20). It occurs in an organized, disciplined manner. This in contrast to nucleation processes where the product phase is only randomly oriented to the parent matrix.

The driving force causing the martensitic transformation is the difference in free energy between the parent and the product phases, (21 p.201, 9 p.418). A temperature exists where both phases can coexist at equilibrium, referred to as (M). If the high temperature phase continues to exist below this temperature, it is considered to be thermodynamically unstable. As the temperature is progressively lowered, the energy difference between the parent and product phases becomes sufficiently large to induce transformation. The temperature at which this transformation occurs is termed the Ms temperature.

The phase change from austenite to martensite occurs by an almost instantaneous shear mechanism parallel to the habit plane. The distortion that causes the change of shape to produce a martensite plate is a homogeneous strain, i.e., every point in the transforming region moves in the same direction and moves by an amount proportional to its distance from the habit plane (22 p.522). The strain causing the shape change is thus also an invariant plane strain, i.e. the habit plane, as well as all planes parallel to it, are unrotated by the strain and remain undistorted, except for a very small dilation or contraction perpendicular to the habit plane (22 p.522). This change of shape can often be observed as tilts on the surface of a specimen (23 p.154).

The original model explaining the martensitic shape change in steel was proposed by Bain in 1924 (24). The plane strain converts the structure of the parent to that of the product phase. This mechanism is illustrated in Fig. 7 . This figure illustrates two adjacent face centred cubic (FCC) structures. This atomic arrangement can also be thought of as a body-centred tetragonal (BCT) structure (dotted lines). If the long vertical axis is contracted and the other two axes are allowed to extend, a body-centred cubic (BCC) structure results.

The octahedral spaces are the largest openings in both these lattice structures (22 p.236), i.e. a space surrounded by six atoms in contact, forming an eight sided crystal structure (Fig. 8).

In steel, these largest indices are, in fact, the only ones that can be occupied by carbon atoms (22 p.237). Due to lattice distortion produced by the interstitial carbon atoms, not all the octahedral positions can be filled. In the FCC austenite iron phase, saturation is reached with 2% by weight of carbon, while in the BCC ferrite phase, the carbon solubility limit is 0.025% by weight at the eutectoid temperature (22 p.512).

It can be seen in Fig. 7 that only positions "X" in the crystal lattice are octahedral index positions for both the BCC and FCC structures. The other index positions, eg. "A", only have octahedral symmetry in the FCC phase.

If, during the phase transformation from the FCC to BCC structure, carbon atoms are located at the positions "X", and there is not enough time to permit carbon diffusion, the carbon atoms maintain the elongation of the vertical axis (C axis). The resulting strained BCT structure is ferrous martensite. This BCT martensite is even formed in steels with less than 0.05% carbon (22 p.514).

The change in shape alone cannot account for the change of crystal structure. The Bain distortion leaves no undistorted planes and therefore the condition of invariant plane strain along the habit plane is not satisfied. A second " invisible" strain is required to generate the final crystal structure. It is termed a lattice-invariant strain, as the unit cell structure, resulting from the previously mentioned shape strain, is not altered. The lattice invariant strain consists of slip on fairly regularly spaced slip planes or of simple homogeneous twinning shear, as illustrated in Fig. 9. To minimize the lattice distortion at the interface, the twins or slip bands are usually finely spaced (19).

The modern phenomenological theories of martensite formation were first proposed by Bowles and Mackenzie and by Wechsler, Lieberman, and Read from 1952 to 1954 (25,26). According to these theories, the martensitic transformation can be completely described in terms of three basic steps (9 p.424).

A) A Bain Distortion: The unit cell structure of the product phase is formed by the shape change.
B) A Secondary Shear Deformation: A lattice invariant strain, which along with (A), produces an undistorted habit plane.
C) A Rotation of the Product Lattice: A "rotation" is usually required to bring both the undistorted lattice of the parent phase to the same orientation in space as the product phase produced by the shape change (A) and secondary shear (B).

These three steps are illustrated in Fig. 10.

The final martensitic structure, as observed under the microscope, is the net effect of the above three distortions. The theories are phenomenological, i.e. they are concerned with the initial and final states and do not specify the route taken by the atoms in achieving the transformation.

Several conflicting theories have been postulated concerning the mechanism of martensite nucleation (18,21 p.209, 27). One point that has been established conclusively, however, is that nuclei cannot form by random fluctuations in a defect free region, i.e. this nucleation does not follow classical nucleation theory. Martensite appears to be nucleated heterogeneously, the nuclei forming at internal positions of high strain termed strain embryos. There are two conflicting theories concerning the temperature at which strain embryos are formed: (27)

a) The embryos form at a relatively high temperature but only become activated by cooling through the Ms temperature.
b) The martensite embryos are formed and nucleated at the Ms temperature, at a suitable dislocation configuration or internal stress field.

Neither postulate has been confirmed conclusively.

The majority of martensite is formed athermally. The nuclei are formed without thermal activation as can be seen by the fact that martensite can be formed at $4^{o}K$ (9 p.436). Martensite begins to nucleate at the Ms temperature.

Each plate grows to its final size with great speed, i.e. in the order of one third the velocity of sound in the material (9). The temperature must be progressively lowered to nucleate more martensite. The rate of growth of individual martensite plate is independent of temperature (9).

Isothermal martensitic transformation is only encountered to a minor extent. The growth of isothermal martensite is characterized by progressive nucleation, each new nucleus growing to its final size just as quickly as athermal martensite (9 ,23 p.147). In isothermal martensite, thermal activation contributes only to martensite nucleation.

Two distinctly different types of martensitic transformation will be described briefly (9,p.422-435).

1) Transformation involving small atomic displacement: eg. the FCC to FCT transformation of In-Tl.

   As the temperature is continually cooled below the Ms temperature, the interface moves along by jerks in an orderly manner. Complete transformation is achieved in a small temperature interval (between 65°C and 72°C), and is reversible with little temperature hysteresis, Fig. 11.

2) Transformation involving large atomic displacements: eg. the FCC to BCC transformation of Fe-Ni alloys.

   During cooling, small lens shaped martensite is first formed just below the Ms temperature. At a lower critical temperature an audible burst produces much more martensite, whose plates are considerably thicker than those which were formed initially. The typical martensite products are lens shaped or acicular, these shapes being due to the constraints of the matrix. The lens shape is actually produced by parallel sections of habit plane, where the interface is interupted by steps. The limiting size of the plates is associated with the magnitude of the strains set up between the martensite plate and the surrounding matrix.

> The plastic flow, produced in the surrounding matrix by the strain, causes loss of atom to atom coherency, so that, as coherency is lost, growth stops. This type of martensite is also typical of Fe-C and steel martensite.

One important aspect of martensite formation is that plastic deformation, per se, may energise the transformation of the parent matrix to martensite (9,21,23 p.25). Plastic deformation increases the internal strain and makes nucleation easier. The highest temperature where martensite can be formed by applied deformation is termed Md, which is higher than the previously mentioned Ms. The reverse process of recrystallizing deformed martensite to austenite occurs at a temperature Ad, lower than the normal recrystallization temperature As. This will be clear from the illustration in Fig. 12. The role of plastic deformation on martensite formation will be discussed in more detail in Section III.

It is important to realize that martensite need not be hard or strong as it is commonly is in steel. In a material undergoing a martensitic reactions, strength is increased by the following factors: (19 p.205).

1) The ultrafine product phase due to internal twins.
2) Significant increase in dislocation density of both the parent and product phases due to work hardening.
3) Refinement of the parent grain size due to the smaller grained product phase.
4) A solid solution hardening increment.
5) A order hardening increment of the product phase.

In the ferrous martensite, the greatest contribution to strength is offered by the interstitial solid solution hardening of carbon retained in solution during the phase change (Fig. 13). The strengthening contribution of the finely twinned product phase alone appears to be minimal (28). As carbon content is increased, and the lattice strain increases, the strengthening effect of the fine structure becomes more

significant. The increased carbon content also changes the morphology of the ferrous martensite, the number of twin increasing with increasing carbon content (19).

The hardness and strength of ferrous martensite can be greatly increased by aging at low temperatures (100°C to 300°C), Fig. 14. A clear theoretical picture, explaining this phenomenon is not available. Possible reasons for this effect are the following : (27)

1) The migration of interstitial carbon atoms during aging produces locking of dislocations.
2) Positive resistance to the movement of dislocations is produced in the form of precipitated carbides.

It is well known that ferritic martensite is extremely brittle and of little commercial value (9). The transformation of austenite to martensite involves expansion, which produces internal stress in the material. Martensitic steels are almost always subjected to a heat treatment process called tempering, i.e. the steel is heated to a value below the eutectoid temperature, held there for a specific time and then cooled (9 p.506). During tempering, the martensite loses some of its carbon and the unit cell of martensite becomes less tetragonal. Epsilon carbides ( ) are formed and are originally crystallographically coherent with the martensite matrix. At this stage, the strength of the material may be increased (18 p.255). Further tempering produces a number of other structural changes; some of the retained austenite converts to ferrite or bainite and carbides separate out of solution, forming non-coherent carbides. Softening occurs at this stage and elongation is increased.

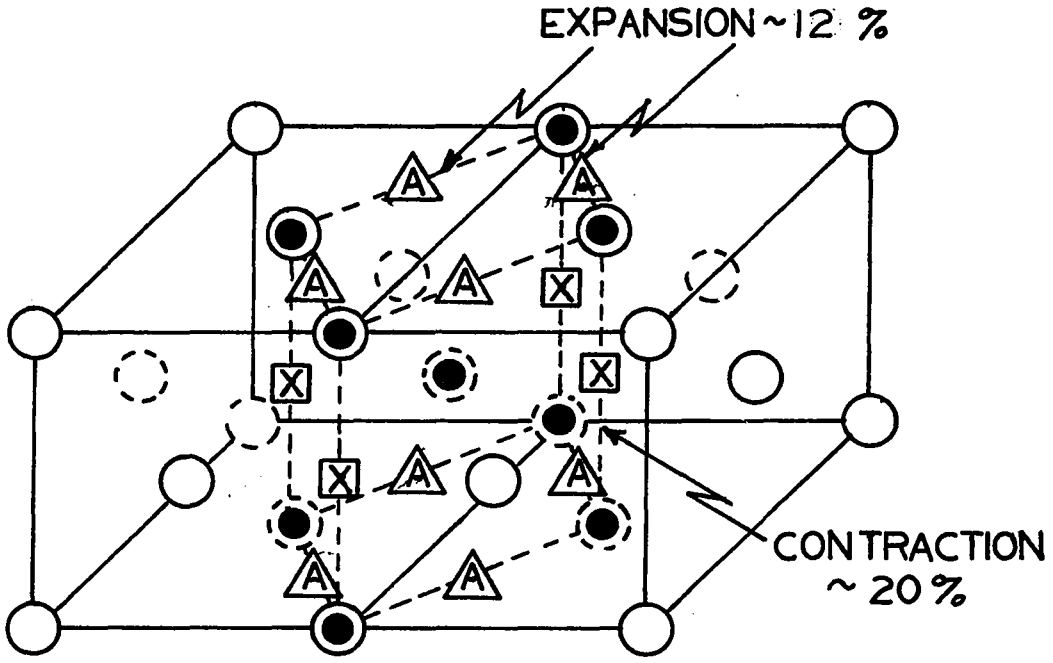

Fig. 7 . The homogeneous FCC → BCT lattice distortion proposed by Bain (24), illustrating the strain produced by interstitial carbon atoms

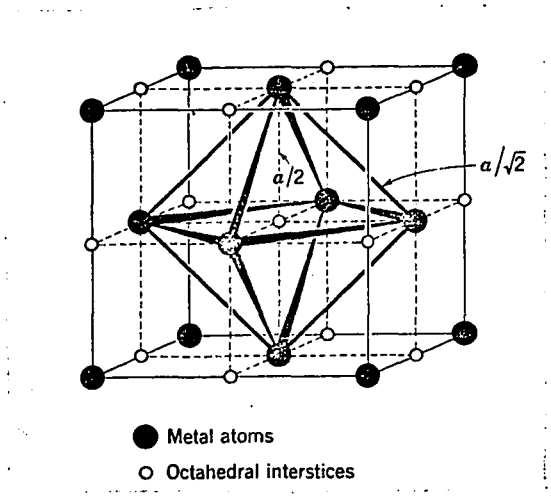

Fig. 8 The interstitial octahedral voids in the F.C.C. structure.

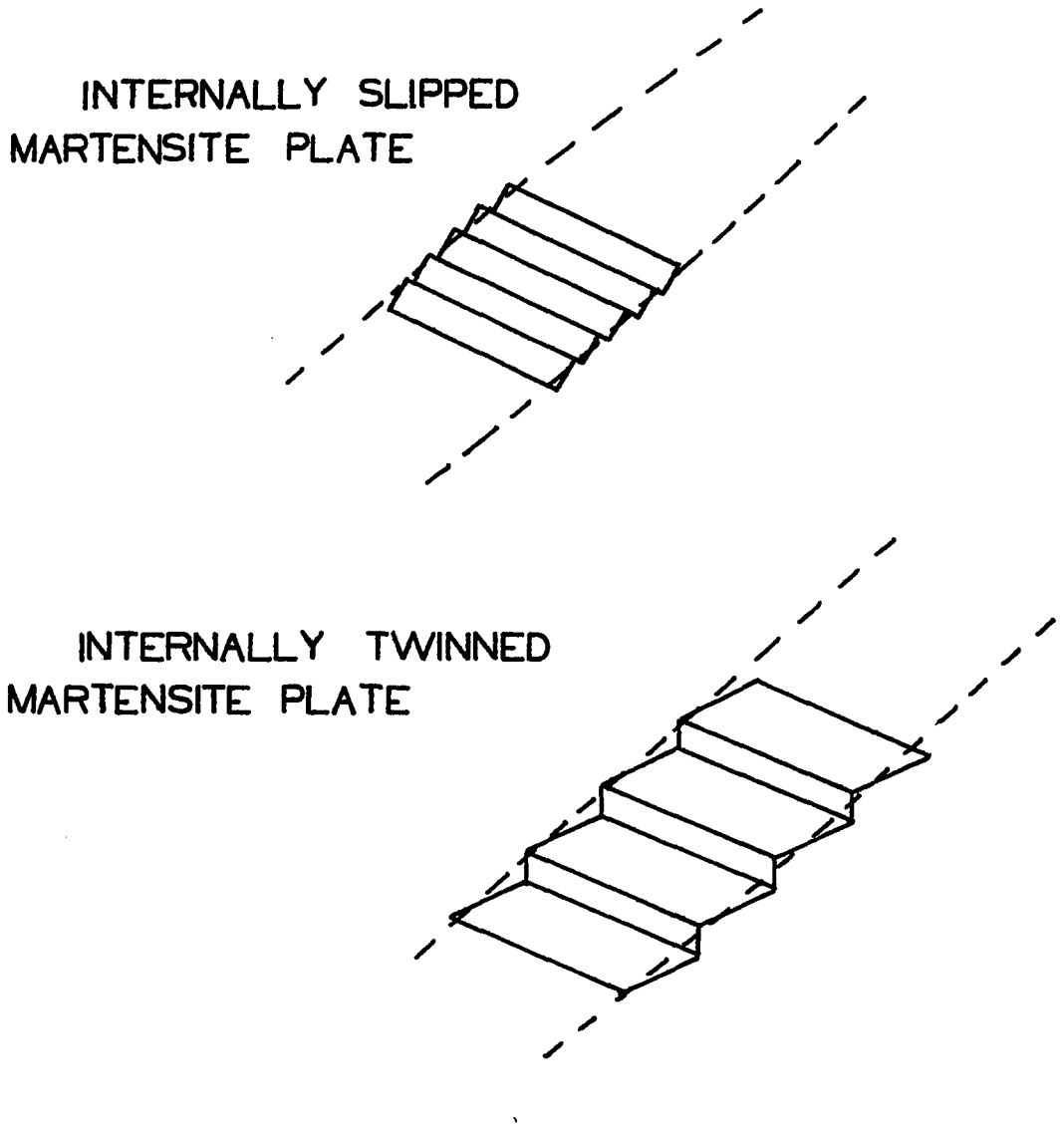

Fig. 9. Schematic representation of martensite plates which are internally slipped and internally twinned (28)

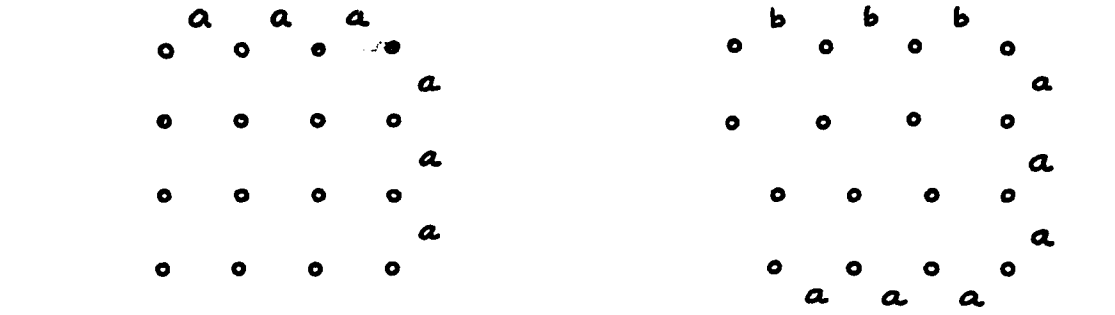

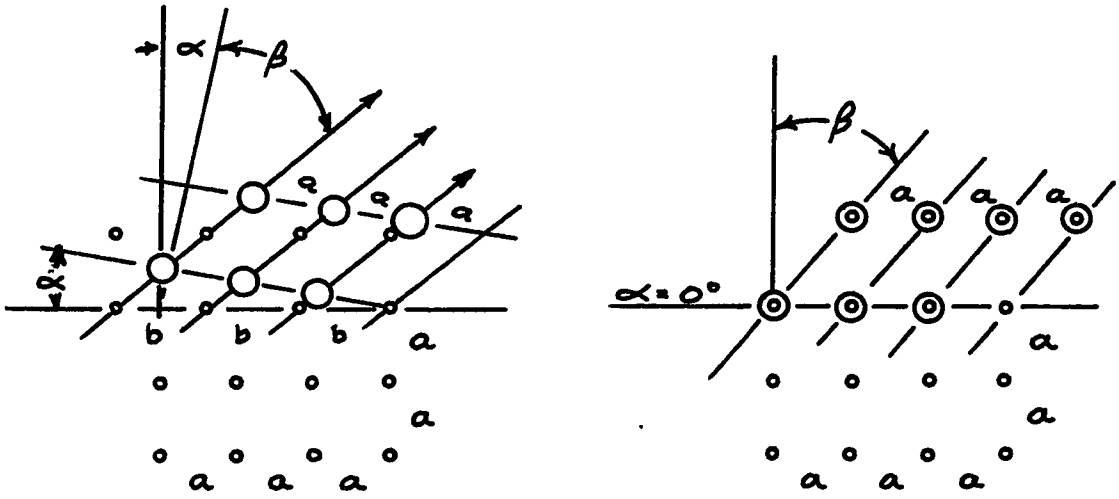

Fig. 10. Phenomenological steps involved in a simple, idealized martensitic phase transformation

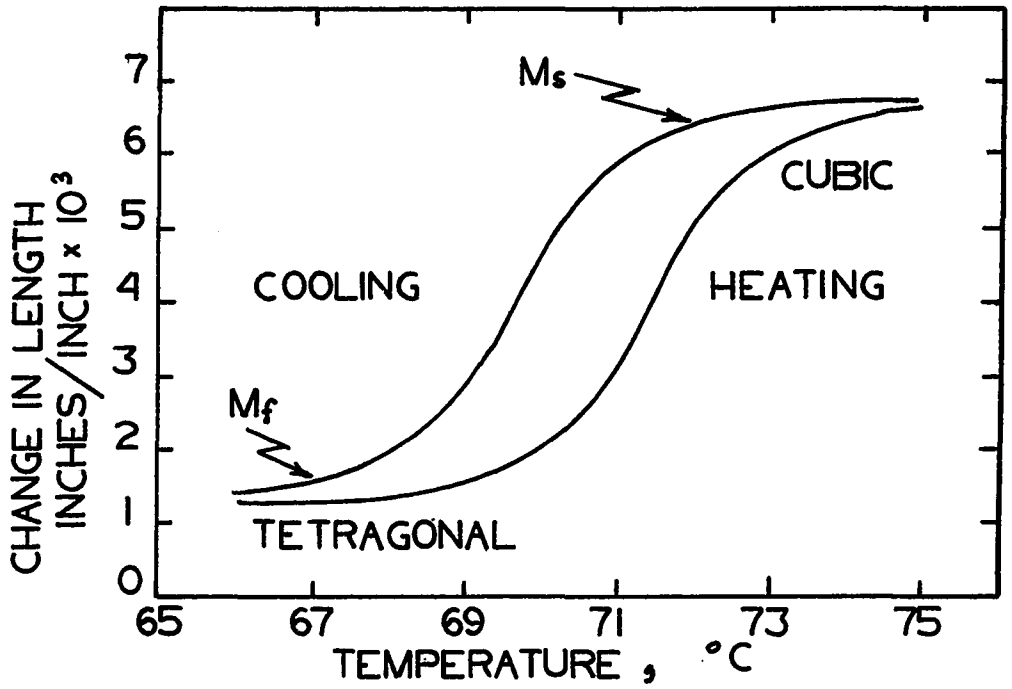

Fig. 11. The temperature dependence of the martensite transformation in the indium-thallium (18% Tℓ) alloy

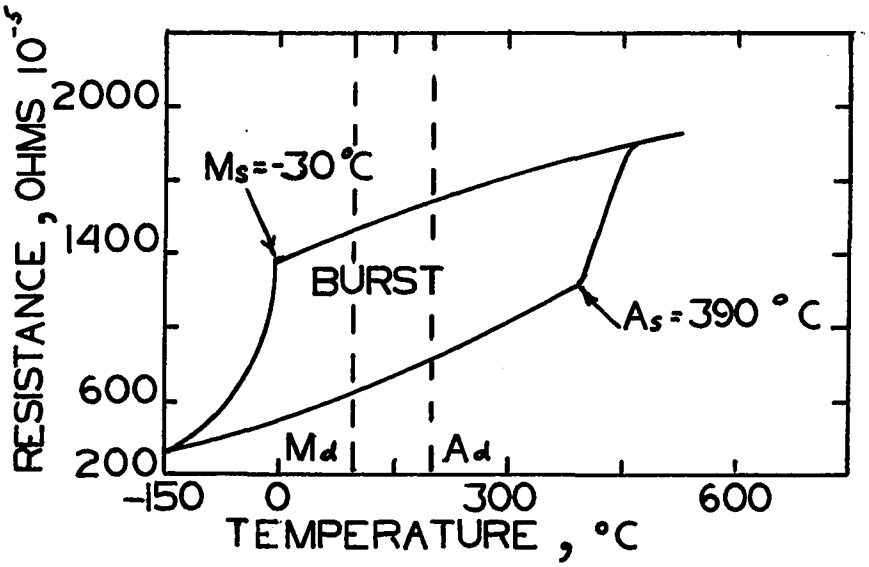

Fig. 12. The martensitic transformation in an iron-nickel (29.5% Ni) alloy, showing the relation of Md and Ad to Ms and As

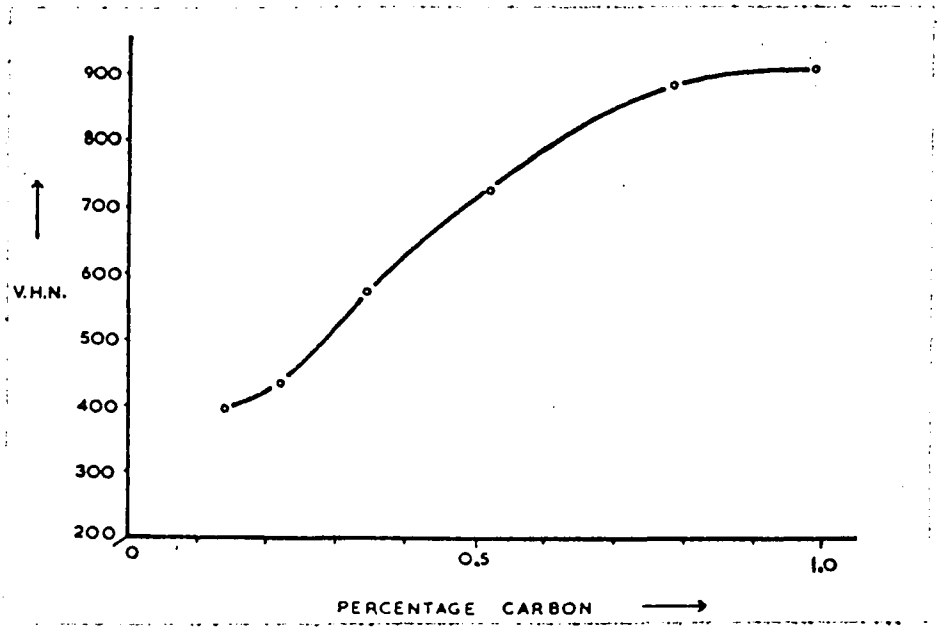

Fig. 13 The effect of carbon content on the microhardness of martensite in carbon steels (19)

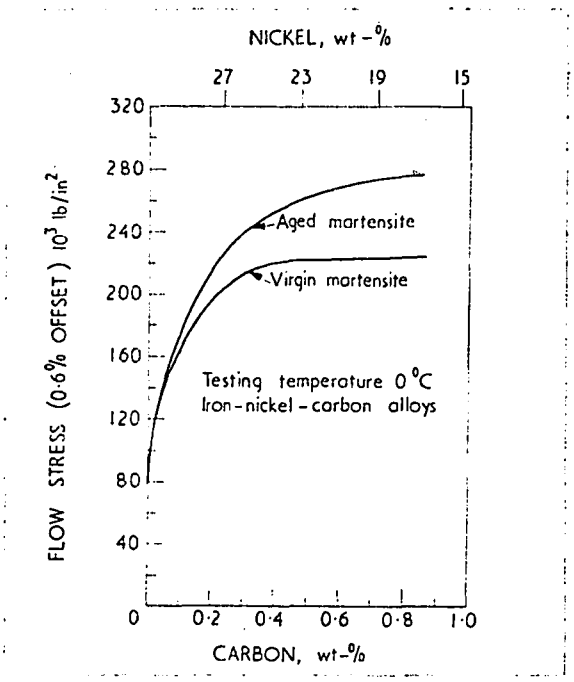

Fig. 14 (28)

Variation of flow stress at 0°C of martensitic Fe-Ni-C alloys (Ms 35°C) as a function of carbon content.

D. A Model for Predicting Temper Rolling and Temper Annealing Behavior

Since the most important aspect of this study was to compare the mechanical properties of temper rolled and temper annealed material, a theoretical analysis of properties of partly recrystallized material vis-a-vis the properties of cold worked material is desirable in trying to analyse experimental data. A model describing the relationship between mechanical properties and the degree of recrystallization of a metal has been presented by S.Adams (17). The analysis is perhaps more accurately described as a theoretical investigation of two-constituent structures, each constituent having different mechanical properties. Adams' treatment is summarized below; the detailed treatment is reproduced in Appendix A.

An attempt was made to estimate the mechanical properties of sheet at various stages of temper rolling and at various stages of temper annealing, using only the readily available data of the annealed and fully hardened states. In order to compare a wide variety of materials, the tensile strength and elongation parameters were expressed in normalized form as follows:

1) $Fs = \frac{S - So}{St - So}$

S = Tensile strength of material being tested.

So = Tensile strength of material in its annealed state.

St = Tensile strength of material in its fully hardened state.

2) $Fe = \frac{(\epsilon_u) - (\epsilon_u)T}{(\epsilon_u)o - (\epsilon_u)T}$

(ϵu) = Max. Uniform Elongation of material being tested.

$(\epsilon_u)o$ = Max.Uniform Elongation of material in its annealed state.

$(\epsilon_u)T$ = Max. Uniform Elongation of material in its fully hardened state.

Fs = Normalized Tensile Strength

Fe = Normalized Elongation

When the parameters are expressed in the normalized form, and if total elongation is a linear function of uniform elongation, total elongation readings may be substituted for the uniform elongation, without loss of accuracy.

In predicting temper rolling behavior, it was supposed that cold rolling prior to testing was equivalent to reducing available uniform strain prior to necking by a strain which was a direct function of rolling reduction. This equivalent rolling strain must, however, be determined experimentally. The true stress at the tensile stress, δ_u, is always constant, and thus the tensile stress S, is only a function of maximum uniform strain, (ϵ_u), i.e. 3)

$$S = \frac{\delta}{(1+\epsilon u)}$$

When a material is cold worked to the stage where the uniform elongation approaches zero, $\epsilon_u = 0$, the tensile strength is denoted by S* and $S^* = \delta_u$. In the normalized form, the same stage Fs*, is reached when:

4) $$Fs^* = (\epsilon_u)o \times \frac{So}{St-So}$$

5) $$Fe = 0$$

Up to Fs*, the normalized tensile strength is described by the following equation:

6) $$Fs = Fs^* \times \frac{1 - Fe}{1 - (\epsilon_u)o\ Fe}$$

The effect of temper rolling on the tensile strength is illustrated in Fig. 10.

It can be seen from equation (4) that Fs* is reduced if

a) St is large, i.e. total reduction is great

b) $^{So}/St$ is small, i.e. strain hardening is rapid

c) $(\epsilon_u)o$ is small, i.e. annealed uniform elongation is small.

Rapid strain hardening, (low $^{So}/St$ value) in metals corresponds to a large value of $(\epsilon_u)o$. When a metal has a low value of $(\epsilon_u)o$, the only way to obtain small values of $^{So}/St$ is by a large amount of cold work, past S*, making St as large as possible. Large cold reductions may, however, be impracticable.

In real systems, the uniform elongation never drops to zero, even after a large amount of cold work. This is probably due to a softening effect, like recovery, occurring during processing.

The discussion of the behavior of temper annealed materials is analogous to a study of a duplex structure. The problem is to relate the average stress, $\bar{\delta}$, to stresses in the separate components as a function of the applied strain and the relative amounts of the components. The following assumptions were made in Adams' analysis:

1) Individual regions have the same properties as the bulk materials; if α is the soft and β the hard component,

7) $$\bar{\delta}_\alpha = k_1 (k_2 + (\bar{\epsilon}_\alpha + b)^n)$$

8) $$\bar{\delta}_\beta = k_1 (k_2 + (\bar{\epsilon}_\beta + c\epsilon_T + b)^n)$$

Where δ = true stress

ϵ = natural strain

b k_1 k_2 n = constants of the system

2). Areal and linear functions of the components remain unchanged during deformation. Further, it is assumed there is no preferred orientation. On any cross-section, the average stress is given by:

(9) $$\bar{\delta} = V \bar{\delta}_\alpha + (1 - V) \bar{\delta}_\beta$$

where V = volume fraction of the annealed material

3). A small increment in the overall strain is related to the increments in the average strain in α and β by;

(10) $$d\varepsilon = V\, d\bar{\varepsilon}_\alpha + (1-V)\, d\bar{\varepsilon}_\beta$$

4). The relationship between $\bar{\varepsilon}_\alpha$ and $\bar{\varepsilon}_\beta$ was assumed to be one of the following:

a) Equi-Stress in the components; i.e. strain only occurs in the soft component until it work hardens sufficiently to reach the same strength as the hardened component.

b) Equi-Strain in the components; i.e. differences in hardness between the two components are ignored.

c) Equi-Work in the components; i.e. the work per unit volume is constant;

(11) $$d\bar{\varepsilon}_\alpha \times \bar{\delta}_\alpha = d\bar{\varepsilon}_\beta \times \bar{\delta}_\beta$$

Using these assumptions and assuming a knowledge of the tensile strength and total elongation of the annealed and fully hardened material, temper annealing curves were calculated. The equi-stress relationship had to be rejected because the results were obviously erroneous, but the other relationships (using 4b or 4c) gave very similar results.

When expressed in normalized form, widely differing reductions and annealed elongations gave about the same temper annealing results, (Fig. 16).

The curvature of the temper annealing curve, however, did become more prominent if:

a) The metal had a high rate of strain hardening.

b) The metal had a high elongation in the annealed state.

c) Greater cold work had been performed, especially if the annealed elongation was large.

All these effects were only minor when compared to the effect of the same variables on the properties of temper rolled material.

In fact, an empirical average curve of available data would be a reasonably good approximation to any unknown temper annealing curve.

The improvement in elongation achieved by temper annealing is greatest if the Fe of the temper annealing and temper rolling curves differ greatly for a given Fs, as illustrated in Fig. 17. The main contributions to this improvement would be:

a) A small amount of elongation in the annealed state

b) A large amount of prior deformation.

When elongation in the annealed state is large, cold worked material is still very ductile , at even high reductions, but the very high reductions required to produce useful temper annealing properties may be impossible to achieve.

On the other hand, if the annealed elongation is low, although a considerable relative increase in ductility is possible by temper annealing, the absolute value may not be large or significant, eg. a 2% elongation is four times a ½% elongation, but the 2% is probably not significant or useful.

In the metals, the effect of a low $^{So}/St$ ratio, i.e. rapid strain hardening, on ductility improvement by temper annealing is usually less significant than the effect of low $(\epsilon_u)o$. In fact, it can be a hindrancewhen attempting to achieve high cold reductions. The relative effect of these parameters, (So/St, St, $(\epsilon_u)o$), on mechanical properties will be discussed in a later section (V-H).

Adams' analysis forecasts that the most impressive improvements should be found in materials with annealed elongations in the range of 15-25%, especially if cold reduction can be continued successfully to high strength values. Possible materials falling in this catagory would be certain aluminum alloys and perhaps ferritic stainless steel.

Results can be expressed in either the normalized form, as in Fig. 17 or in the more standard stress-elongation curve form as seen in Fig. 18. The conversion of readings is obtained through the following equations:

(12) $S = Fs(St-So) + So$

(13) $\epsilon = Fe((\epsilon_u)o - (\epsilon_u)t) \quad (\epsilon_u)t$

Adams' analysis is borne out by the limited amount of data available on partially annealed and partially cold reduced material. His techniques could be used in predicting which metals may be usefully temper annealed. This theoretical analysis was being developed at the same time as the present experiments were being conducted on the temper annealing of stainless steel. As will be shown in Section VI-H, some of the findings of the present research contributed to the development of this model, although the data was difficult to interpret.

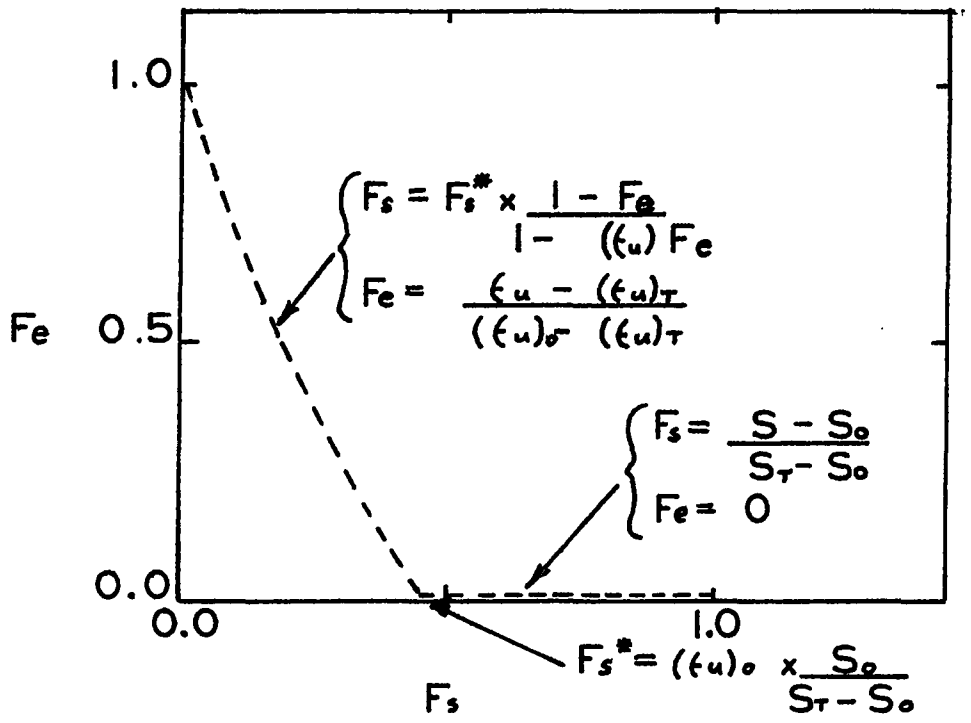

Fig. 15. Temper rolling data, in normalized form

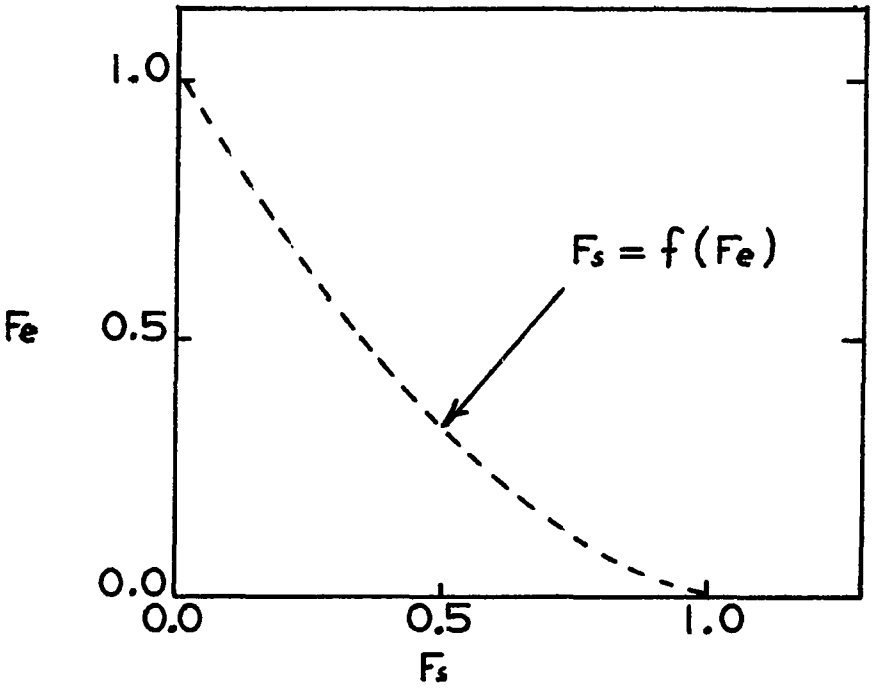

Fig. 16. Temper annealing data, in normalized form

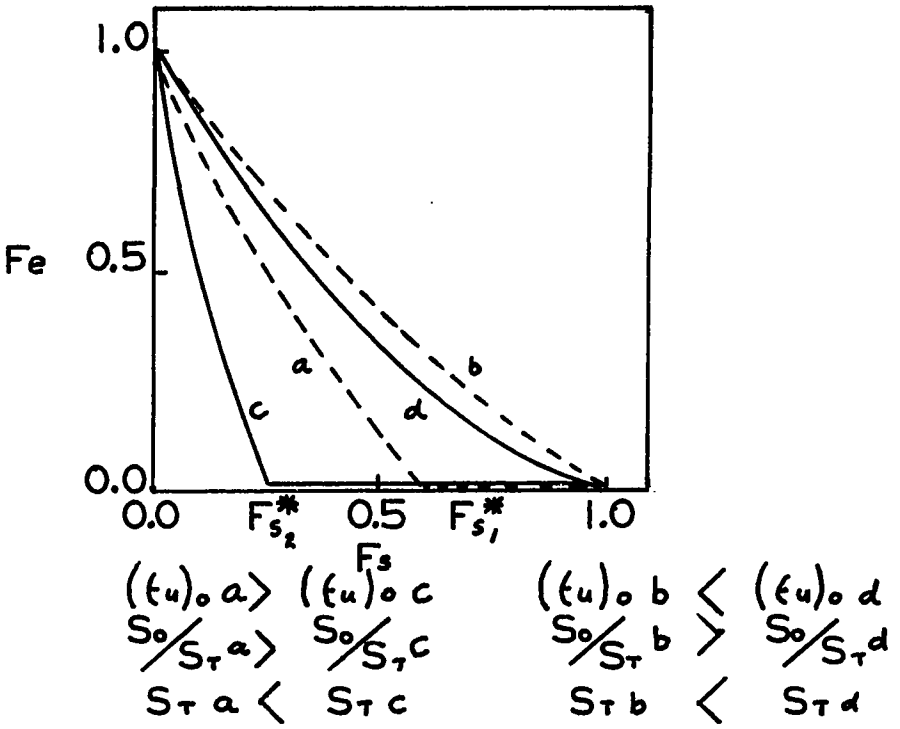

Fig. 17. Effect of critical mechanical properties on the temper rolling and temper annealing curves

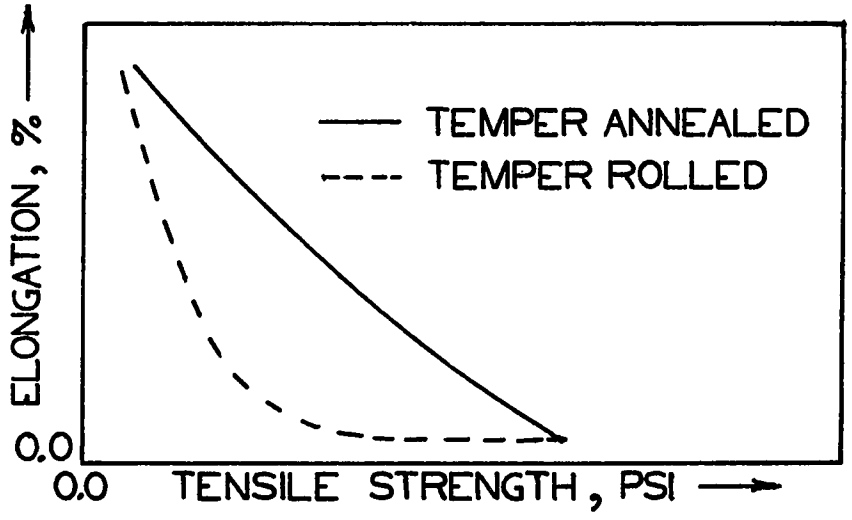

Fig. 18. Temper rolling and temper annealing curves expressed in the "Strength-Elongation Form"

Section III

METALLURGY OF STAINLESS STEEL

III METALLURGY OF STAINLESS STEEL

A. Classification of Stainless Steel

Stainless steels form a versatile series of alloys composed of iron, chromium, nickel and carbon. The effect of chromium on the corrosion resistance of iron was first recongized by Brearly in 1912 (29 p.3). Chromium-nickel steels were developed about the same time by Maurer and Strauss (29 p.3) to give the steels more workability and an improved corrosion resistance to certain low oxidizing acids such as HCl & H_2SO_4 (30 p.380). For convenience, stainless steels are divided into five classes, involving three distinct crystallographic structures (31 p.3).

1) Ferrite stainless steel (BCC Structure)
2) Martensitic Stainless Steel (BCT Structure)
3) Austenitic Stainless Steel (FCC Structure)
4) Manganese Substituted Austenitic Stainless Steel.
5) Precipitation Hardening Stainless Steel.

The latter two classes of steel may be considered merely variations of the first three, which are characterized by three distinct crystallographic structures. They have, however, many unique properties to justify their separate classification, eg. precipitation hardened steels have better creep properties; both have good high temperature properties. The last two classes will be excluded from further discussion as they are not directly related to the present research.

B. The Chemistry of Stainless Steel

Before proceeding to a more detailed examination of the properties of stainless steels, it is useful to have an understanding of the different phase transformation possible in Fe-Cr alloys.

The essential solute element in all stainless steels is chromium. It imparts excellent corrosion resistance to iron against a variety of atmospheres as well as to most acids except HCl and H_2SO_4 (30 p.38). The minimum amount of chromium required to confer this protection depends greatly on the corroding agent. According to AISI standards (32), a minimum of 4% by weight Cr is required to classify a steel as " stainless".

The basic phase diagram to consider, therefore, is the Fe-Cr system (Fig. 19) (4). When this diagram is compared to the Fe-C diagram (Fig. 20) (4), it can be seen that increased Cr promotes the formation of a gamma loop i.e. a closed austenitic region. As the amount of Cr is increased, the A_4 critical line is lowered, while A_3 critical line is first lowered, then raised. At about 12.5% Cr, these two lines meet, thus closing the loop. The austenite or gamma phase cannot exist beyond the closed loop, even at elevated temperatures. The high Cr phase has the BCC structure of alpha iron, is magnetic at room temperature and thus is termed alpha (or delta) ferrite. Ferritic stainless steel has this BCC structure. These steels are difficult to fabricate and are generally limited in their applications to simple shapes, requiring a minimum of fabrication, eg. automobile trim.

As in the heat treatment of ordinary carbon steels, Fe-Cr alloys up to 12.5% Cr can be heated into the austenite region, and then quenched into the ferrite region, thus producing the hard, distorted phase, martensite. In the Fe-Cr alloys, the cooling rate need not be severe, as in most cases the metastable martensite phase can be produced by air cooling.

With only 12.5% Cr, however, the steel would only just be passive to most atmospheres. The addition of 0.2% carbon to this alloy can expand the gamma loop, as shown by the dashed line in Fig. 19(29,30,31,32).

It is really the expansion of this loop by carbon addition that enables the manufacture of martensitic stainless steel. Most of these steels are thus in the 10%-18% Cr range (29, 32). An example of the use of this type of steel is in the stainless steel cutlery.

The effect of nickel, as opposed to chromium, is to open up the stable region of austenite. The Fe-Ni phase diagram is shown in Fig. 21 (32p. 1111). As Cr is added to a Fe-Ni solution, in order to produce corrosion resistence, the region of stable ferrite is increased as illustrated in Fig. 22.

These diagrams would imply that even at high Ni contents, the austenite would still transform to ferrite as the alloy is cooled to room temperature. This transformation is, however, so sluggish that the austenite can be retained at room temperature or at even cryogenic temperatures. The retained austenite is, in fact, a metastable phase (31 p.27).

An additional aspect shown in these diagrams is that, at 18% Cr, a common stainless steel analysis, a minimum Ni content is required to produce any austenite at all, i.e. about 6.5% Ni. Further Ni additions serve to increase the stability of the austenite (32 p.79). The Ni and Cr analysis may be varied or other elements may be added to the steel in order to obtain almost any desired mechanical or corrosion resistant properties. A series of austenitic stainless steels is thus derived, based on the standard composition of 18% Cr and 8% Ni (the well-known 18/8 series).

The addition of carbon adds a further complication to this system. Austenite can hold about 2% carbon in solution, while ferrite can only hold about 0.1% carbon. The effect of carbon additions to a typical 18/8 stainless steel is illustrated in Fig. 23 (32 p.1123). Below about 1000°C, mixed carbides can precipitate from solution as stable phases.

Prolonged heating below this temperature and above about 700°C, which permits sufficient atomic mobility, will result in the precipitation of metal carbides. In austenitic stainless steel, these precipitates are usually chromium rich carbides of the composition (Cr, M_1, M_2) $_{23}C_6$ (34,35). This results in a depletion of the solid solution of chromium in the area adjacent to the carbides causing a loss of corrosion resistance in this area. This depletion is most readily encountered at grain boundaries as they are the preferred sites for precipitate nucleation (9). This type of loss of corrosion resistance is termed sensitization and it poses a very critical problem when heat treating or welding austenitic stainless steels. It must be kept in mind that any commercially useful heat treatment must still avoid sensitization.

The problems of sensitization can be minimized either by producing a low carbon stainless steel or by adding other elements such as titanium or columbium, which will combine with the excess carbon more readily than chromium, forming their own stable carbides, the full corrosion resistance offered by solid solution chromium being thus retained (29,31,32).

In further discussion of Fe-Cr-Ni-C alloys and their structures it is useful to consider the diagram in Fig. 24 (29). This shows the phases in an Fe-Cr-Ni alloy, containing 0.1%C (a typical carbon content in austenitic stainless steel), after rapid cooling from a temperature of maximum austenite formation. The point R denotes the analysis of a typical 18/8 stainless steel. It will be noted that this analysis has the minimum Ni content that can maintain the austenitic structure and still have sufficient Cr available for corrosion resistance.

Other common elements, such as Mn,Si,P,S, which are always found in steel, are all in substitutional solid solution, while carbon and nitrogen are in interstitial solid solution.

All these elements contribute, in widely varying degrees to the stability of the phases found in stainless steel. These elements can be expressed as either ferrite stabalizers or austenite stabilizers. Elements which promote ferrite formation are Cr, V, Ti,W,Al, Mo,Si,Cb, while austenite stabilizers are C, Ni, Cu, Co, N, Mn (31,36).

A useful diagram, illustrating the effect of each of these elements, is the Schaeffler Diagram, Fig. 25(31 p.88,36) . This diagram was devised only for predicting the phase structure of weld metal, but it can still be used to predict general effects of alloy addition on the structure of stainless steel. In this diagram the important ferrite stabilizers are each multiplied by a potency factor, and the results are added together. The total is expressed as a Cr equivalent and is read on the horizontal axis of the diagram. Similarly, the austenite stabilizers are expressed together as a Ni equivalent and this total is shown on the vertical axis. Any given Ni and Cr equivalent combination, together define a point of this diagram, from which the phase composition of a weld metal can be predicted.

On this diagram the point P denotes the analysis of a typical 18/8 stainless steel. While it is obvious that an increase of Ni equivalent will stabilize austenite, either an increase or decrease of Cr equivalent will remove this analysis point from the region of stable austenite. Increased Cr encourages ferrite formation, while a decrease in Cr produces martensite directly by quenching (the thermodynamically stable phase is ferrite). The same situation was observed in Fig. 24.

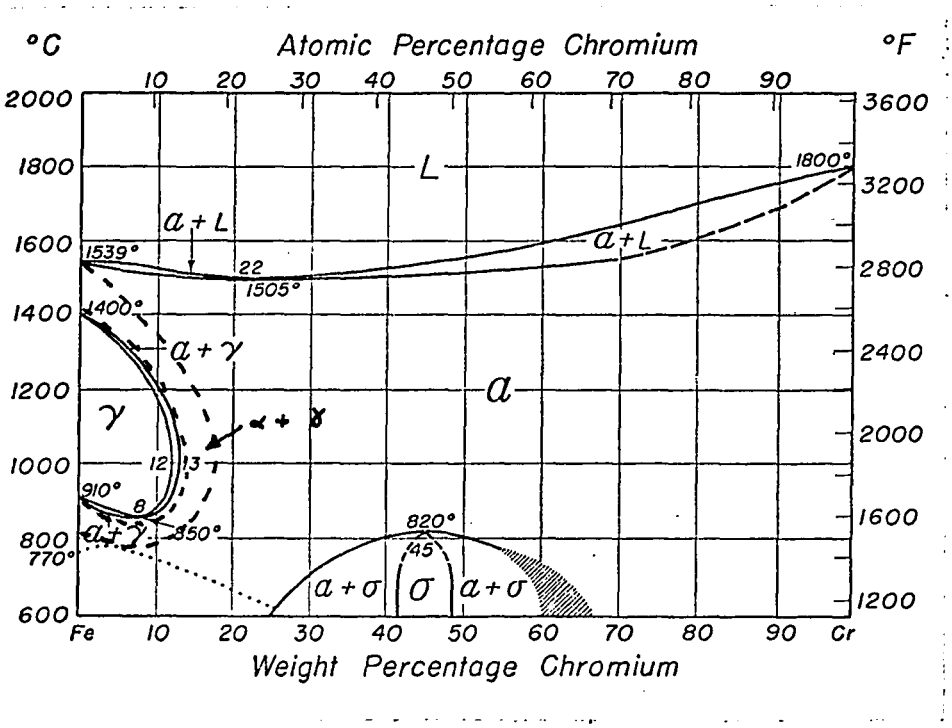

Fig. 19 (4)

The iron-chromium constitution diagram.

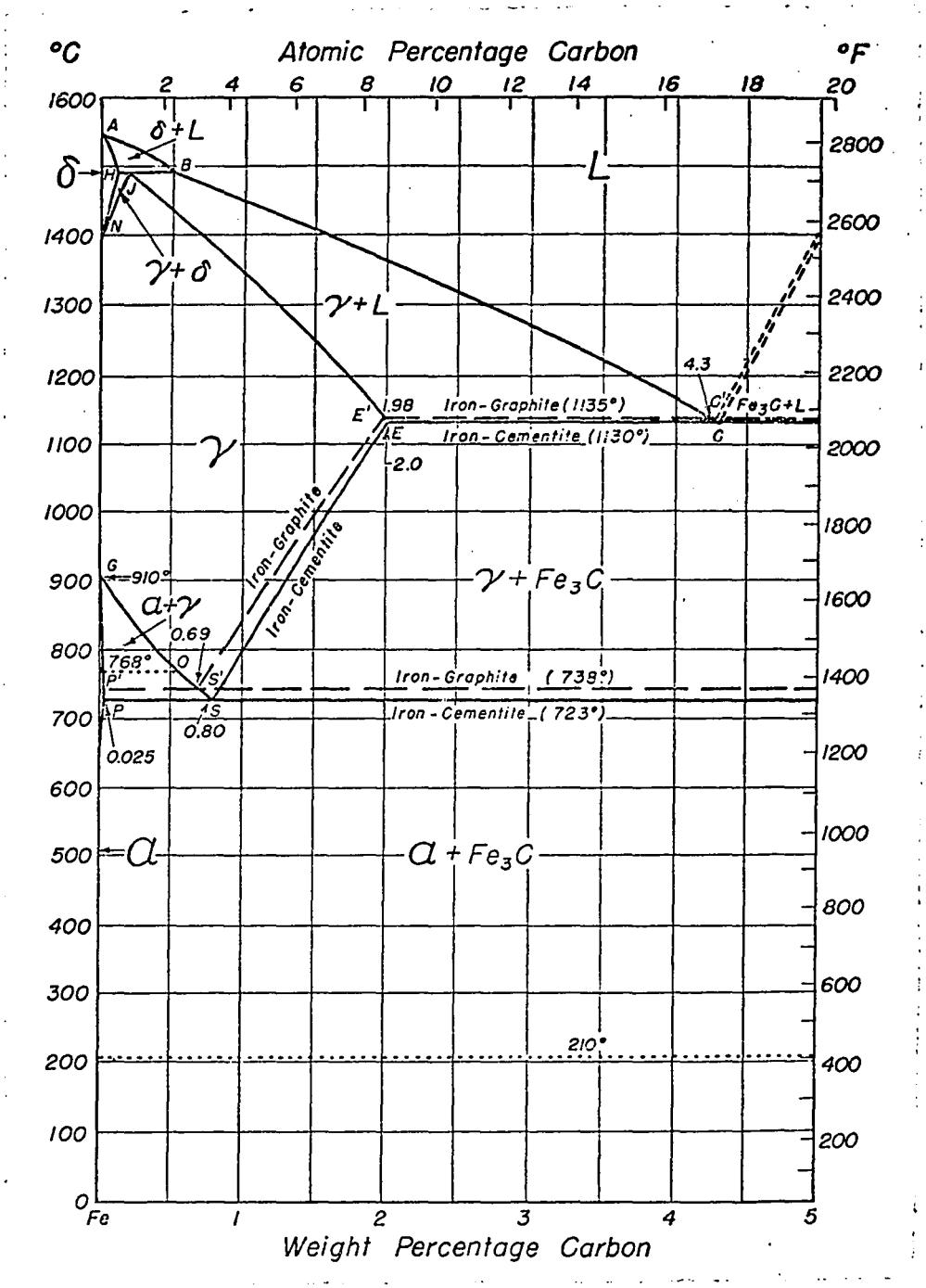

Fig. 20 (4)

The iron-carbon constitution diagram

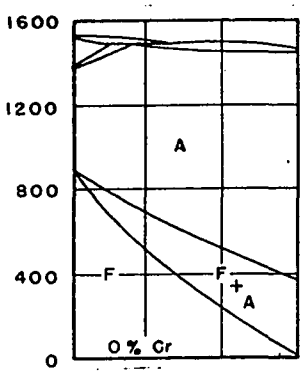

Fig. 21 (32)

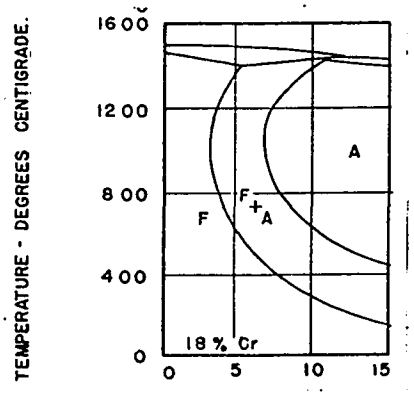

Fig. 22 (32)

The iron-chromium-nickel diagram at constant chromium content. The symbols A and F stand for austenite and ferrite, respectively

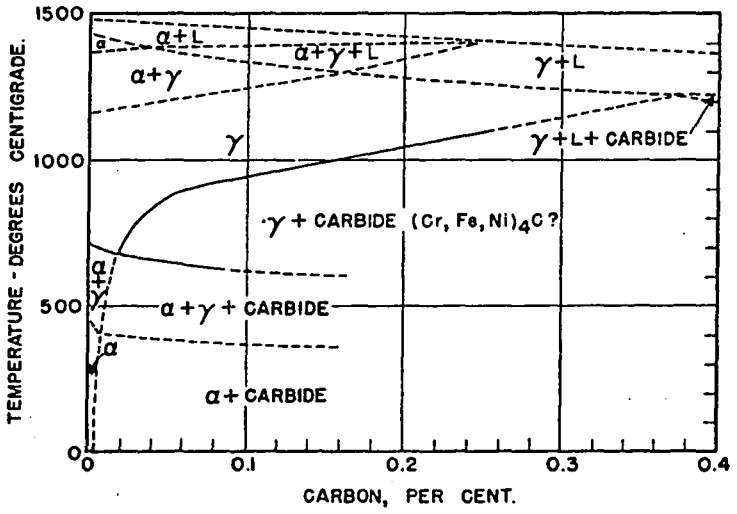

Fig. 23 (32)

The effect of carbon on the constitution of stainless steel containing 18 percent chromium and 8 percent nickel.

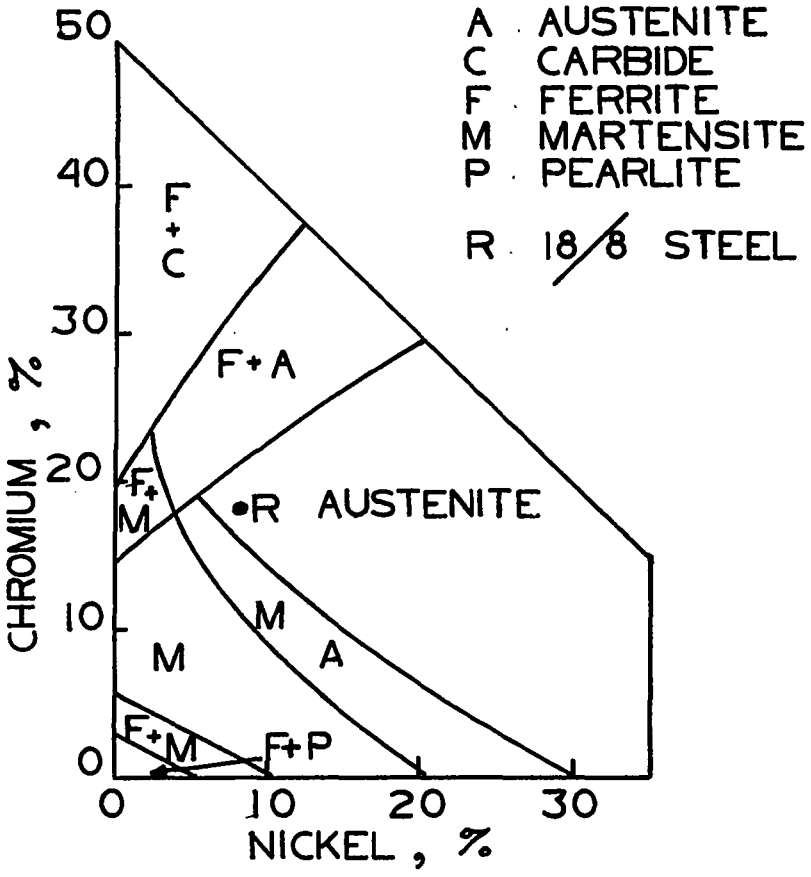

Fig. 24. Phases in Fe-Cr-Ni Alloy with 0.1%C quenched to room temperature (29)

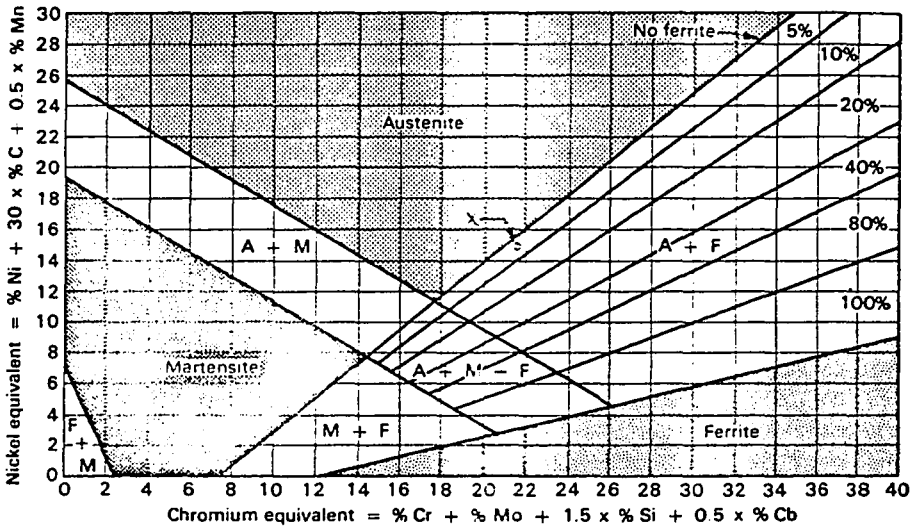

Example: Point X on the diagram indicates the equivalent composition of a 318 (316 with columbium) weld deposit containing 0.07% carbon, 1.55% manganese, 0.57% silicon, 18.02% chromium, 11.87% nickel, 2.16% molybdenum, and 0.80% columbium. Each of these percentages was multiplied by the "potency factor" indicated for the element in question along the axes of the diagram, in order to determine the chromium equivalent and the nickel equivalent. When these were plotted, as point X, the constitution of the weld was indicated as austenite plus from 0 to 5% ferrite. Magnetic analysis of the actual sample revealed an average ferrite content of 2%. For austenite-plus-ferrite structures, the diagram predicts the percentage ferrite within 4% for the following corrosion-resistant steels: CH-20, CH-20C, CK-20, CF-12M, and CF-8MC.

Fig. 25. Schaeffler diagram for estimating ferrite content from composition.

C. Mechanical Properties of Austenitic Stainless Steel

The mechanical properties of annealed austenitic stainless steel may be summarized, in very general terms, as follows: (7)

1. Tensile Strength : 80,000 - 120,000 psi
2. Ductility : 65% - 75%
3. Yield Strength: 25,000 - 60,000 psi
4. Impact Resistance: 70 - 120 Ft-lb Izod.

The AISI standard tempers for cold rolled austenitic stainless steel and strip are given in Table II (7).

Cold work, in addition to bringing about the properties indicated in Table II, increases the fatique strength of austenitic stainless steel but at the same time increases its notch sensitivity.

The outstanding feature of austenitic stainless steel is the drastic change in mechanical properties which can be achieved by cold work, as is clear from the data in Table III and Fig. 26. A number of investigations have put forward possible reasons for this accelerated work hardening (34,35,37,38,39,40). Ludwigson and Berger recently proposed a model to describe the plastic behavior of metastable austenitic steel (37). Their empirical equation, describing the stress developed in response to strain, included the contribution of three strengthening parameters:

a) Strain hardening of austenite
b) The extent of strain induced transformation of austenite to martensite
c) The strength of the product martensite

They examined the effect of alloying on the different parameters expressed in their equation. It was found that the principal contributors to the strength of the cold worked material were 1, the amount of martensite formed, and 2, the strength of this martensite. Many elements, notably C and N, had effects that increased strength and at the same time had opposing softening effects.

An increase of either C or N, for instance, retarded the phase transformation to martensite but, the martensite which was formed, was stronger. The anomalous effect of Cr, depending on other alloying elements present was mentioned previously. Both an increase or decrease of Cr can make austenite less stable. A suitable chemical alloy balance must be determined in order to obtain maximum work hardening in a steel.

The effect of cold work on two different stainless steels of the same series can be seen from the data in Fig. 27. These illustrations refer to AISI 301 and 304 Steels, which have the following typical compositions (7).

	C	Mn	Si	Cr	Ni
AISI 301	.15	2.00 max	1.00 max.	17.0	7.0
AISI 304	.08	2.00 max	1.00 max.	19.0	9.5

The AISI 301 steel has a much higher rate of work hardening (7, 29,31,32). It can be seen from the metal analysis that the critical elements are C, Ni, Cr. In this comparison, the lower Ni content in grade 301 promotes increased transformation from austenite to martensite, while at the same time, the increased carbon increases the strength of the martensite formed, as well as the strength of the residual austenite. The lower Cr analysis in this range of Ni analysis also promotes martensite formation.

TABLE II

MINIMUM TENSILE PROPERTIES OF VARIOUS TEMPERS OF COLD ROLLED CHROMIUM-NICKEL STAINLESS STEEL SHOOT AND STRIP

Temper	Tensile Strength psi	Yield Strength (0.2% Offset) psi	Elongation (in 2 in.) %	Rockwell C Hardness
1/4 Hard	125,000	75,000	25	25
1/2 Hard	150,000	110,000	15 or 18	32
3/4 Hard	175,000	135,000	10 or 12	37
Full Hard	185,000	140,000	9 or 9	41
Extra Full Hard	200,000	-	-	45

TABLE III

Effect of Short- Time Aging on Properties at Room Temperature

AISI Type	Conditions of Rolling	Subsequent Heat Treatment	Yield Strength PSI	Tensile Strength PSI	Elongation (in 2 in.) %
301	As received	none	34,000	102,000	72.0
	10% at R.T.	none	78,000	120,000	44.5
		550F-24Hr.	86,000	119,500	46.5
	10% at-105°F	none	84,000	153,000	32.5
		550F-24Hr	86,000	142,000	40.0
	10% at-320°F				
		550F-24Hr	95,000	155,000	31.0
	20% at R.T.	none	96,000	139,500	32.
		550F-24Hr	117,000	146,000	33.
	20% at-105°F	none	128,000	206,000	18.5
		550F-24Hr	159,000	193,500	15.5
	20% at-320°F	none	182,000	236,000	10.
		550F-24Hr	218,000	241,000	5.5
	40% at R.T.	none	156,000	186,000	9.
		550F-24Hr	166,000	194,000	8.5
	40% at-105°F	none	268,000	273,000	3.5
		550F-24Hr	275,000	276,000	2.
	40% at-320°F	none	291,000	295,000	3.5
		550F-24Hr	308,000	309,000	3.
	60% at R.T.	none	209,000	236,000	3.
		550F-24Hr	216,000	242,000	2.
	60% at-105°F	none	311,000	318,000	1.5
		550F-24Hr	313,000	316,000	1.5

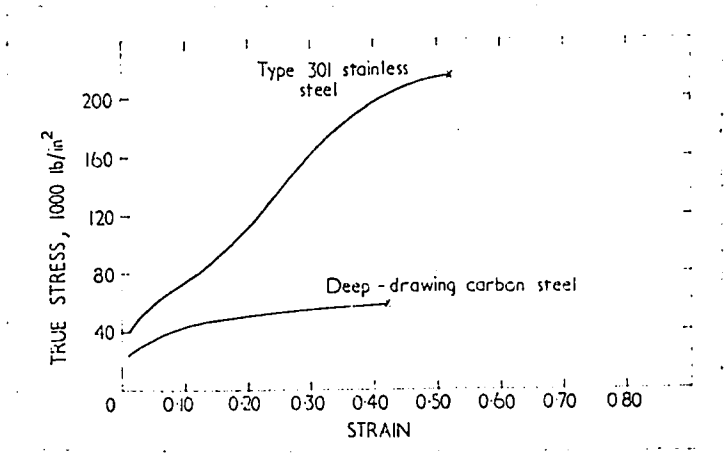

Fig. 26 (37)

Differences in the plastic behavior of deep drawing carbon steel and type 301 stainless steel in uniaxial tension.

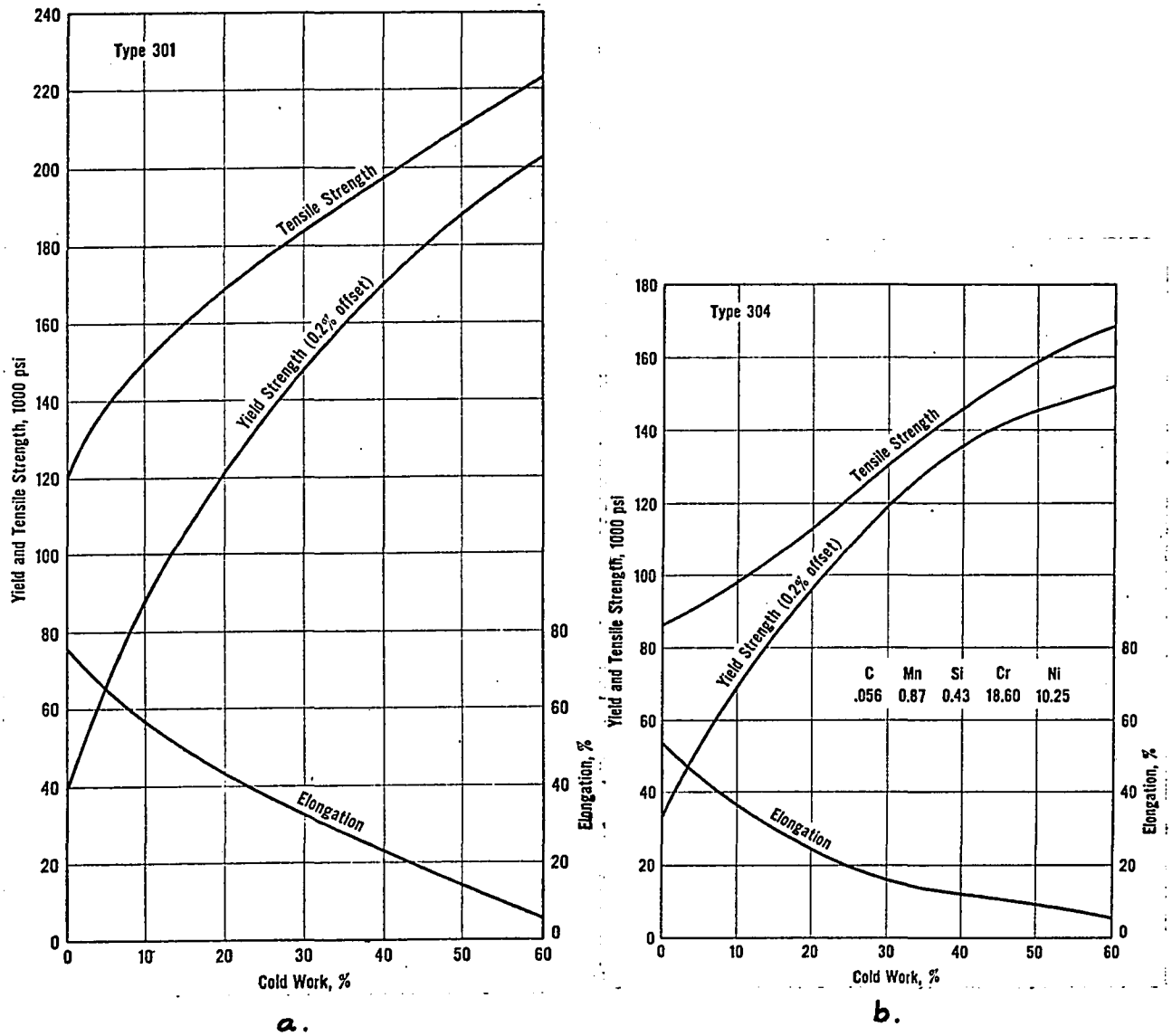

Fig. 27 (7)

Effect of cold working on the mechanical properties of type 301 and type 304 steel - Data from Allegheny Ludlum Steel Corp.

D. Theoretical Aspects on Plastic Deformation of Stainless Steel

Plastic deformation energises the martensite transformation in austenitic stainless steels where the Md temperature is above the deformation temperature (9,34,40). As the Ms temperature of a steel is raised by suitable alloying and approaches room temperature, the steel is termed meta-stable, i.e. room temperature strain will induce martensite formation. As the temperature of plastic deformation is reduced, towards the Ms, martensite formation is enhanced (39,40).

For example, a typical stainless steel of composition C 0.044%, Cr 18.8%, Ni 7.99% has a Ms temperature of $-30^{\circ}C$ (40), which is raised about $50^{\circ}C$ for each 1% decrease in nickel (40). As was seen earlier, when discussing phase diagrams, low nickel austenitic stainless steels are typically metastable. In some cases, the temperature of complete martensite formation, Mf, may never be attainable, eg. the above mentioned steel, quenched to $-263^{\circ}C$ (approaching absolute zero), in the absence of cold work, can never contain more than 15% by volume of martensite. Table III shows the effect of cold working temperature on the mechanical properties of austenitic stainless steel.

In stainless steel the martensite transformation products are either a hexagonal close packed (HCP) or a body centred phase (BCC or BCT). The HCP phase is referred to as Epsilon Martensite ε (38,41), and it is a special type of martensite where the austenite-martensite interface is fully coherent (20).

With decreasing temperature, the stacking fault energy decreases in 18/8 alloys, since it essentially depends on the free energy differences between the hexagonal and the face centred cubic phases.

A decrease of stacking fault energy would promote the formation of sheets of stacking faults, i.e. the partial dislocations are farther apart. The local faults produce a hexagonal structure, the same as the previously mentioned ε phase (41,42). Whether the hexagonal configuration acts as a nucleus for formation of BCT martensite or changes itself first to ε martensite has not been proven conclusively (42,43). Stable ε martensite appears to be transient, in any case (38,43,44). At 0°C, a AISI 301 grade of steel produces a maximum ε martensite at 10% strain, and even this is only about 10% of the martensite formed at that stage of cold work. At 50% reduction, the ε phase disappears (38). The same steel strained at 50°C shows no ε phase at all, at any amount of strain (38).

The nature of the applied stress also exerts considerable influence on the transformation of martensite, i.e. more martensite transformation is obtained by tensile than by compressive stress (45).

Less martensite transformation is observed at higher strain rates (46). This is generally attributed to the increased temperature induced during rapid deformation.

It is clear that more than steel chemistry determines the rate of martensite transformation. The transformation is influenced by temperature, stress system, amount of plastic strain, microstructure, and even specimen geometry (43).

E. Discontinuous Yielding

During the mechanical testing, under controlled conditions, some austenitic stainless steels show discontinuous yielding (43,46).

Bazinski (47) postulated that this instability was due to localized softening, caused by heat evalution in testing at a temperature where the specific heat of the metal is low and the flow stress is highly temperature dependent, i.e. deformation under these conditions produces localized heating, which can resoften a metal at the point of strain. He maintained that even structurally stable materials will exhibit discontinuous yielding at low temperatures.

An alternative theory was proposed by Watson & Christian (48). They contend that the discontinuous flow is due to an induced burst type martensite transformation as necking begins. This would re-strengthen the metal. In the more recent literature, the Bazinski theory is the one more generally favoured (43,46). The "Burst" phenomenon of Watson & Christian is believed to be a result of yield strain and note the cause of serrated flown (43).

The total elongation of a metastable austenitic steel is at a maximum if the following two conditions are satisfied (38).

1. A large amount of deformation is available in the austenite before the martensite transformation starts.
2. Once local contraction occurs, martensite is gradually induced and the increment in strength caused by this martensite is responsible for the increment in the applied stress at the necked portion and thus prevents early failure by necking.

When martensite is formed early during strain, it hinders elongation. The martensite has a BCT structure, which has a very much lower total elongation than the FCC austenite. When formed, this martensite contributes its low increment to the total elongation, resulting in premature necking. Beyond a minimum stability that eliminates the above condition , elongation improves with decreasing austenite stability (39), an exactly opposite effect.

F. Annealing of Austenitic Stainless Steel

The annealing of metastable austenitic stainless steel is considerably more complex than the recovery, recrystallization and grain growth phenomena encountered in the annealing of single phase materials. In stainless steels, other metallurgical changes occur: martensite tempering, carbide precipitation, and the reverse martensite to austenite phase reaction. During the heating of a typical fully cold worked austenitic stainless steel, the following sequence of events is observed (35,37,40):

Up to 200°C	- No measurable effects.
200°C-300°C	- Initial softening and stress relief occurs. Yield strength increases.
300°C-400°C	- Carbide precipitation begins at slip planes. These precipitations are spread more uniformly than during the heating of non-cold-worked material, as they do not only form at the grain boundaries.
400°C-700°C	- Carbide precipitation continues at twin and grain boundaries.
At 550°C	- The martensite phase starts to disappear. The carbide precipitation and phase change processes overlap.
600°C-650°C	- The phase change of martensite to austenite progresses at great speed.
700°C	- magnetic properties disappear at about this temperature (Curie point).
750°C	- The martensite to austenite phase change is complete
800°C	-At this stage the carbide precipitates are coarse and often form a continuous network around the grains
Above 800°C	- Prolonged heating in this range causes carbide coalescence. The carbides progressively re-dissolve as stable austenite temperatures are reached.

At 1000°C - Depending on the carbon content of stainless steel, most of the carbide precipitates should be in solution. The rate of dissolution is very rapid.

During annealing, the martensite transforms rapidly to the austenitic phase, any stable ferrite phase present, however, dissolves more slowly.

A partially cold worked austenitic stainless steel will first harden and increase in tensile strength, then soften during annealing, i.e. submicroscopic coherent precipitates form first, and then these precipitates lose their coherency with the matrix. In highly cold worked material, this initial hardening phenomenon is not observed (49). More carbide precipitation occurs when heavily cold worked, rather than annealed, stainless steel is annealed.

In the present work, an attempt was made to minimize carbide precipitation during the annealing of cold worked austenitic stainless steel, so as not to adversely affect corrosion. Prime consideration, however, was given to the study of the change of mechanical rather than corrosion resistive properties brought about by cold work and annealing.

Section IV

EXPERIMENTAL PROCEDURE

IV EXPERIMENTAL PROCEDURE

The preparation of temper rolled and temper annealed specimens is discussed in this section. Brief description of the testing methods employed for assessment of structural and mechanical properties are also included.

A. Material

The experimental samples used throughout the work originated from the same production heat of AISI 301 stainless steel. The material was received from Atlas Steels Company in the form of annealed strip with the following process history:

1. Teemed Continuous Casting - 6 5/8 in. X 24 in. section
2. Primary Rolling - to 2¼ in. X 19½ in. section at 2380°F.
3. Secondary Rolling - by Planetary Mill to 0.180 in. to 0.008 in. at 2220°F.
4. Annealing - Preheated to 1700°F and held at this temperature for 5 sec. Heated in main furnace at 2150°F for 1 minute and air cooled.

Thus, the as-received material consisted of strip, approximately 2 ft. wide and 0.180 in. thick. The chemical ladle analysis of this steel is given in Table IV.

TABLE IV

CHEMICAL LADLE ANALYSIS OF THE EXPERIMENTAL MATERIAL

C	Mn	P	S	Si	Cr	Mo
0.12	1.31	0.024	0.011	0.68	17.28	0.20

Co	Ni	Cu	Al	Sn	Pb	B
0.10	8.03	0.12	0.022	0.010	0.002	< 0.000001

B. Preparation of Temper Rolled Material

In the investigation of the effect of temper rolling on stainless steel, the mechanical properties were measured as a function of increasing cold work. In order to eliminate the experimental variable of sample thickness, all tests were performed on material close to 0.036 in. gauge. This gauge was selected, as it represented the maximum reduction obtainable with the laboratory rolling mill, from the as received gauge of 0.180 in. The maximum cold work possible was thus, an 80% reduction in thickness.

The as-received material was cut into 3 in. X 8 in. strips and annealed as shown in Table V. This preanneal was considered necessary for the following reasons.

1. The material had previously received only an industrial anneal and it was uncertain if the metal was completely austenitic.
2. The as-received material still contained a considerable number of undissolved carbides. Maximum carbide solution was desired.
3. Bands of nickel rich zones (determined by electron microprobe) were observed,running parallel to the rolling direction. This structure was probably due to nickel segregation produced during solidification of the concast slab. The added anneal promoted more homogenization of solute atoms, causing the nickel rich bands to virtually disappear.
4. The preanneal ensured a uniform grain size prior to cold reduction.

All cold reduction was performed on a STANAT 2-high laboratory rolling mill, using 4 in. diameter rolls. The reduction per pass was very small (less than 0.5%). This was necessitated by the limited capacity of the rolling mill and the fact that specimen heating had to be avoided. After every pass, the material was cooled in a room temperature water bath.

No lubricant was used on the rolls, other than the water adhering to the surface of the specimens after cooling.

Some slipping of the material occurred in the rolls during cold reduction and, at a certain stage during the reduction, the strips become slightly bowed. This problem was, however, overcome by continuing the rolling with very small reductions per pass.

In order to obtain maximum cold reduction at the final stages of rolling, when the material become extremely hard, a 4 high rolling arrangement with 0.75 in. diameter working rolls was tried. Due to the lack of rolling tension, however, the samples became hopelessly rippled and this 4-high rolling technique had to be discarded. The maximum reduction that could be obtained with the 4 in. diameter rolls was only 80%.

The rolling schedules to produce the different intermediate thicknesses are given in Table V.

Prior to the final cold work, all the samples (except those reduced 80%) had to be annealed. The annealing was performed in a Lindberg Hevi Duty Muffle Furnace. After holding at 1100°C for varying times, as discussed below, the samples were quenched in water, which was always maintained at room temperature. As no protective atmosphere was used, the annealed test strips had to be "pickled" prior to further processing.

The cleaning or pickling was performed using Aqua Regia (75% HCl, 25% HNO_3). The solution was maintained at 70°C. Stubborn oxide flakes were removed using 600 grit silicon carbide paper. The surface of some of the samples being cleaned became seriously pitted when over-pickled. These samples had to be discarded.

The annealing temperature of 1100°C and the annealing times at this temperature were chosen in order to achieve the same hardness and microstructure in the annealed specimen as existed before cold reduction.

Some difficulty was encountered in obtaining a suitable annealing temperature. At 1000°C, the temperature of the preanneal, the carbides precipitated during the annealing process did not dissolve sufficiently before full recrystallization was achieved. When the annealing temperature was raised to 1100°C, however, most of the carbides redissolved before the desired recrystallized condition was reached. The highly reduced samples recovered their original hardness more quickly, as would be expected from the theory of recrystallization (8,9) , and from the fact that they were thinner and could be heated more readily. Two annealing times were found to be sufficient to satisfactory anneal the full range of cold reduced specimens; three minutes for reductions of 30% to 80%, and five minutes for reductions for 2% to 30%. The hardness readings obtained after annealing are recorded in Table V. The differences in hardness of the annealed material could be clearly correlated with grain size, (the softer material possessed a larger grain size).

After annealing at 1100°C,the specimens were cold reduced to the finished thicknessess shown in Table V, i.e. reductions ranging from 79.5% to 2.8%. The resulting mechanical properties will be discussed in Section V .

TABLE V

Annealing Schedules for Preparation of

Temper Rolled Material

Orig. Hard. Rb	Pre-Anneal Time at 1000°C min.	Start. Hard. Rb	Start. Gauge in.	Inter. Gauge in.	Int.-Anneal Time at 1100°C min.	Inter. Hard. Rb	Cold Redn. %	Final Gauge in.	Final Hard. Rc
88	30	80	0.178	0.0381	5	80	2.8	0.0370	9.0
88	30	80	0.177	0.0350	5	80	11.4	0.0310	24.0
88	30	80	0.178	0.0390	5	81	15.4	0.0330	-
88	30	80	0.178	0.0440	5	79	19.0	0.0360	-
88	30	80	0.177	0.0350	5	79	20.0	0.0280	28.0
88	30	80	0.178	0.0485	5	80	26.0	0.0360	-
88	30	80	0.178	0.0530	3	79	32.0	0.0360	-
88	30	80	0.177	0.0530	3	81	36.0	0.0340	36.6
88	30	80	0.177	0.0710	3	78	52.1	0.0340	40.0
88	30	80	0.177	0.0840	3	79	63.1	0.0310	41.0
88	30	80	0.177	0.1070	3	78	68.2	0.0340	42.6
88	30	80	0.177	0.1170	3	77	73.5	0.0310	43.6
88	30	80	0.177	0.1710	3	78	79.5	0.0350	46.3

C. Preparation of Temper Annealed Material

The material to be used for partial annealing was cut into 3 in. X 8 in. strips and preannealed at 1000°C for 30 mins. in the Lindberg furnace, without using any protective atmosphere. This was exactly the same pre-anneal as was given to the temper rolled material. The annealed strips were then pickled and cold reduced 80%.

Three temperature ranges were considered for temper annealing:

350°C-500°C	: Method for low temperature annealing
500°C-850°C	: Sensitization region
850°C-1050°C	: Method for high temperature annealing

At temperatures below 350°C, any heat treatment would have brought about a type of martensite tempering, which might have been expected to increase tensile strength and reduce ductility (7). Some softening would occur, but only if the material became overaged.

At temperatures above 1050°C, on the other hand, the rate of recovery and recrystallization was expected to be too rapid for practical experimental control.

1) 350°C-500°C Range

Preliminary low temperature annealing trials in this range were conducted using two methods.

(i) Lindberg Hevi-Duty Furnace: No protective atmosphere was used. The annealing temperatures used, as well as test results, are indicated in Fig. 28.

(ii) Low Temperature Salt Bath: The salt bath used was 12" in diameter and was heated by an electric coil within the bath. The salt used, Houghton Draw Temp 275, was a mixture of 55% Potassium Nitrate and 45% Sodium Nitrite. The bath was stirred continuously in order to maintain an even temperature. A Bristol

proportional controller maintained the bath temperature to ±1°C of the value desired. The results are illustrated in Fig. 29.

As can be seen from Fig. 28 and Fig. 29, neither annealing technique, even after annealing for over 48 hours, produced any significant softening of the material. The hardness reading of the annealed state was not even approached. Optical microscope examination revealed gross carbide precipitation. Any softening observed was believed to be only due to overaging of the martensite present, i.e. precipitated ferrous carbides lost their lattice coherency, as was explained in Section III - no recrystallization process was involved.

Temper annealing in this temperature range was therefore abandoned.

2) 500°C-825°C Range

As was discussed in previous sections on sensitization, heating of austenitic stainless steel in this region produces precipitation of chromium rich carbides. The areas surrounding these precipitates are denuded of chromium and thus lose their corrosion resistance. No annealing trials were attempted in this temperature range.

3) 825°C-1050°C Range

Two annealing techniques were tried in this temperature range.

(i) Lindberg Hevi-Duty Furnace:

The air chamber in this furnace was large and had severe temperature gradients. In order to obtain a zone of uniform temperature, a graphite tube (1½ in. ID) was located centrally in the furnace, with an opening that coincided with the existing opening in the furnace door. Because the graphite tube had good thermal conductivity, a 9 in. length of uniform temperature (±1°C) was obtained.

At high temperatures, the graphite tube became oxidized fairly quickly and because of this, provided a partially reducing CO_2 atmosphere. A specimen could be held in the furnace at 1000°C for periods of over one hour, without scaling. Only minor pickling was required. This air annealing process, however, proved to give heating rates which were too slow, i.e. the heating up period was as long as the time held at temperature, (a full 20 seconds was required to heat the sample to temperature). Using this method, therefore, the recrystallization was virtually completed during the heating up period. Further, gross carbide precipitation was observed in the specimen as a result of the slow heating through the sensitization range. For these reasons, this method of annealing had to be abandoned.

(ii) High Temperature Salt Bath:

A laboratory Leeds and Northrup Hump furnace was fitted with a 5½ in. Dia. X 14 in. Muffle. The maximum recommended operating temperature for this muffle was 1010°C. An Inconel pot, 3 in. Dia. X 12 in. deep, was fabricated as illustrated (Fig .30), and suspended in the muffle by its ledges. A single piece of insulating brick, (14 in. Dia. X 4 in.) was used to cover the whole top of the furnace. A 1 in. diameter opening was made in the center of the covering brick in order to allow access to the bath. Even this small hole allowed excessive temperature loss (10°C in 2 minutes) and thus was always kept covered except when actually inserting or withdrawing a specimen. The salt used was a 15% NaCI-85% $BaCl_2$ mixture, prepared from pure anhydrous compounds. This salt mixture, which melted at approximately 760°C, provided an effective molten operating range of 815°C to 1090°C. When the bath was operated over 950°C, some salt fuming took place, but not enough to hinder any experimental work. A Leeds and Northrup 10876 D.A.T. control system, supplied with a Speedomax H Recorder, maintained the muffle temperature within 1°C of the desired temperature. A Chromel-Alumel thermocouple, the junction located 2/3 up the muffle wall, was used to activate the controller. The salt temperature was measured accurately, using an external thermocouple that had been accurately calibrated against the melting points of several pure

At high temperatures, the graphite tube became oxidized fairly quickly and because of this, provided a partially reducing CO_2 atmosphere. A specimen could be held in the furnace at 1000°C for periods of over one hour, without scaling. Only minor pickling was required. This air annealing process, however, proved to give heating rates which were too slow, i.e. the heating up period was as long as the time held at temperature, (a full 20 seconds was required to heat the sample to temperature). Using this method, therefore, the recrystallization was virtually completed during the heating up period. Further, gross carbide precipitation was observed in the specimen as a result of the slow heating through the sensitization range. For these reasons, this method of annealing had to be abandoned.

(ii) High Temperature Salt Bath:

A laboratory Leeds and Northrup Hump furnace was fitted with a 5½ in. Dia. X 14 in. Muffle. The maximum recommended operating temperature for this muffle was 1010°C. An Inconel pot, 3 in. Dia. X 12 in. deep, was fabricated as illustrated (Fig .30), and suspended in the muffle by its ledges. A single piece of insulating brick, (14 in. Dia. X 4 in.) was used to cover the whole top of the furnace. A 1 in. diameter opening was made in the center of the covering brick in order to allow access to the bath. Even this small hole allowed excessive temperature loss (10°C in 2 minutes) and thus was always kept covered except when actually inserting or withdrawing a specimen. The salt used was a 15% NaCI-85% $BaCl_2$ mixture, prepared from pure anhydrous compounds. This salt mixture, which melted at approximately 760°C, provided an effective molten operating range of 815°C to 1090°C. When the bath was operated over 950°C, some salt fuming took place, but not enough to hinder any experimental work. A Leeds and Northrup 10876 D.A.T. control system, supplied with a Speedomax H Recorder, maintained the muffle temperature within 1°C of the desired temperature. A Chromel-Alumel thermocouple, the junction located 2/3 up the muffle wall, was used to activate the controller. The salt temperature was measured accurately, using an external thermocouple that had been accurately calibrated against the melting points of several pure

metals (Sn, Zn, Al). A calibration curve relating the true bath temperature and control recorder temperature was obtained. The difference between these two temperatures was always less than $5^{o}C$.

The salt bath was 11 in. deep and, with constant stirring, the temperature profile, as indicated in Fig.31, was maintained, i.e. an 8 in. depth of uniform ($\pm 1^{o}C$) temperature is indicated. If the bath was not agitated, however, the temperature profile was as shown in Fig.32 , i.e. only a 5 in. length of constant temperature could be achieved. This was considered to be unsatisfactory. As the salt bath was maintained at the desired temperature, it was constantly agitated by a stainless steel mechanical stirrer. Just before a specimen was to be annealed, the stirrer was removed. Only one specimen was heat treated in the salt bath at one time. After the desired holding time, the sample was quickly withdrawn and quenched in water, which was maintained at room temperature. A maximum of 5 specimens could be annealed in succession, before the temperature gradient in the bath changed. When this change occurred, the stirrer was replaced and heating continued until the temperature of the bath again became stabilized. The results of these preliminary trials are indicated in Fig.33. From these results, an annealing temperature of $850^{o}C$ was chosen as suitable for the temper annealing experiments. Any higher temperatures produced almost complete recrystallization within 20 seconds. At temperatures lower than $850^{o}C$, complete carbide dissolution was not obtainable. Even at this low temperature, the specimens were completely recrystallizated in 60 seconds. It took the immersed specimen 7 sec. to reach the temperature of the salt bath. As will be seen later, it was necessary to use some annealing times that were very short indeed, eg. 1-7 sec. In these cases, it is probable that the standard annealing temperature of $850^{o}C$ was never reached, and the maximum temperatures reached in these cases were within the severe sensitization range. It was hoped that the short residence time in this dangerous range would not allow sufficient chromium depletion, so as to adversely affect corrosion resistance. Consequences of this heat treatment will be pointed out

in the analysis of the results.

It should be also mentioned, that in order to approach the grain size required for the softer, completely annealed material, a temperature of 900°C was used for some of the work. These results complemented the results previously obtained by annealing at 850°C.

The final mechanical properties obtained for temper annealed material will be discussed in Section V.

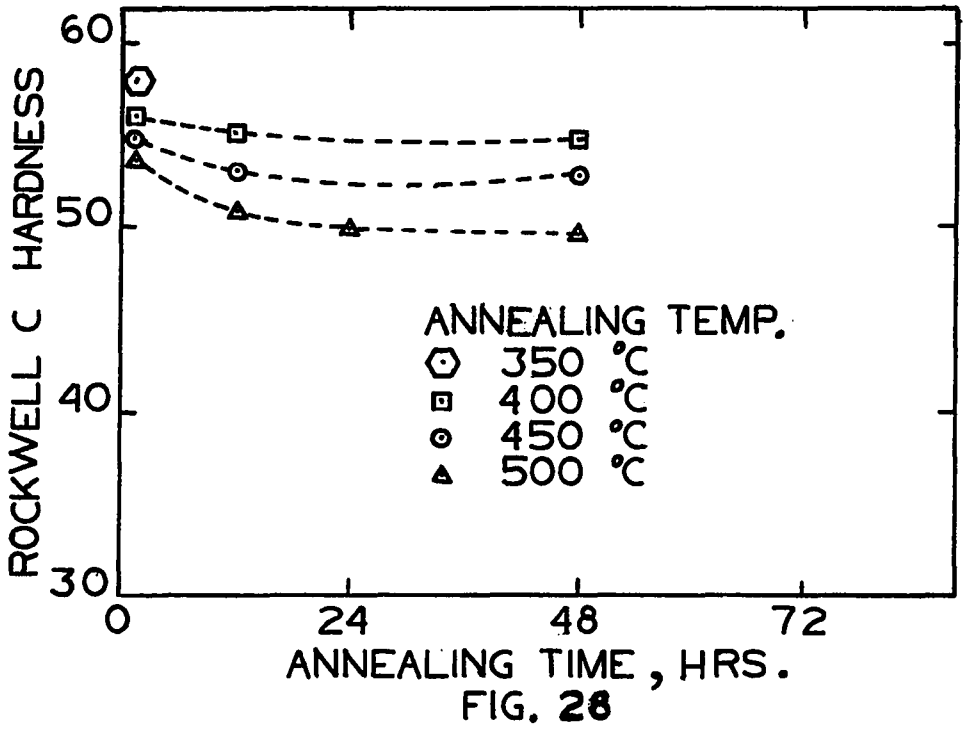

FIG. 28

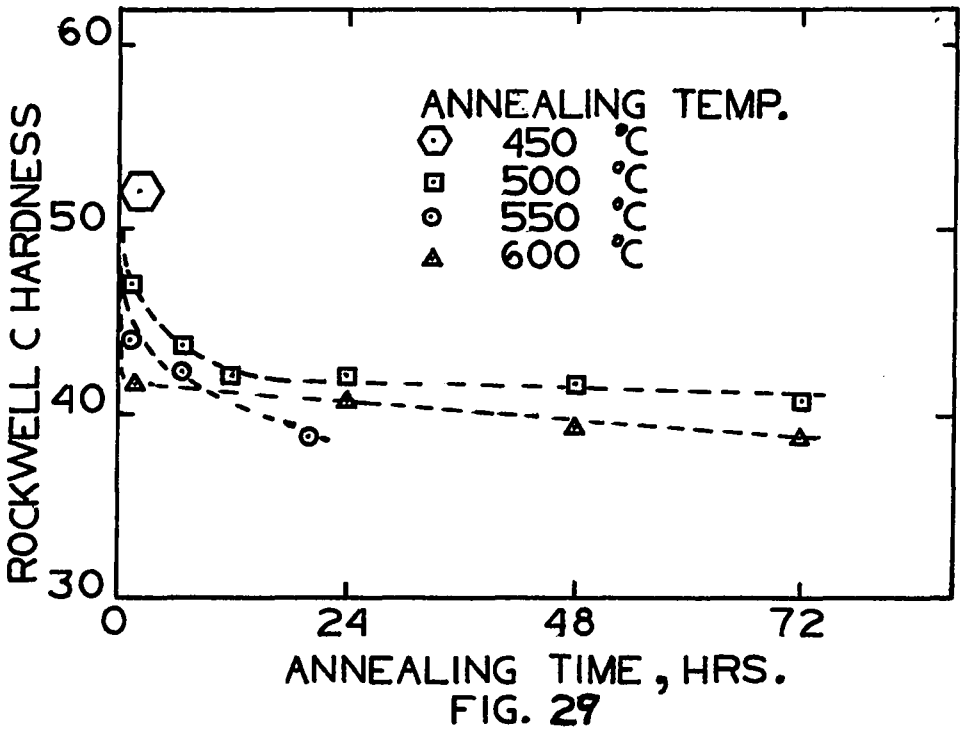

FIG. 29

Hardness versus annealing time of low temperature exploratory tests

Fig. 28 - Annealed in Air Furnace
Fig. 29 - Annealed in Salt Bath

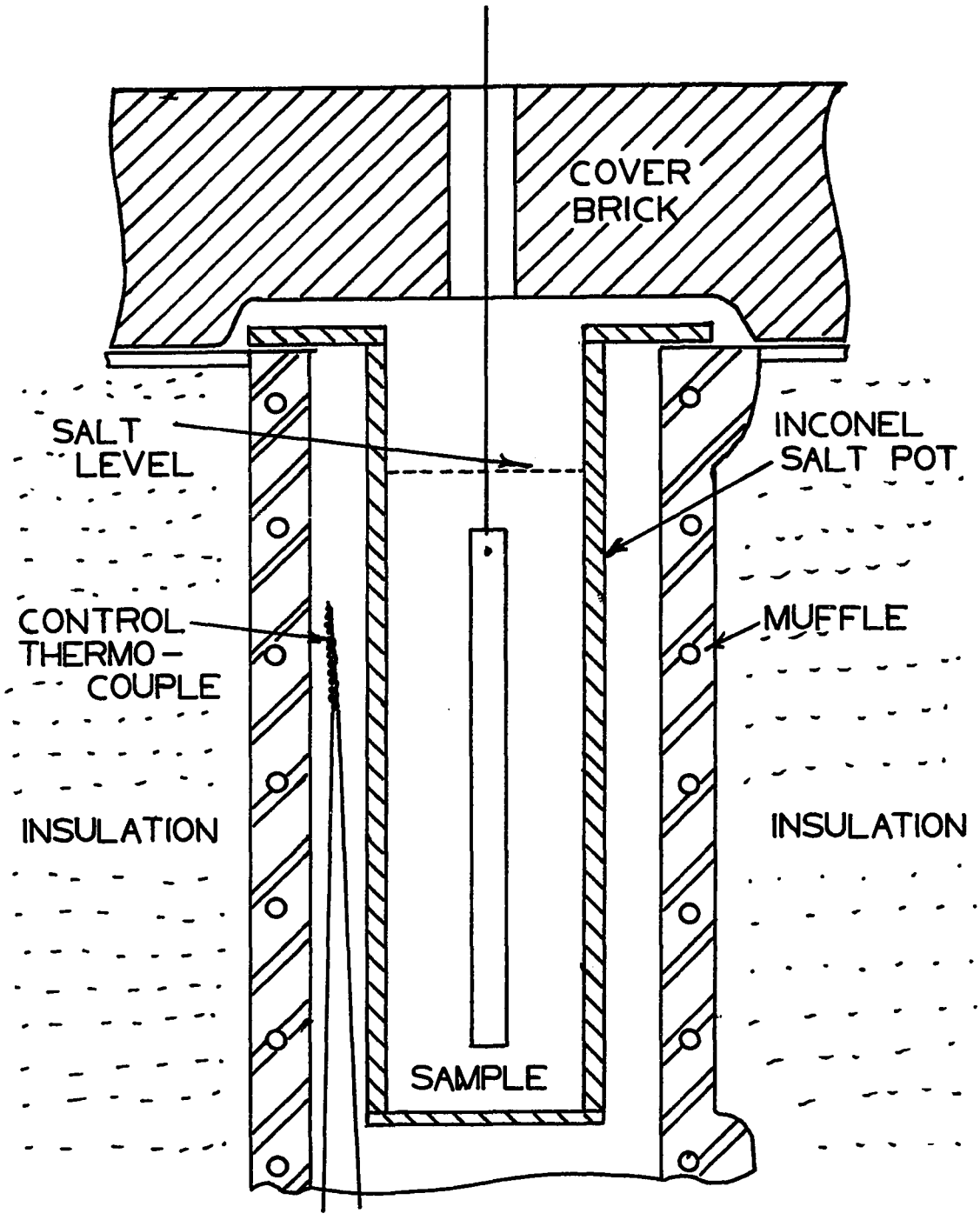

Fig. 30. High temperature Salt Bath Testing Apparatus

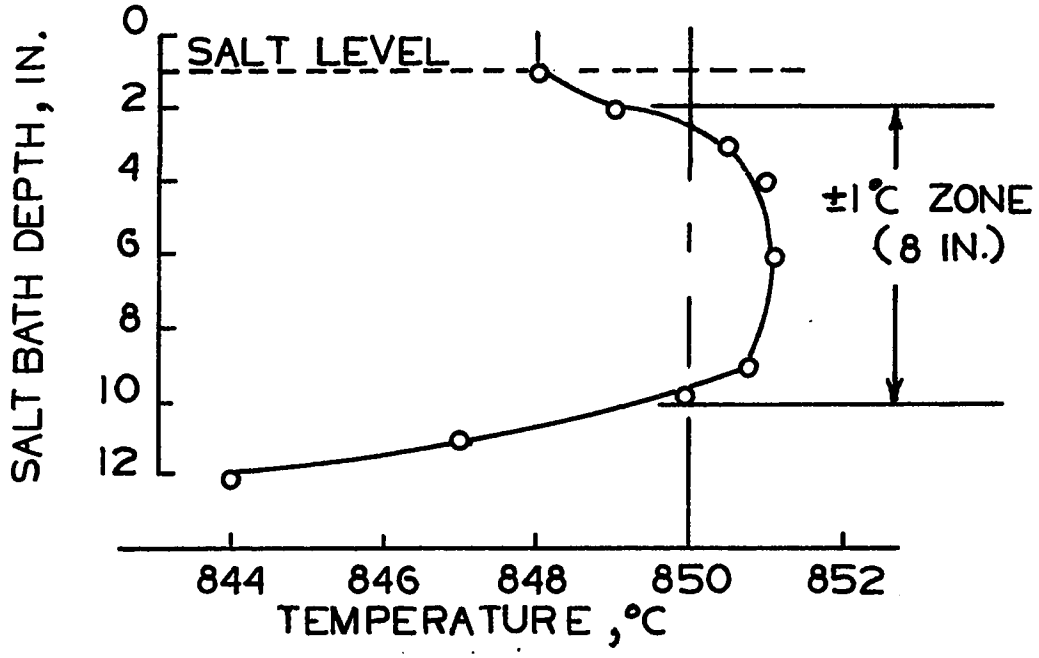

Fig. 31. Temperature profile in the high temp. salt bath, using constant stirring

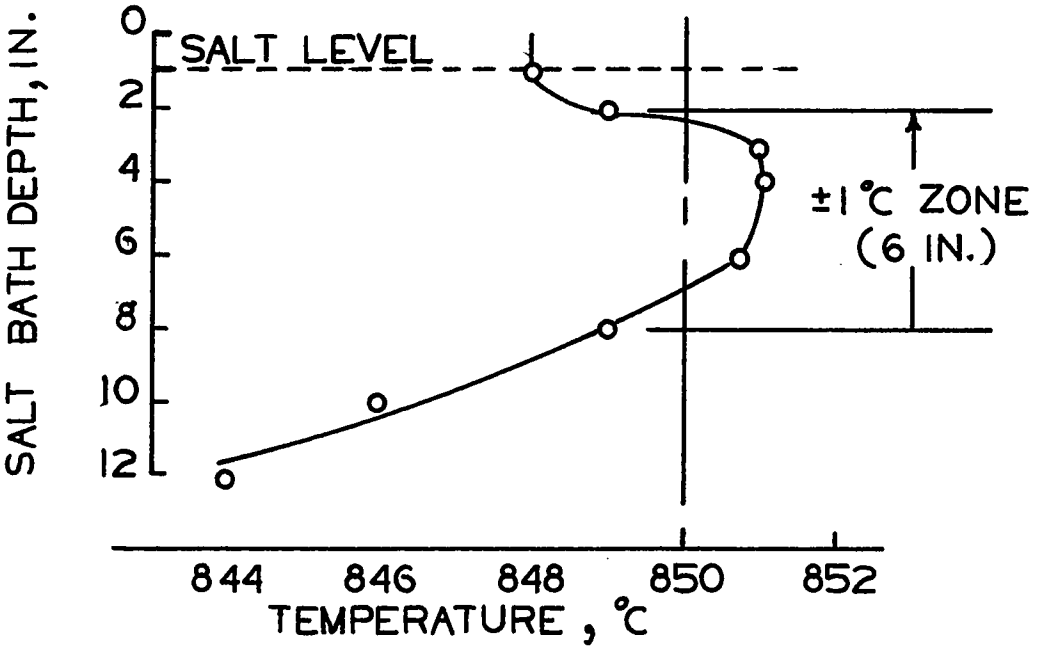

Fig. 32. Temperature profile in the high temp. salt bath, without stirring

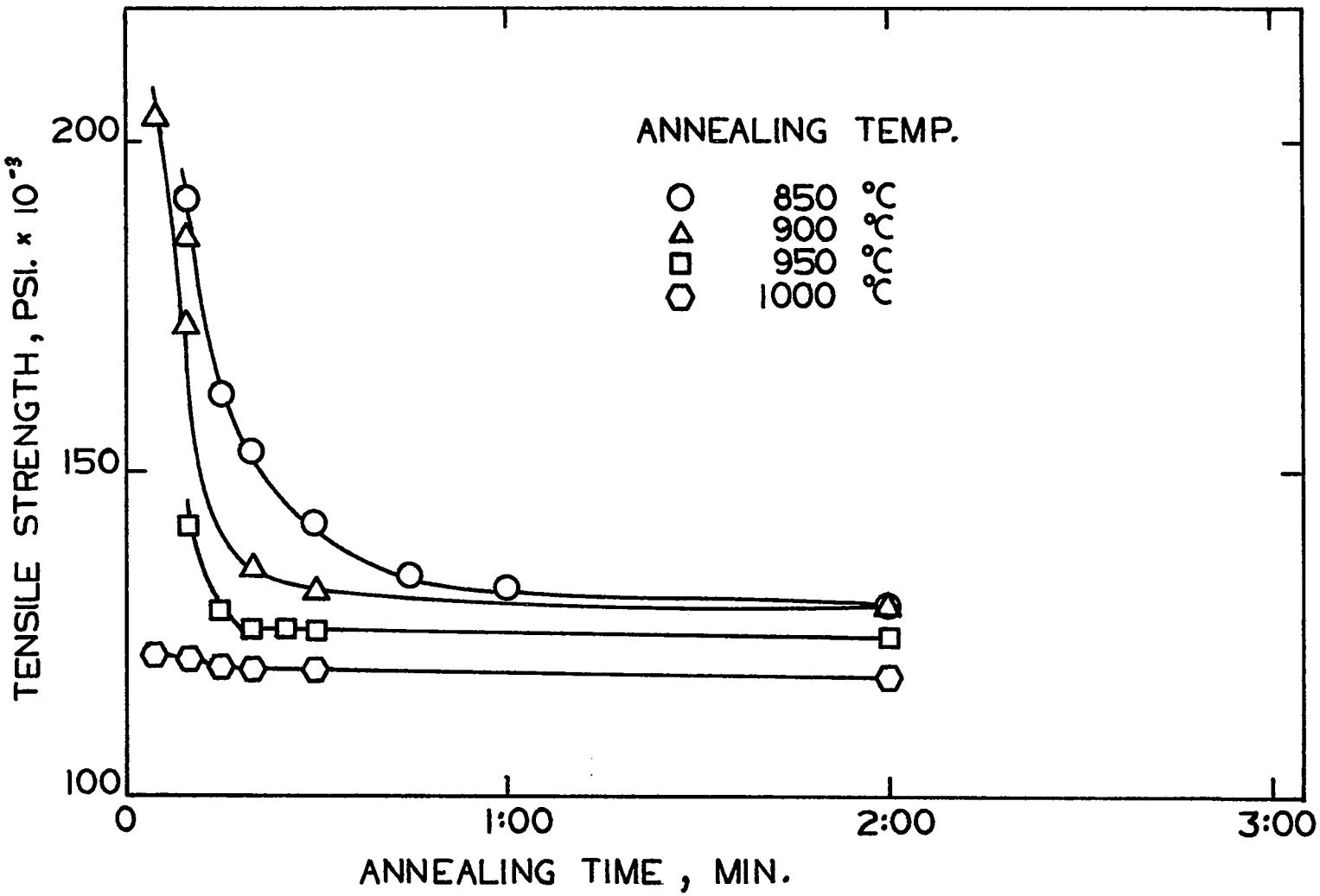

Fig. 33. Tensile strength versus annealing time of high temperature exploratory tests of AISI 301 steel - Annealed in Salt Bath

D. EXPERIMENTAL TECHNIQUES

1) Preparation of Tensile Specimens

The tensile specimens were prepared from strips 3/4" wide, cut in the rolling direction of appropriately treated material. All test material was cut on a Doall Band Saw, using friction cutting. The heat affected zone produced by sawing was subsequently removed by milling, as the specimens were further shaped on a "Tensilkut" shaping mill to a modified ASTM E-8 specification (50). The overall length of the specimen was 8 in., i.e. one inch shorter than standard. Due to the extreme hardness of most of the samples, only one sample was milled at a time. As the milling bits became worn, the increased cutting friction produced heating in the sample, and to avoid any tempering or heat effect on the material being tested, the whole template and sample assembly was frequently cooled in a room temperature water bath. The " Tensilkut" template is designed with a blended taper of 0.003 in., to insure a minimum cross section at the center of the specimen so that fracture would occur within the gauge length (Fig. 34).

Width and thickness measurements on the specimens were made with an " ETALON" micrometer. This is a very precise instrument, and has a jeweled dial gauge that can be measured accurately to ± 0.00002 in. (3). Each width and thickness measurement recorded was an average of five readings, taken near the center of the gauge length and across the width of the specimen.

Four specimens were prepared for each experimental condition.

2) Tensile Testing

The tensile tests were performed on an Instron TT-D Universal Testing Machine at room temperature.

Wedge action grips were used. The loads were measured with a GR Instron Load Cell and the extension was measured using an Instron strain gauge extensometer, with a 1 in. gauge length and a 1 in. maximum extension. The maximum extension obtainable with Instron strain gauges was 1 in. and ,as some of the test samples were expected to have total elongations of over 50%, the more common 2 in. gauge length used by previous workers in this field (1,2,3) could not be used.

The Instron cross-head movement was supplied with an accurate control dial which could be adjusted to read 0.002 in. This dial was used to calibrate the extensometer. Thus an extensometer error of 0.2% could be expected, i.e. ($1.0 \pm 0.2\%$) or ($10.0 \pm 0.2\%$). This error is well within experimental accuracy of normal tensile testing. The Instron X-Y Chart drive system was used to measure elongation. Thus, a gauge extension of 1 in. represented 100% elongation on the recorder chart. The sensitivity of the recorder was varied to obtain 6 in. to 10 in. of chart movement for a complete specimen extension to fracture.

The yield strength was measured by the 0.2% offset method as shown in Fig.35. Only the engineering Tensile and Yield Strengths were derived from the curves, i.e. the appropriate loads were simply divided by the original cross-section area of the sample. Each recorded value in the results represents the average of readings from four samples, except for the instances when fracture of some samples occurred outside the gauge length.

The rate of crosshead travel was maintained at 0.2 in.per minute for all tensile testing.

Three distinct types of chart curve were obtained during tensile testing.

a) A smooth flat topped stress-strain curve was typical for annealed austenitic stainless steel (Fig.36).

A 0.2% offset yield strength had to be used as no precise yield point was measurable.

b) At intermediate strengths, a discontinuous yielding phenomenon was observed. This is illustrated in Fig. 37. A fairly sharp upper yield point was observed, followed by a plateau of lower uniform yield strength. The specimen sometimes fractured at this lower yield strength and sometimes more " work hardening" was produced prior to fracture. The resulting curves were similar to the curves normally obtained with annealed mild steel, except that the " work hardening" stage was always very short (2% maximum). The reasons for this phenomenon were discussed in section III-E.

c) With very highly cold worked specimens, virtually no yielding was observed (Fig. 38). The specimens fractured within 1% of yielding, without any observable necking.

In all cases, the total strain was defined as the horizontal distance from the line of proportionality to the point of fracture. The uniform strain was defined as the horizontal distance from the line of proportionality to the first drop from maximum load. For very ductile material, in order to obtain an accurate value for yield stress as well as a convenient chart size, it was necessary to decrease the elongation sensitivity once the yield stress was passed. In Fig. 39 is outlined the procedure used to interpret the change of scale (3).

Previous work with similar procedures, and using the same testing equipment, confirmed the accuracy of this indirect method of obtaining elongations (3). This procedure gives more accurate results than can be obtained by direct measurement of the sample.

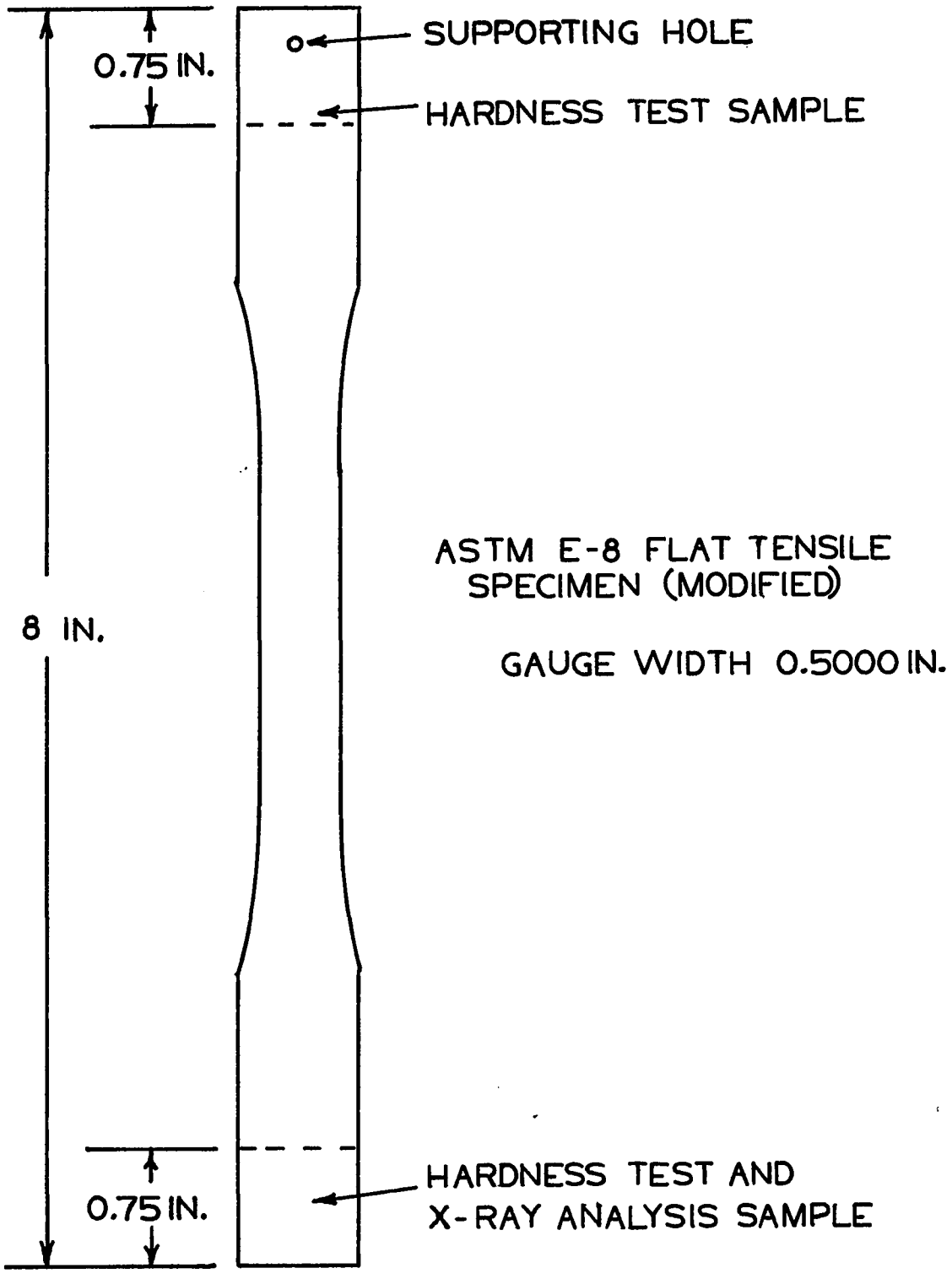

Fig. 34. Tensile Specimen

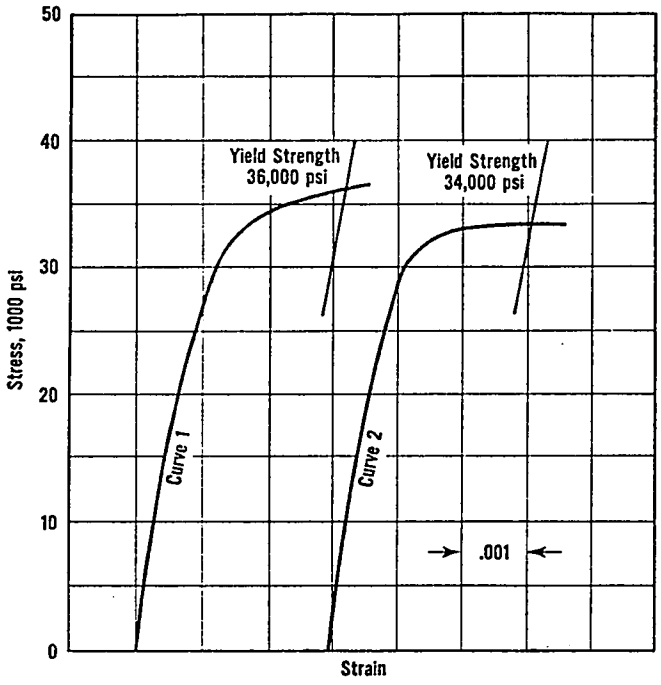

Fig. 35 (7)

Typical stress-strain curves in tension for annealed stainless steel of the 300 series.
Curve 1- parallel to rolling direction
Curve 2- perpendicular to rolling direction.

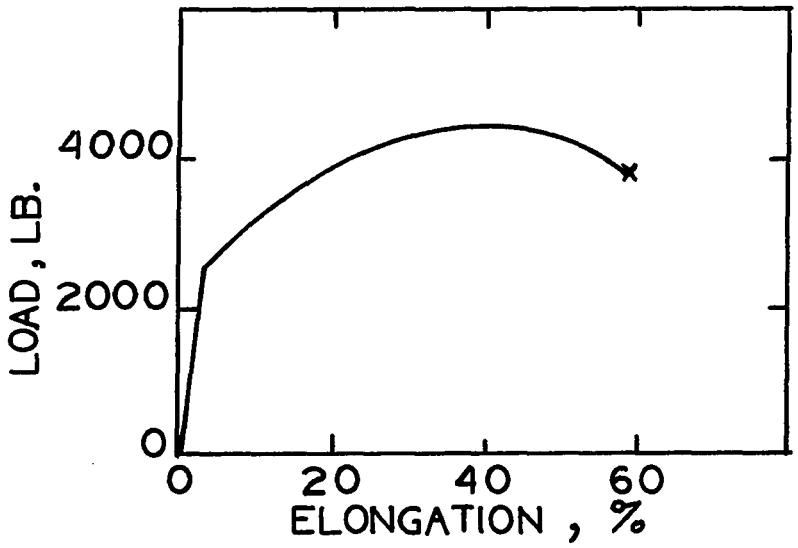

Fig. 36. Typical load-elongation curve for annealed 18/8 stainless steel

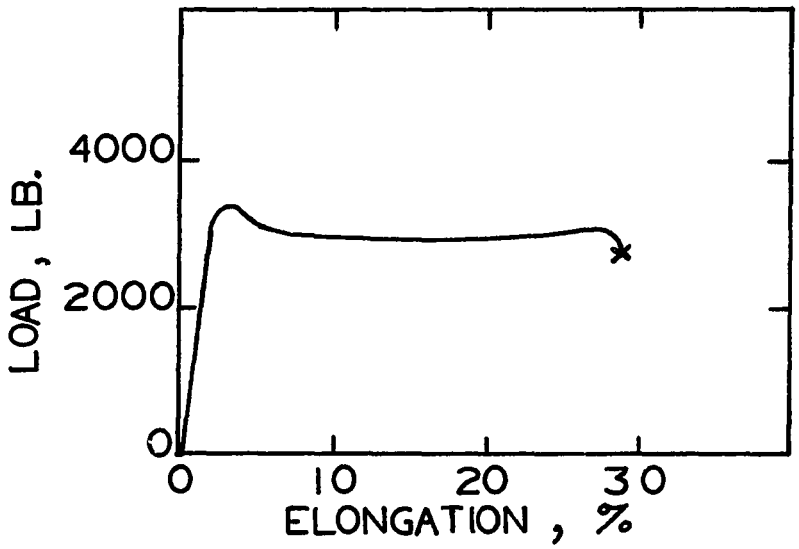

Fig. 37. Typical load-elongation curve showing discontinuous yielding in 18/8 stainless steel

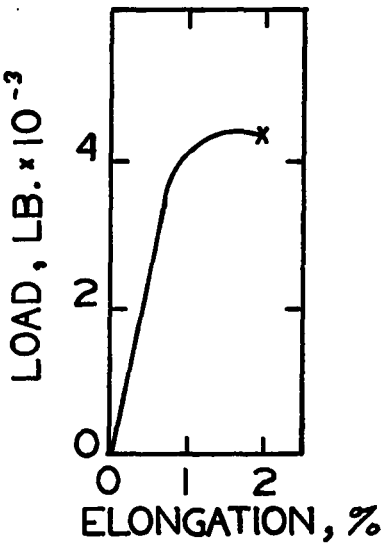

Fig. 38. Typical curve for highly cold worked 18/8 stainless steel

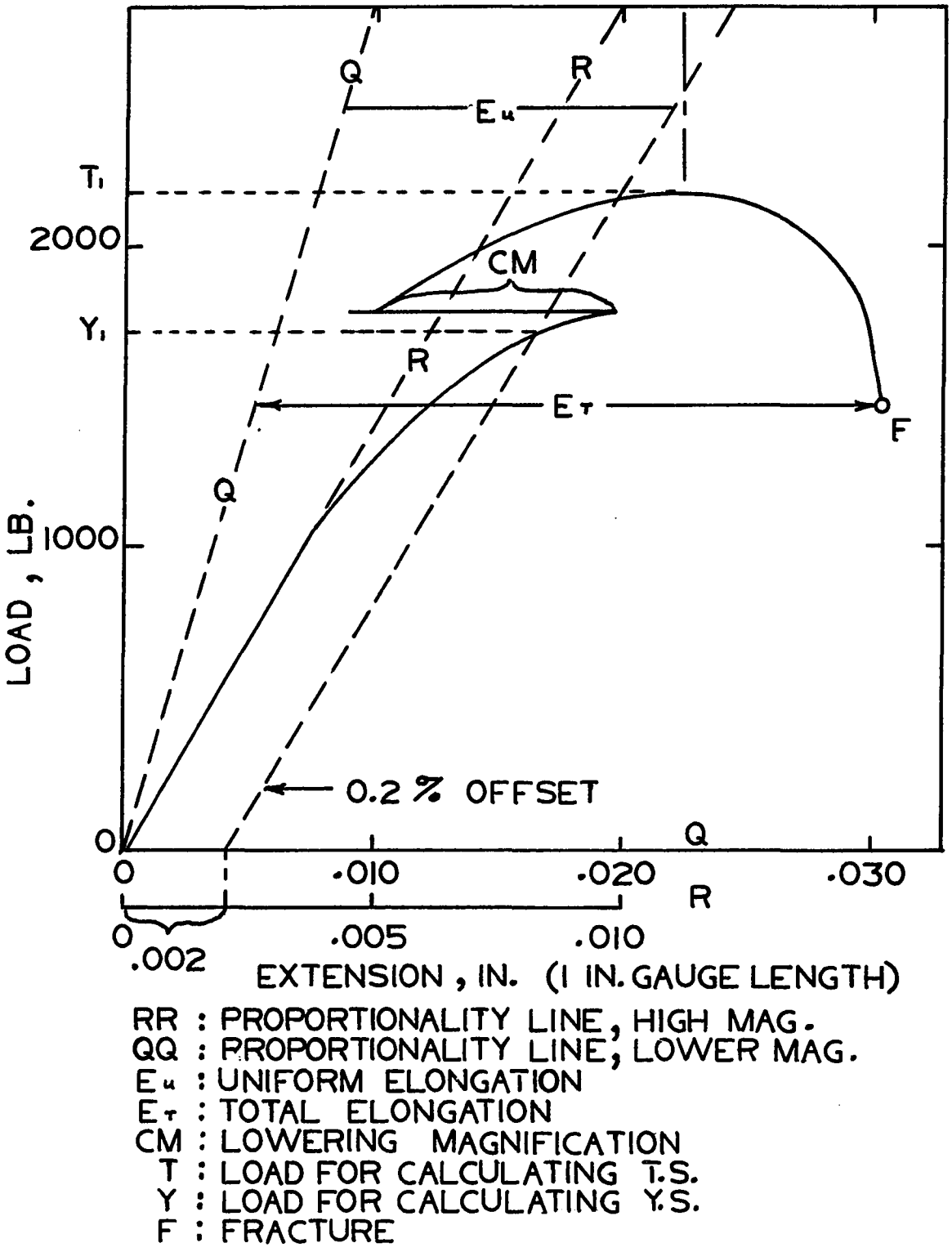

Fig. 39. Interpretation of the Load-Extension curve

3) Erichsen Testing

The Erichsen Test is a common industrial test for ductility. It is defined as a cupping test in which the depth of impression at fracture, made by forcing a cone shaped, spherical end plunger into the sheet specimen, is measured in inches or millimeters(1). It is generally agreed that this test can give widely varying results, varying from operator to operator or from machine to machine. Variation in clamping pressure, lubrication, and die smoothness can also affect the readings. However, because of the industrial importance of this test, some representative samples were tested.

The testing machine was a Louis Small model ductility tester, supplied with automatic hydraulic clamping equipment, which maintained the clamping pressure at a fixed ratio to the punch pressure. The same dies were used for all testing. The lubricant used was polythene sheet, 0.0002 in. thick, ensuring similar and effective lubrication. The end point was determined by slowly applying the load and carefully watching the punch pressure dial and the cup depth indicator to the point of specimen fracture. At the point of fracture, the pressure gauge needle dropped suddenly. The depth of cup reached when the pressure needle dropped was taken as the Erichsen value. The same operator performed all the tests, using the same experimental technique. Three samples were tested at each experimental condition.

4) Hardness Testing

Small test pieces were cut from the tensile specimens as shown in Fig. 34. Hardness was measured using an ordinary Rockwell Machine. Rockwell B and C scales were used, as the superficial testings scales, 30T, produced a very wide scatter of readings (the equivalent of 5 RB). On soft and thin material the depth of penetration of the test head was almost half as deep as the specimen thickness, thus giving an inaccurate reading.

When these samples were mounted on edge in Bakelite, more valid results could be obtained by performing the hardness tests on these mounted samples.

Five hardness readings were obtained for each specimen. The hardness recorded for an experimental value was an overall average of the hardness results obtained from all four tensile specimens.

5) Metallography

Representative samples were obtained from the experimental specimens for metallographic examination. The samples were studied for sensitization effects as well as for the correlation of mechanical properties with microstructure. Longitudinal sections of the same samples used for hardness testing were mounted in Bakelite. A hole was drilled into the back of the Bakelite mounting in order to make electrical contact with the metal for electrolytic etching purposes. The samples were wet ground on a 80 grit belt, followed by hard grinding, successively on 220,320,400, and 600 grit silicon carbide papers. The specimens were then polished with a 5 micron alumina slurry, on a nylon covered wheel. The final polish was performed on a low speed wheel, covered with "microcloth", using a 0.3 micron alumina slurry.

The etching was performed electrolytically according to ASTM specification A-262 (outlined in Table VI(51)).

The hole drilled into the rear of the bakelite mounting was filled with mercury to ensure good electrical contact. As the electrical current was applied to the system, a gas film started to form on the anode. This was noted by a drop of current. The sample had to be tilted periodically to destroy this gas envelope. When the required etching time was completed, the sample was removed from the electrolyte and quickly rinsed

with water, followed by an acetone rinse and rapid drying under a hot air blast.

The final polish and etching was repeated three times to ensure that surface effects were minimized.

TABLE VI

Electrolytic Etching Technique
(Modified ASTM Specification A-262)

Power:	15 V and 20 amp. D.C.
Cathode:	Piece of Stainless Steel
Anode:	Sample to be etched
Electrolyte:	10% Oxalic Acid by weight aqueous Solution-($H_2C_2O_4$) 2 H_2O
Sample Area:	At least 1 sq. cm. Up to 1 sq. in.
Current Density :	1 amp. per sq. cm.
Time of Exposure :	20 sec. to 1.5 min., depending on relief desired.
Temperature:	Electrolyte to be kept below $50^{o}C$

6) X-Ray Analysis

As was pointed out earlier in Section III-C, one of the results of cold working austenitic stainless steel is the transformation of some of the austenite to martensite. The extent of this transformation plays a significant role in the mechanical properties of the plastically deformed material.

Metallographic methods of determining the martensite content are unreliable for metastable austenitic stainless steel. The martensite formed by cold work has the appearance of slip bands in the predominantly austenite structure (23 p.25). With increased deformation, these bands become distorted and, at about 50% reduction, the microscopic structure becomes indistinguishable and the estimation of martensite content is impossible.

Magnetic and dilatometric methods have been used to estimate the austenite/martensite phase analysis. These methods, however, become inaccurate when one phase is less than 10%, the steel is highly alloyed, or the steel contains an appreciable amount of carbides (52).

With the advent of accurate diffractometer apparatus, X-Ray diffraction techniques have become the most popular tests for this type of analysis. As little as 0.3% of a component can be analysed (52). In the present work, the direct comparison X-Ray diffraction technique, as described in Cullity (53 p.391-396), was found to be suitable for phase analysis.

The following assumptions were made by Durnin & Ridal (52) concerning this experimental procedure, and were incorporated in the present work.

1. The absorption factors for austenite and martensite differ only by 4% and are thus considered equal for calculation purposes.

2. Extinction is negligible for the peaks used for analysis.

3. The Debye-Weller Temperature Factor for ferrite is also suitable for stainless steel.

4. A correction is required for the atomic scattering factor, as the Fe Kα radiation used is very close to the absorption edge of iron (stainless steel).

5. The carbide precipitates formed in this stainless steel are almost exclusively $Cr_{23} C_6$ (34,35). These carbides, if present in sufficient amounts, could affect the peaks as follows:

(200) γ	strong overlap
(200) α	weak overlap
(220) γ	medium overlap
(211) α	medium overlap
(311) γ	strong overlap

Since carbides would only account for a very small volume percent, well within the accuracy of the X-Ray readings, they were neglected in phase analysis calculation.

6. Austenite peaks show more preferred orientation, as texture is introduced during hot working. The 220 γ peak is greatly increased by rolling, as it is parallel to the (110) principal plane of rolling for austenite.

7. The effect of texture can be minimized, but never completely overcome, by spinning the sample.

8. In Durnin's and Ridal's work, the retained austenite results obtained by using the 211 α peak for comparison were higher than results obtained using the 200 α peak.

9. The retained austenite results found by using 311 γ peak corresponded most closely to results obtained by magnetization techniques. This diffraction line was the line of lowest symmetry and was expected to be least affected by rolling texture.

10. The peaks considered suitable for comparison purposes were 200 α ,211 α ,200 γ ,220 γ ,311 γ . These peaks did not interfere with each other, i.e. did not overlap. The 220 α ,110 α ,222 γ ,111 γ peaks were only included for determining the lattice parameters of the γ and α phase, i.e. the position of the peak was measured, not the intensity.

Other factors relevent to this technique will also be mentioned. The peak position measured for the body centred tetragonal martensite (002,200) is exactly the same as position for the corresponding (200) body centred cubic structure, ferrite (α) (53). The martensite peak appears as a very broad ferrite peak. The broadening of this peak is aggravated further by cold working of the martensite (54).

Iron Kα radiation was used in the present X-ray work, as the only other target available, Cu , was unsuitable for ferritic analysis due to excessive fluorescence (55).

Face centred cubic (FCC) metals exhibit predominantly two distinct types of rolling textures: (22 p.541, 56 p.325)

a) " Brass Type" - (110) parallel to the rolling plane. This is characteristic of FCC metals of low stacking fault energy (high stacking fault frequency).

b) " Copper Type" - (123) parallel to the rolling plane. These metals have a high stacking fault energy.

The annealing textures of FCC material follow a similar pattern: (22 p.568, 56 p.331)

a) " Brass Type" - a material with a Brass Type rolling texture will exhibit a Brass Type annealing texture, i.e.- (113) parallel to the rolling plane.

b) " Cube Type" - (sometimes called Copper Type) - a material with a Copper Type rolling texture will show a Cube Type annealing texture, i.e. (100) parallel to the rolling plane.

Austenitic stainless steel exhibits the " Brass Type" of texture after both annealing and rolling (57). The annealing texture during the recovery stage, however, duplicates the cold worked texture (22 p.572).

For body centred cubic (BCT) metals the rolling texture is generally - (100) parallel to the rolling plane (22 p.541). The annealing texture of BCC metals can be described as a combination of (22 p.568):

a) (111) $[\bar{2}11]$ predominantly
b) (001) [110]
c) (112) $[\bar{1}10]$ very slightly

The ferrite or martensite phase would probably exhibit similar tendencies as the BCC structure.

The plastic strain on the surface of a material may differ from the strain in the bulk of the material and could lead to erroneous results.

The direct comparison method involves the comparison of the integrated intensities of selected plane refletions (hkl) of the martensitic and austenitic phases. The following equation expresses the integrated intensity of a diffraction line (53):

$$I\ (hkl) = \frac{Io\,e^4}{m^2 c^4}\left(\frac{\lambda^3 A}{32\pi r}\right)\left(\frac{1}{v^2}\right)\left[|F|^2 p\left(\frac{1+\cos^2 2\theta}{\sin^2\theta\cos\theta}\right)\frac{e^{-2M}}{2m}\right]$$

I = integrated intensity per unit length of diffracted line

Io = intensity of incident beam

e = charge of electron

m = mass of electron

c = velocity of light

λ = wavelength of incident radiation

r = radius of diffracting circle

A = cross-section area of incident beam

v = volume of unit cell

F = structure factor

P = multiplicity factor

θ = Bragg Angle

e^{-2M} = Temperature factor - function of θ

μ = linear absorption coefficient

$\frac{1}{2\mu}$ = absorption factor

$\left(\frac{1+\cos^2 2\theta}{\sin^2\theta\cos\theta}\right)$ = Lorentz-Polorization factor

The above equation can be rearranged so that:

K_2 = a constant, independent of the kind and amount of diffracting substance,

$$K_2 = \frac{I_o e^4}{m^2 c^4} \frac{\lambda^3 A}{32\pi r}$$

R = a variable, dependant on θ, hkl, and the kind of substance,

$$R = \left(\frac{1}{v^2}\right)\left[|F|^2 \; p\left(\frac{1+\cos^2 2\theta}{\sin^2\theta\cos\theta}\right)\right] e^{-2M}$$

Therefore, the equation can be expressed as,

$$I\ (hkl) = \frac{K_2 R}{2\mu}$$

In a multiphase system, where the volume fraction of each component is denoted by Vi,

$$Va + Vb + \cdots + Vn = 1$$

Each component produces its own pattern of diffraction lines. The intensity of each line is a function of the volume percent of that component in the mixture, i.e.

$$Ia = \frac{K_2 Ra\ Va}{2\mu a}$$

The relationship between the intensity of a diffraction line and concentration of a component, however, is not necessarily linear. When using this technique to analyse the austenite-martensite mixture, the following equations apply:

$$I_\gamma\ (hkl) = \frac{K_2\ R_\gamma\ V_\gamma}{2\ \mu_m} \qquad I_\alpha\ (hl\ kl\ ll) = \frac{K_2\ R_\alpha V_\alpha}{2\ \mu_m}$$

Where μ_m is a mean absorption coefficient. This simplification is valid in this system as the difference in absorption coefficient, μ, between martensite and austenite is only about 4% and can be considered as negligible. The absolute value of this μ_m is immaterial in the direct comparison method, as it cancels out in the calculations, as will be seen below.

$$\text{If } P = \frac{I_\alpha}{I_\gamma} \qquad \text{and} \qquad G = \frac{R_\gamma}{R_\alpha}$$

$$\text{then } P = \frac{R_\alpha V_\alpha}{R_\gamma V_\gamma} = \frac{V_\alpha}{V_\gamma} \times \frac{1}{G}$$

or expressed in an other way $V_\alpha = V_\gamma \cdot P \cdot G$ (34).

If α and γ are the only phases present,

$$V_\alpha + V_\gamma = 1.$$

Therefore
$$V_\gamma = 1 - V_\alpha$$
$$= 1 - V_\gamma \cdot G \cdot P$$
$$V_\gamma = \frac{1}{(1 + G \cdot P)}$$

In the present experiments, the formula used to calculate the volume percent austenite was the following:

$$V_\gamma\ \% = \frac{100}{(1 + G \cdot P)}$$

Procedures:

a) Representative specimens (1 in. X 1 in.) were obtained from the cold rolled and temper annealed material for X-Ray analysis in order to determine the effect of phase structure of the stainless steel on the mechanical properties,

The X-ray experimental conditions were as follows:

Instrument	: Phillips Standard Diffractometer
Counter	: Proportional Counter
Radiation	: Fe Target, Mn Filter Voltage 40 Kv. Current 10 ma.
Diffractometer Motion	: $1/2^{o}$ per min.
Chart Motion	: 20 mm per hr.
Sensitivity	: from 10^{2} to 10^{5} cps - varied to achieve maximum resolution.

In an attempt to minimize the effect of preferred orientation in the specimens, each specimen was scanned at six different orientations in the sample holder, i.e. at 0^{o}, 20^{o}, 45^{o}, 60^{o}, 75^{o}, 90^{o} to the rolling direction. The average of the intensity measurements obtained at the different orientations was expressed as the peak intensity.

b) In order to determine the extent of recrystallization and the effects of cold work, back reflection X-ray films were obtained. There is a voluminous literature on the interpretation of these back reflection films (22 ,53) and therefore the theoretical aspects will not be discussed.

Radiation	: Fe Target, Mn Filter Voltage 40 KV Current 20 ma.
Collimator	: Fine
Exposure Time	: 10:00 Hours

Reflection planes observable with the available equipment:

311 γ $2\theta = 126.6^{\circ}$

222 γ $2\theta = 137.8^{\circ}$

220 α $2\theta = 145.6^{\circ}$

Film to sample distance: 1 1/2 in.

Film: Medical X-Ray film 5 in. X 7 in.

c) The forward reflection X-ray analysis method (22,53) was used to determine texture (preferred orientation) in the specimens, as back reflection techniques may not effectively indicate texture, especially if the preferred orientation is only slight.

Radiation	: Fe Target, Mn Filter
	Voltage 40 KV
	Current 20 ma.
Collimator	: Fine
Exposure Time	: 3:00 Hours

Reflection planes observable with the available equipment:

110 α $2\theta = 45.4^{\circ}$

111 γ $2\theta = 55.7^{\circ}$

Film to sample distance: 22 mm.

Film	: Medical X-Ray film 8 cm. X 8 cm.
Thinning Solution	: 15% HCl
	30% HNO_3
	10% HF
	45% H_2O
Temperatue	: simmering
Time	: .030 in. to .010 in. thickness in 2 min.
Thickness of Test Sample	: 0.002 in.

Section V

RESULTS AND DISCUSSION

V RESULTS AND DISCUSSION

A. Introduction

The mechanical properties of temper rolled and temper annealed AISI 301 stainless steel are presented in this section. These properties are compared, especially with respect to differences in ductility achieved by the two treatments, and the results correlated with differences in phase composition and microstructure.

B. Temper Rolled Materials

The mechanical properties of the experimental materials obtained after different amounts of cold work, up to 80%, are presented in Table VII, Fig. 40 and Fig. 41. There is no published data for mechanical properties corresponding to reduction of more than 60%, but up to that reduction, the present results compared favourably with published data (7,29) (Fig.42). The curves compared very closely in shape, but the data from the present work showed tensile strengths consistently lower for the same amount of cold reduction. This lower tensile strength in the experimental samples could have been due to slight variations in steel composition or the effect of a larger grain size in the experimental material prior to cold work. There was much less variation when comparing yield strength results. Up to about 30% cold reduction, yield strength values were extremely close. Beyond this reduction, the material used in the present work showed lower yield strengths. This low yield strength region was also the region of discontinuous yielding, where the true yield point was more difficult to determine.

The outstanding phenomenon observed from this data is the rapid rate of strain hardening. The tensile strength increased from 101,100 psi to over 283,000 psi by 80% cold reduction. The strain hardening was most severe above 70% reduction. The improvement in yield strengths was even more dramatic, eg. from 40,000 psi to over 260,000 psi.

Rockwell hardness readings (Fig. 41a) indicated this rapid hardening up to about 40 Rc (corresponding to 50% cold reduction). Beyond this hardness, the Rc scale became insensitive, and did not reflect the very rapid increase in strength still obtainable. The Vickers hardness test was considered to be more sensitive in measuring higher hardness. (9 p.502) but this did not turn out to be the case in the present work (Fig. 41b).

Total elongation of the annealed material was almost 75% and the uniform elongation was about 57%. These values, of course, are very high and well above the elongations encountered in any other commercial metals. It is for this reason that austenitic stainless steel is used in such great amounts for applications requiring good formability. After full cold reduction, however, the total elongation was reduced to less than 3%, while the uniform elongation was only about 1%.

The stress-elongation curves of stainless steel exhibited three distinct shapes.

1) Up to about 30% Cold Reduction: The stress-elongation curve was smooth, without a sharp yield point (as Fig. 36). The total elongation was always about 10% greater than the uniform elongation. Normal necking occurred prior to fracture. For the experimental material, this type of plastic flow occurred in material with tensile strengths from 101,000 psi to about 140,000 psi.

2) From 30% to 65% Cold Reduction: The method of necking and failure changed completely. The total plastic deformation prior to failure was increased significantly by the discontinuous necking phenomenon discussed in Sec. III-E. The uniform elongation was only about 1%. This was followed by up to 25% of elongation in the form of a discontinuous yielding plateau. Normal necking added 3% to 5% of total elongation prior to failure (as Fig.37). Although the total elongation may have been over 30%, the material could not be really considered ductile, as the majority of this

elongation was actually necking. The maximum discontinuous necking occurred at the first onset of this behavior, i.e. at 30% cold reduction. The amount of discontinuous necking decreased with increased cold reduction, and at about 65% cold reduction, it disappeared.

3) Above 65% Cold Reduction (above 200,000 psi): The material was brittle. Uniform elongation was still about 1%, but the material failed with minimum necking (1% to 3%) (as Fig.38). Although tensile strength increased dramatically with increased cold work beyond this value, the amount of elongation was practically unchanged.

Since the yielding occurred very differently in the above three situations, interpretation of the variations in yield strength and elongation with increased cold work became complex. Total elongation may be a misleading measure of formability.

TABLE VII

Mechanical Properties of Temper Rolled AISI 301 Steel

Experimental Data

Cold Reduction %	Tensile Strength psi. TS	Yield Strength psi. YS	Uniform Elongation % Eu	Total Elongation % Et	Hardness Number R_C
0	101,100	40,500	57	73	@ 0/Rb 80
2.8	102,500	50,840	55	70	9.0
11.4	121,800	74,400	44	53	24.0
15.4	125,200	94,800	40	50	-
19.0	133,700	105,700	33	42	-
20.0	134,600	108,700	31	41	28.0
26.0	144,800	119,600	20.5	30.5	-
32.0	155,000	127,300	2.0	23.5	-
36.0	165,800	135,000	1.2	-	36.6
52.1	184,600	162,900	1.2	11.0	40.0
63.1	200,600	176,100	1.1	5.4	41.0
68.2	214,900	193,600	1.0	3.2	42.6
73.5	250,100	215,600	1.1	2.2	43.6
79.5	283,500	250,200	1.1	2.6	46.3

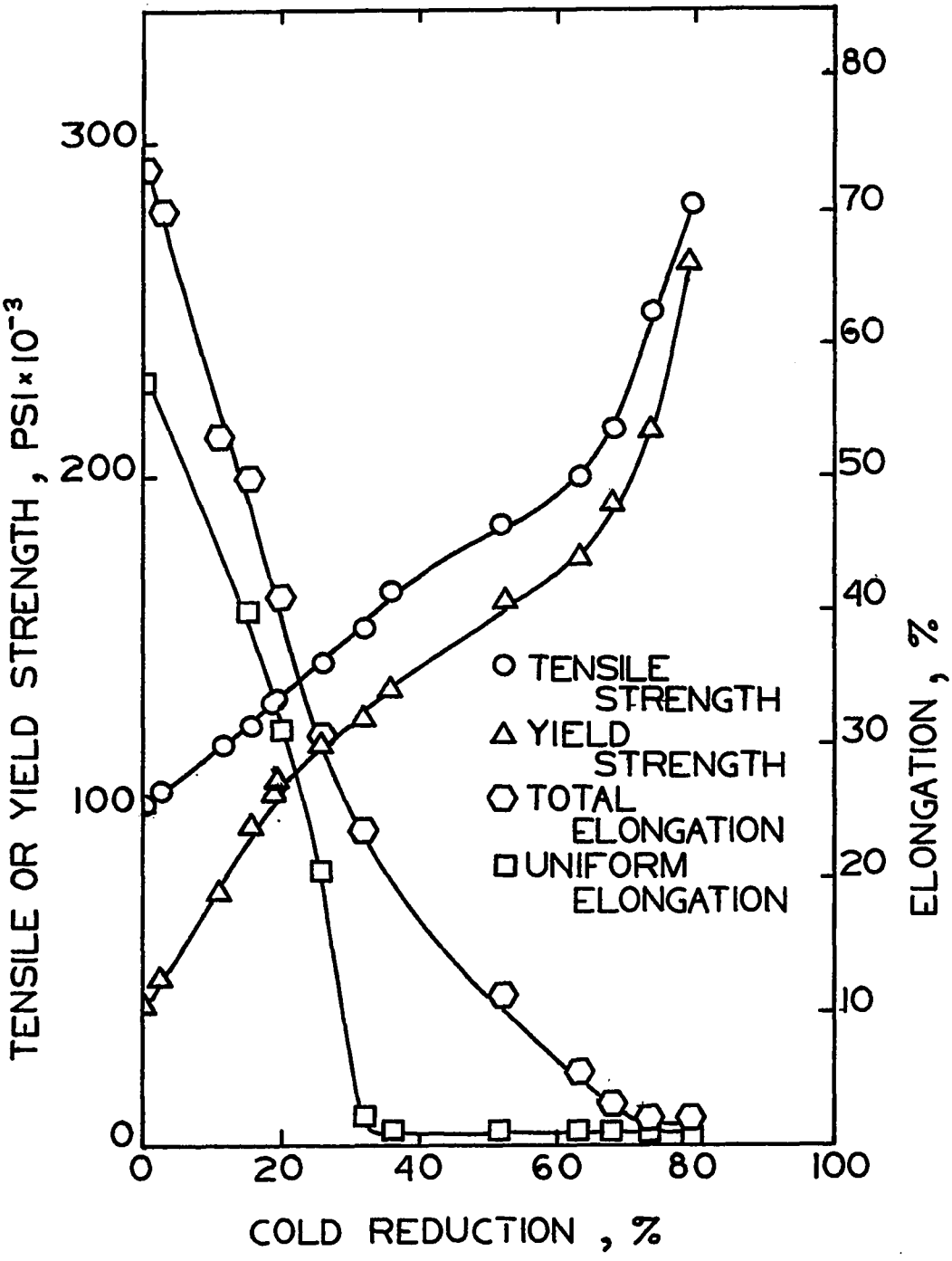

Fig. 40. Variation of mechanical properties with rolling reduction for AISI 301 steel - Experimental Data

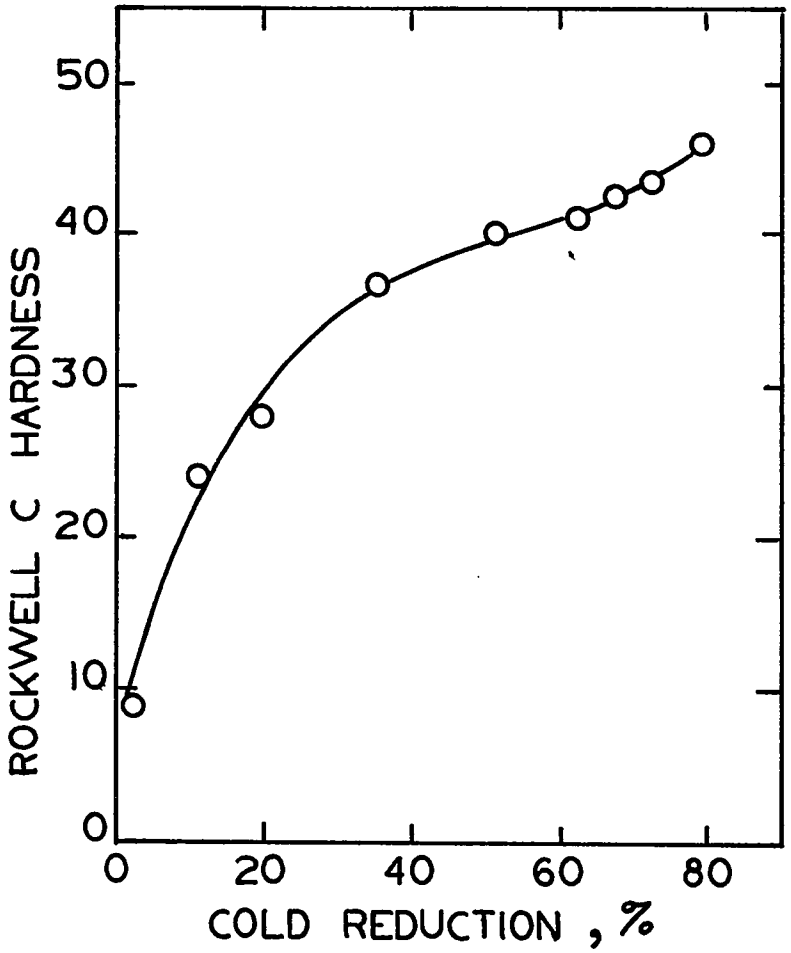

Fig. 41a. Rockwell hardness versus percentage reduction of AISI 301 steel

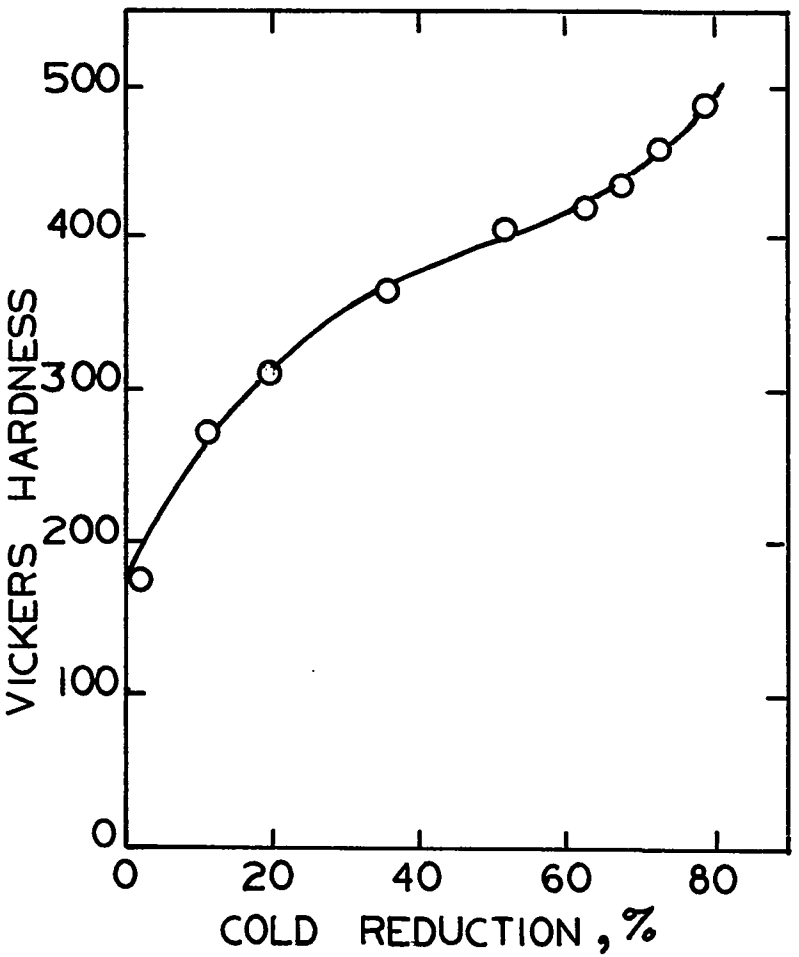

Fig. 41b. Vickers hardness versus percentage reduction of AISI 301 steel

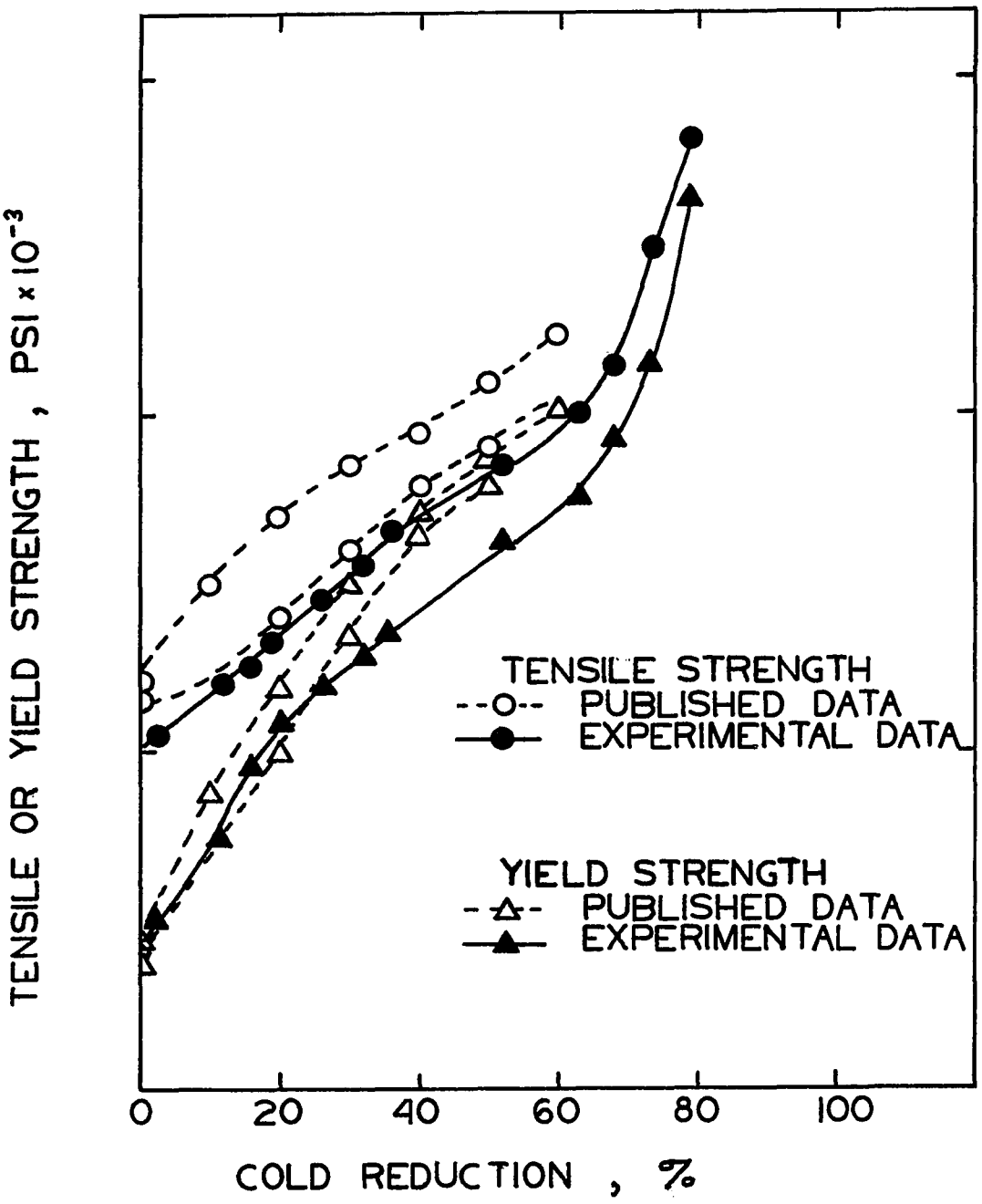

Fig. 42. Variation of mechanical properties with rolling reduction for AISI 301 steel - Experimental and published data.

C. Temper Annealed Materials

The mechanical properties obtained by temper annealing at 850°C, for various times, are illustrated in Fig. 43(a), while the same properties, obtained by temper annealing at 900°C are illustrated In Fig. 43(b). Only long holding times are recorded for 900°C, as this temperature was only used to expedite grain growth, so as to obtain a grain size corresponding to the size found in the starting material. By annealing at 900°C, it was possible to approach the mechanical properties of the starting (annealed) material.

The full range of mechanical properties was obtained by using five separate runs, as indicated in Table VIII . Considering the short time of annealing (virtually full recrystallization within one minute) and the high annealing temperatures, 850°C - 900°C, very good reproducibility was obtained. At any one annealing time, the scatter in the tensile strength was about 10,000 psi. The variation in elongation corresponded to tensile strength scatter.

Great precision was essential in temperature measurement and control. Each specimen had to be heat treated separately in order not to disturb bath temperature or heat transfer conditions.

The annealing time was measured using a stop watch and material transfer times were kept consistent. The sensitivity of the results to annealing time can be seen from the fact that tensile strength dropped from 283,600 to 181,000 psi. by increasing the annealing time, at 850°C, from 0 to 10 seconds.

It was also imperative that the starting material used for all temper annealing trials always had the same properties. If a different rate of rolling or material cooling, or a different rolling temperature was used, different mechanical properties resulted. If

the tensile strength after 80% reduction was not within the rage of 283,000 psi. to 284,000 psi., the complete rolled strip was rejected.

As was noted in the previous section on temper rolled material, discontinuous necking was observed within a certain range of tensile strengths, i.e. between 150,000 psi. and 200,000 psi. Material with tensile properties outside this range behaved exactly the same as temper rolled material. In temper annealed material as well, total elongation would be a misleading criterion for ductility, eg. at 155,000 psi. (annealed 20 sec. at 850^{o}C) the total elongation was 33% while the uniform elongation, which may be a better measure of ductility, was only 1.0%.

Tensile strength values were higher than expected from hardness readings, but were still well within the ranges expected. At very high strengths, the Rc scale again became insensitive, eg. in the range of tensile strength from 245,000 psi. to 283,000 psi. the Rc value remained virtually unchanged at about Rc 46.5

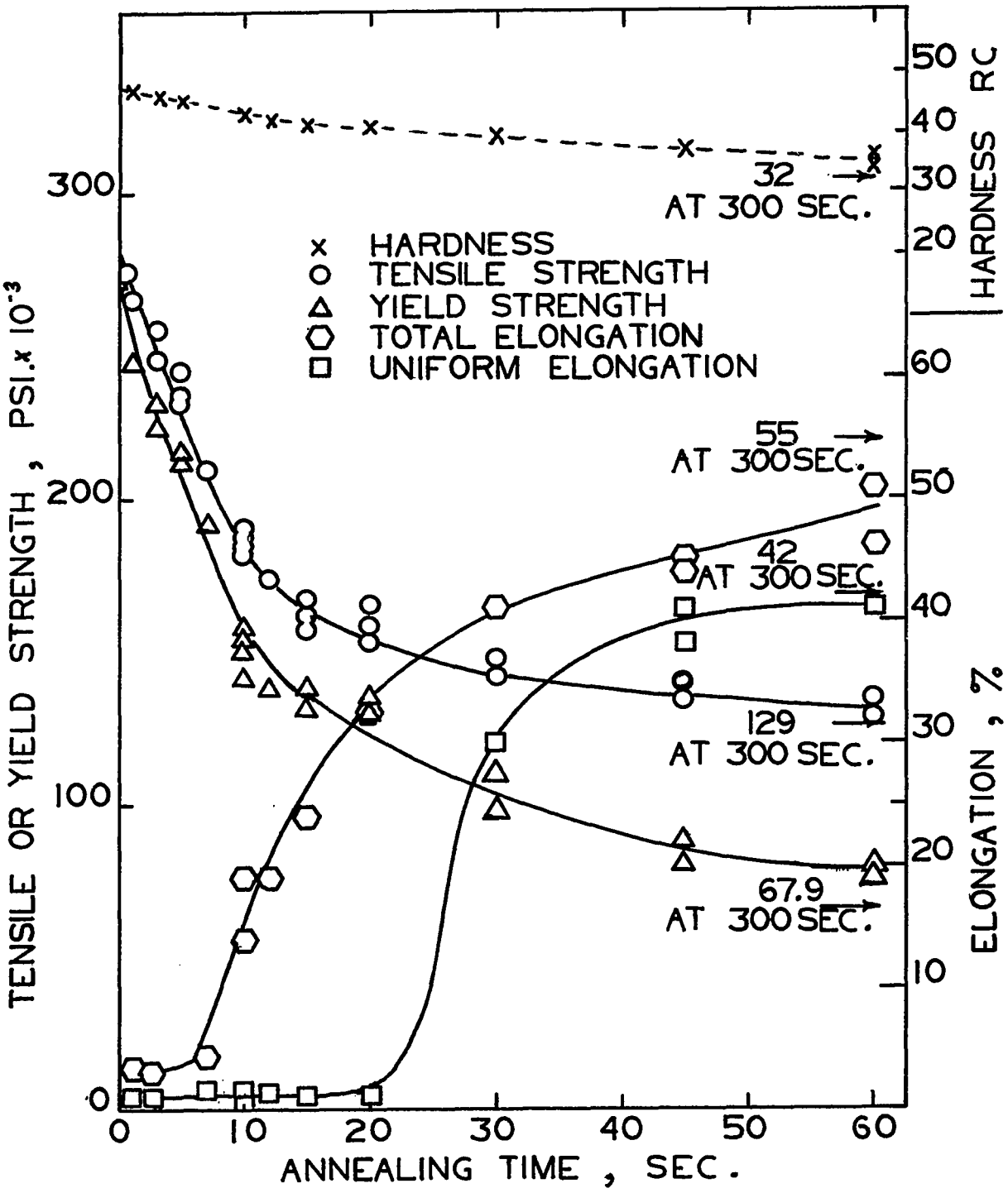

Fig. 43a. Variation of mechanical properties with annealing time at 850°C for AISI 301 steel

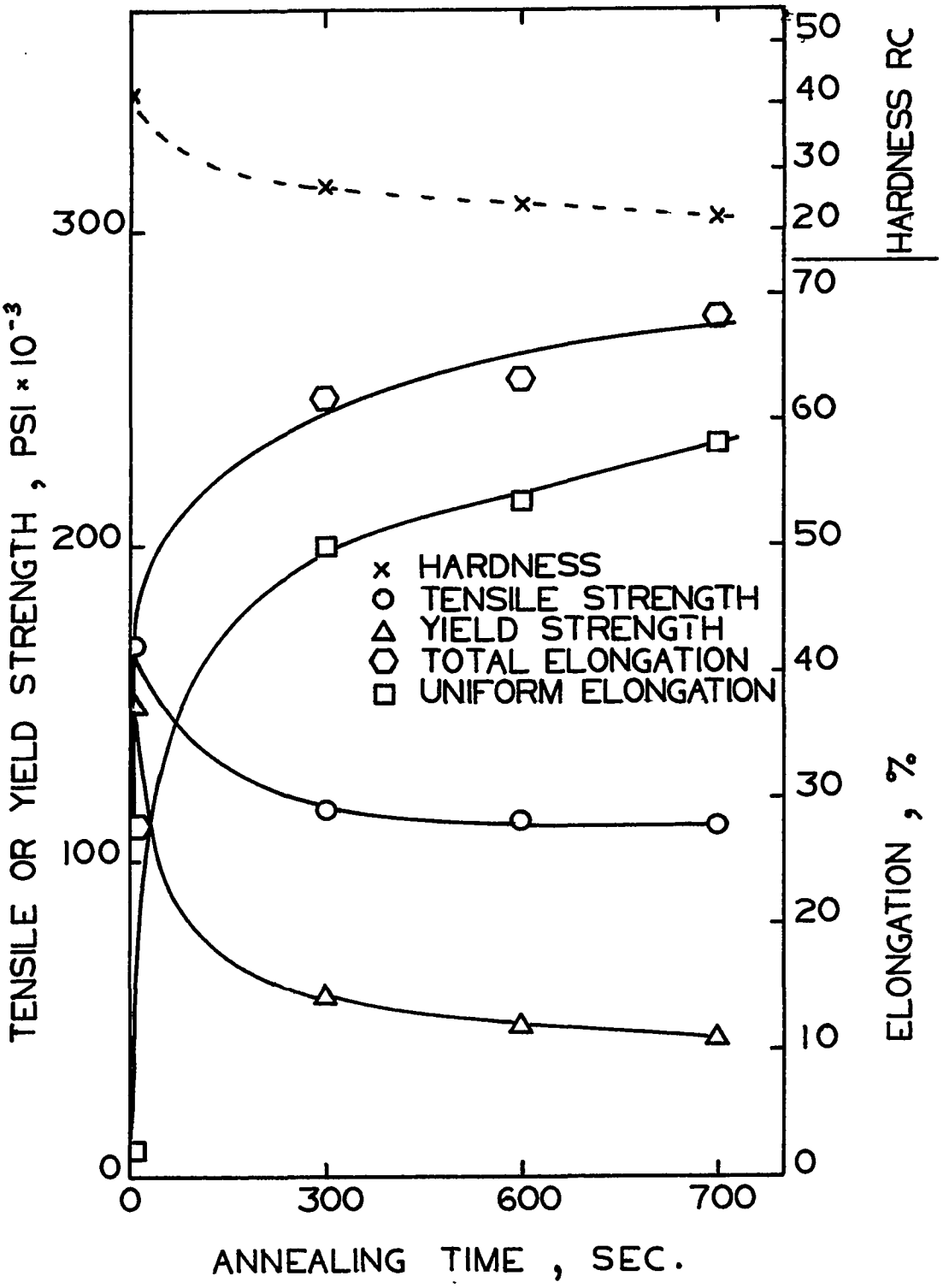

Fig. 43b. Variation of mechanical properties with annealing at 900°C for AISI 301 steel

TABLE VIII part 1

Mechanical Properties of AISI 301 Steel - Temper Annealed at 850°C - Runs No. 1 & 2

Annealing Time Sec	Run No. 1 T.S. psi.	Y.S. psi.	Eu %	Et %	Hardness Rc	Run No. 2 T.S. psi.	Y.S. psi.	Eu %	Et %	Hardness Rc
00	283,600	274,000	0.5	0.9	46.3					
01										
03						256,300	232,700	0.8	3.1	46.5
05						243,200	213,000	1.3	-	45.5
07										
10	191,100	186,300	-	-	-	180,800	153,500	1.1	19.0	43.0
12										
15	163,000	139,300	1.1	29.0	-	166,900	132,500	1.2	24.0	41.6
20	153,500	136,800	-	-	-					
30	141,900	98,700	-	-	-	148,600	110,100	30.0	41.0	40.0
45	134,700	89,000	41.0	45.0	-	140,400	92,600	38.0	44.0	37.0
60	132,000	80,000	41.0	51.0	-	133,600	79,500	41.0	48.0	34.0
300										

TABLE VII part 2

Mechanical Properties of AISI 301 Steel - Temper Annealed at 850°C - Runs No. 3 & 4

Annealing	Run No. 3					Run No. 4				
Time	T.S.	Y.S.	Eu	Et	Hardness	T.S.	Y.S.	Eu	Et	Hardness
Sec.	psi.	psi.	%	%	Rc	psi.	psi.	%	%	Rc
00										
01	266,600	245,600	1.5	3.6	-	265,300	243,600	-	-	46.8
03						245,400	224,000	1.5	-	41.0
05	230,100	213,400	1.4	-	-	233,800	215,400	-	-	45.0
07	209,700	191,900	1.7	4.6	-					
10	181,500	140,800	-	-	-	189,600	159,400	1.5	14.0	43.5
12						173,500	138,600	1.5	19.0	42.0
15										
20						154,100	132,600	1.0	33.0	41.0
30										
45										
60										
300						129,000	67,900	42.5	55.0	32

TABLE VIII part 3

Mechanical Properties of AISI 301 Steel

Temper Annealed at 900°C

Run No.5

Annealing	Run. No.5				
Time Sec.	T.S. PSI.	Y.S. PSI.	Eu %	Et %	Hardness
05	168,200	149.800	1.9	28.0	42.0
300	118,400	57,600	50.0	62.0	27.0
600	112,800	47,900	53.5	63.5	24.0
900	111,600	44,100	58.0	68.3	22.0

D. Comparison of Properties of Temper Rolled and Temper Annealed Material.

The tensile strength vs. elongation curve is the most convenient curve for comparing properties of temper rolled and temper-annealed material. This was the type of curve that was used by S. Adams in his theoretical analysis os temper annealing (17) (Appendix A).

In the material tested, both the uniform and total elongation values showed modest but useful improvements when a desired tensile strength was produced by temper annealing rather than temper rolling (Fig.44 and 45). The maximum improvement in total elongation obtained by temper annealing and was about 10% Et (Total Elongation), occurring in the vicinity of 150,000 psi. tensile strength. Beyond about 210,000 psi., tensile strength, the total elongation obtained by either treatment became almost the same, i.e. less than 3%, but the elongation in the temper annealed material was always slightly higher (see Table VII and Table VIII.

The shape of the tensile strength vs. uniform elongation curve was very different from the tensile strength vs. total elongation curve. Uniform elongation dropped off more quickly with increasing tensile strength, for both temper annealed and temper rolled materials. Above 155,000 psi. the material was effectively brittle, i.e. the uniform elongation was only 1%. The maximum improvement in uniform elongation brought about by temper annealing was about 15% Eu (Uniform Elongation), occurring at about 150,000 psi. i.e. at the same tensile strength where maximum improvement in total elongation was obtained. The humped shape of the temper annealing curve was probably due to experimental error.

The absolute improvement in elongation may have been only 15% Eu, maximum, but at 150,000 psi., this represented an improvement from 10% to 25%, i.e. 150%.

An increased ductility may have useful industrial applications, where design considerations might require slightly more ductility than obtainable when using normal temper-rolled material. Designers and users of sheet and strip are constantly demanding improvements in ductility with no significant loss of tensile strength.

The curves in Fig. 44 and 45 formed almost a closed loop and would have closed exactly if the grain size and other structure features, (e.g. carbides) of the starting material for temper rolling had been exactly the same as grain size and other structural features of the final temper annealed material. A material with a large grain size strain hardens more uniformly over its plastic range and so loses its ductility during cold rolling at a lower rate than material with a fine grain size (58,59). There is also the Hall-Petch equation which shows that the strength of a material decreases with increasing grain size (59). The above facts determine the shape of the temper rolling curve. A starting material with a grain size larger than that resulting from the temper annealing experiments tends to opern the top end of the loop by changing the shape of the temper rolling curve as seen in Fig. 46 (3). In the present experiment the closing gap between the curves was very small and any error due to variation in grain size was considered minimal.

Hardness readings are often used to predict other mechanical properties. From Fig. 47a and 47b, it can be seen that there was a great difference in elongations between the temper annealed and temper rolled materials at the same hardness readings, eg. at Rc 35 the uniform elongation of temper rolled material was 1%, while the uniform elongation of temper annealed material was 40%, the total elongation of temper rolled material was 22%, while, for temper annealed material it was 48%. Hardness readings are thus not always a very good measure of ductility.

In Fig. 48, an unusual phenomenon was observed. At a particular value of tensile strength, the temper annealed material showed higher hardness readings. This was unexpected since, at the same time, elongation was greater and yield strength was lower for the temper annealed material. Adams' results, plotted on an equivalent scale, are shown in Fig. 49. Up to tensile strength values of 90,000 psi. and Rb 90, the temper rolled material was harder than temper annealed material at the same tensile strength, as would be expected. Above 90,000 psi. the hardness differences between the two materials was negligible, although this seemingly anomalous behavior can be observed as well. In the present work the anomalous behavior was always observed.

This seemingly anomalous behavior could have been due to differences in microstructure or the excessive presence of chromium carbides in the temper annealed stainless steel. Any explanation, however, would be quite speculative.

The yield to tensile strength ratio is a measure of the amount of plastic flow occurring in a material (3), i.e. a low value of this ratio indicates a low yield strength followed by an ample range of plastic deformation until necking commences at the tensile strength reading. A high ratio indicates a yield strength close to the tensile strength, with little capacity for uniform elongation. The yield to tensile strength ratio for the temper rolled and temper annealed material was plotted against tensile strength in Fig. 50. Up to about 200,000 psi., the yield strength to tensile strength ratio of the temper annealed material was lower than for temper rolled material. Between 150,000 psi. and 200,000 psi., a considerable scatter of readings was observed for both the temper annealed and temper rolled material. This corresponded to the region of discontinuous yielding. Beyond 200,000 psi., the yield strength to tensile strength ratios were similar (about 0.9). Up to about 200,000 psi., therefore, the temper annealed material was expected to have better cold fabrication properties due to the greater plastic flow region. Beyond 200,000 psi., any possible improvement brought about by temper annealing was considered negligible. This can also be seen from Fig. 44, i.e. above about 200,000 psi., total elongation readings for both materials became practically identical.

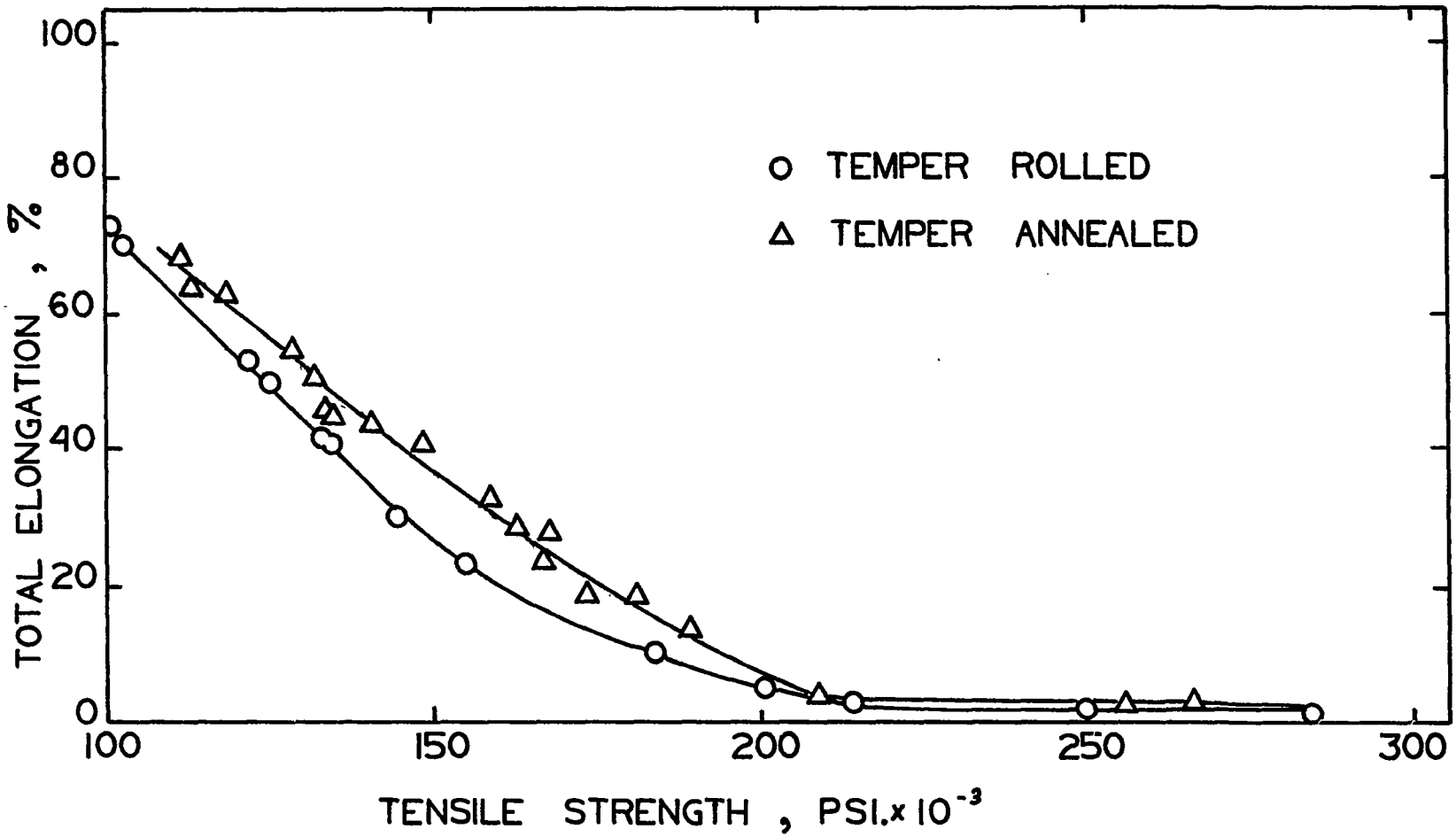

Fig. 44. Comparison of percentage total elongation for temper annealed and temper rolled sheet for AISI 301 steel

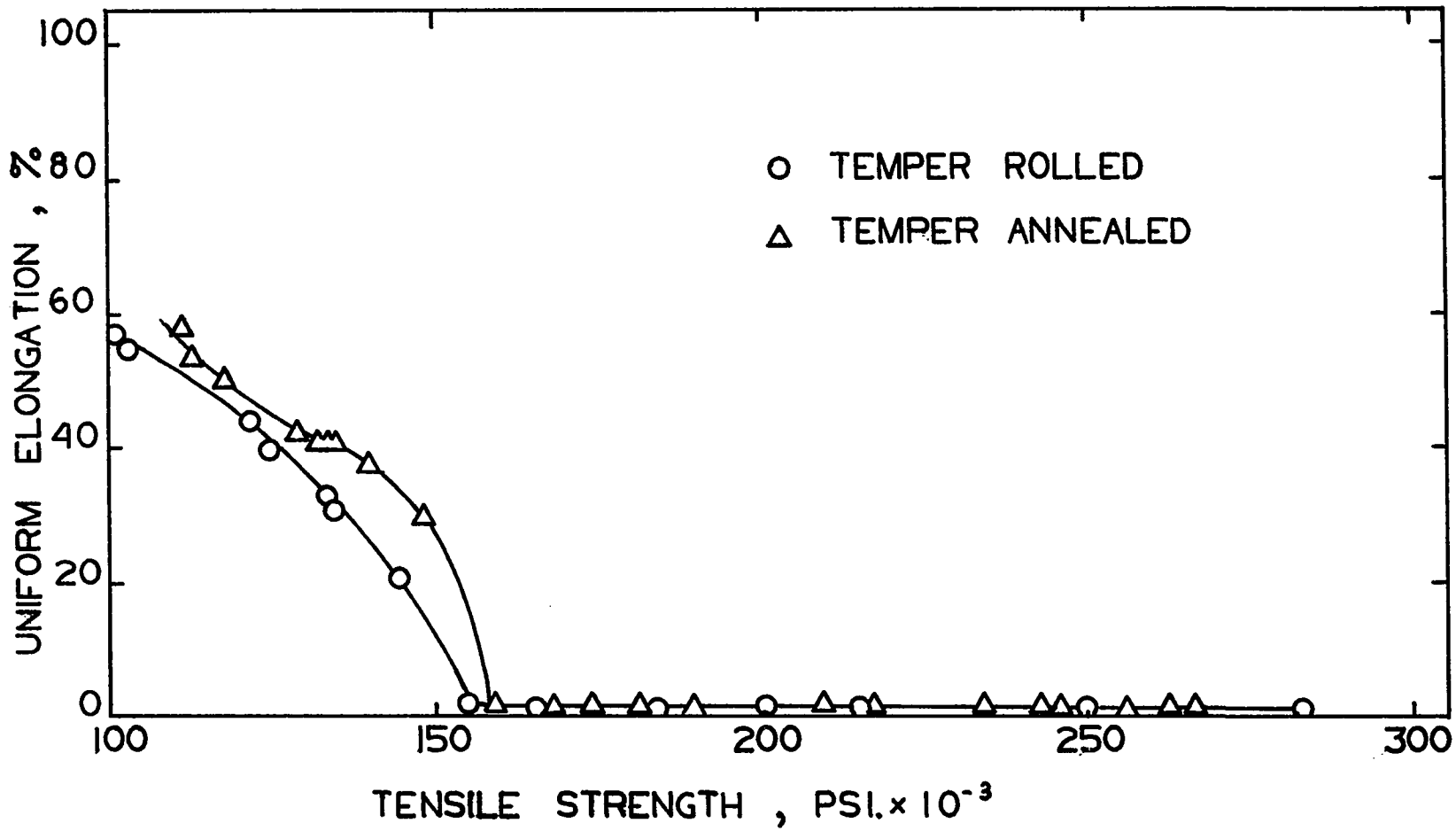

Fig. 45. Comparison of percentage uniform elongation for temper annealed and temper rolled sheet for AISI 301 steel

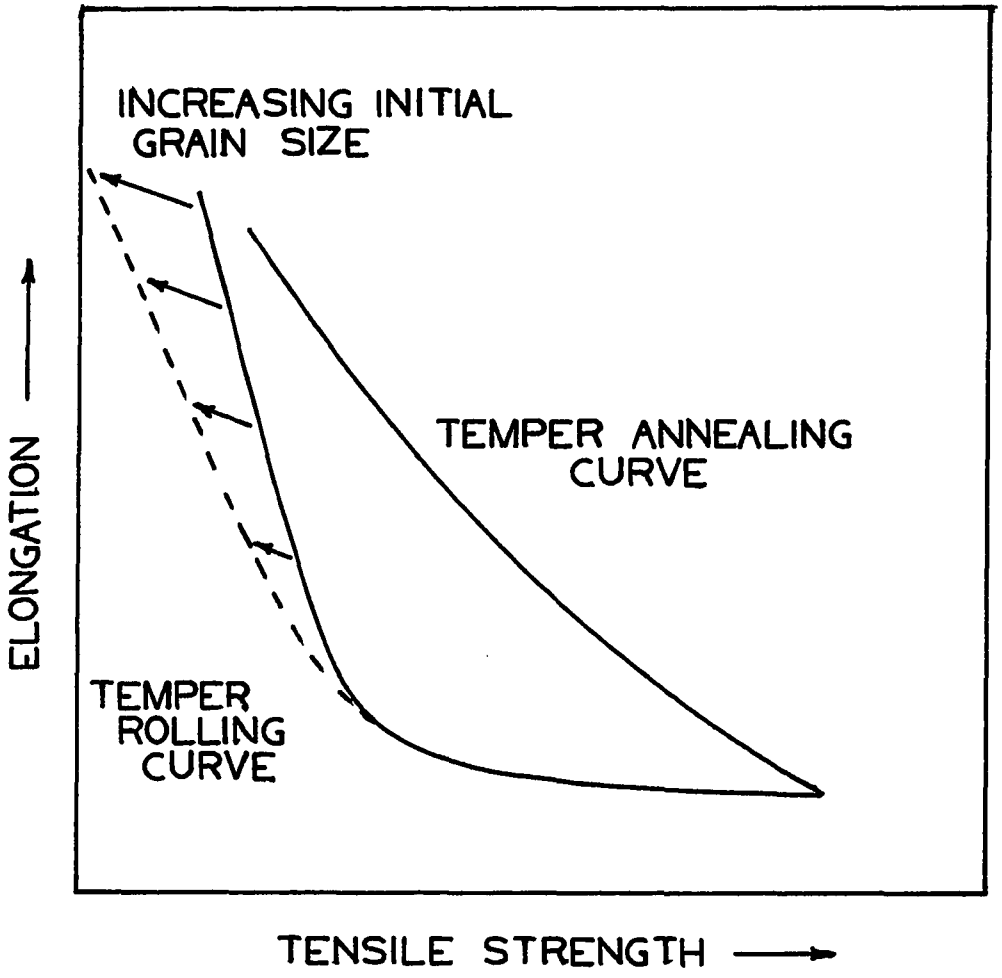

Fig. 46. Effect of grain size on temper rolled material.

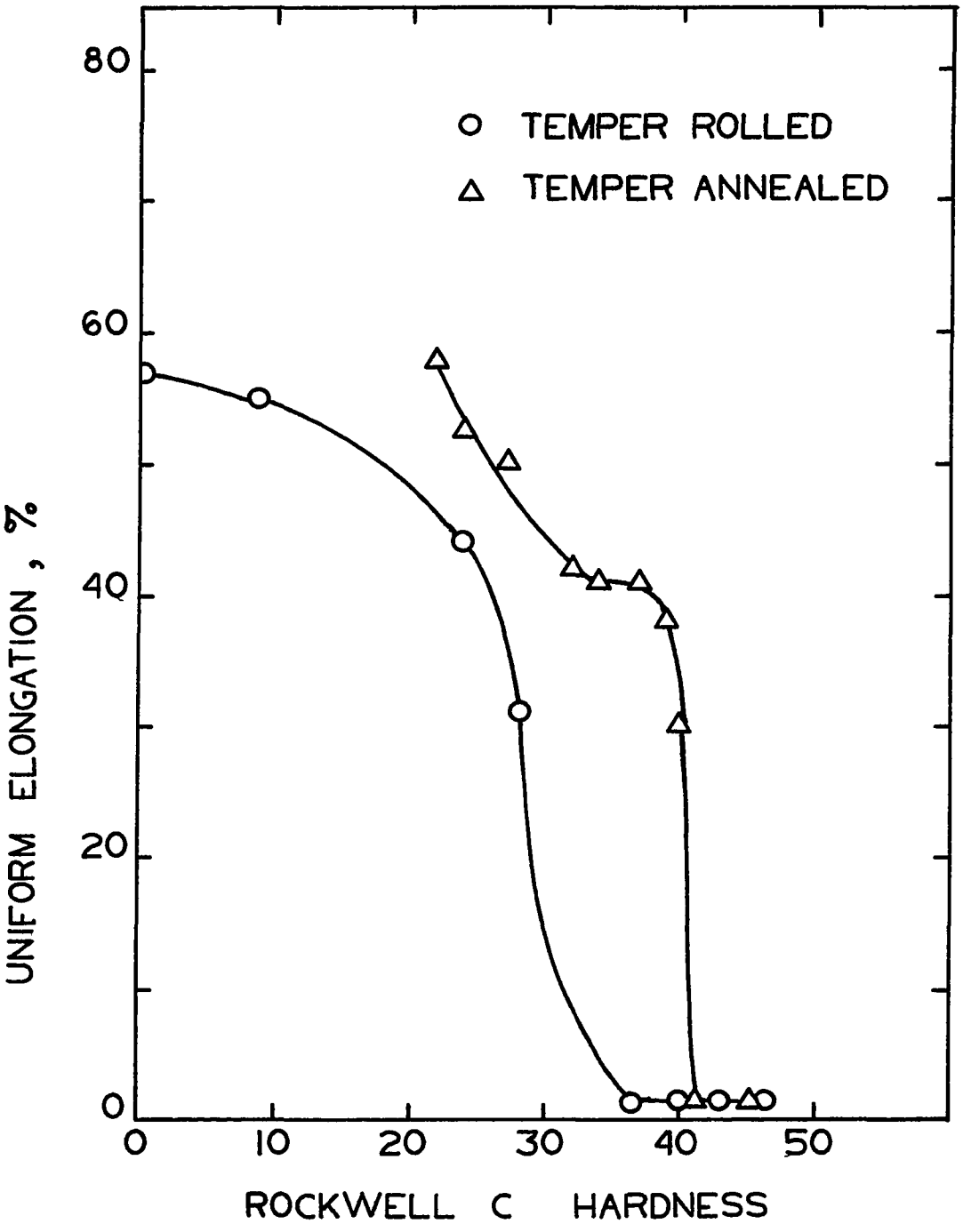

Fig. 47a. Percentage uniform elongation versus hardness for temper rolled and temper annealed AISI 301 steel

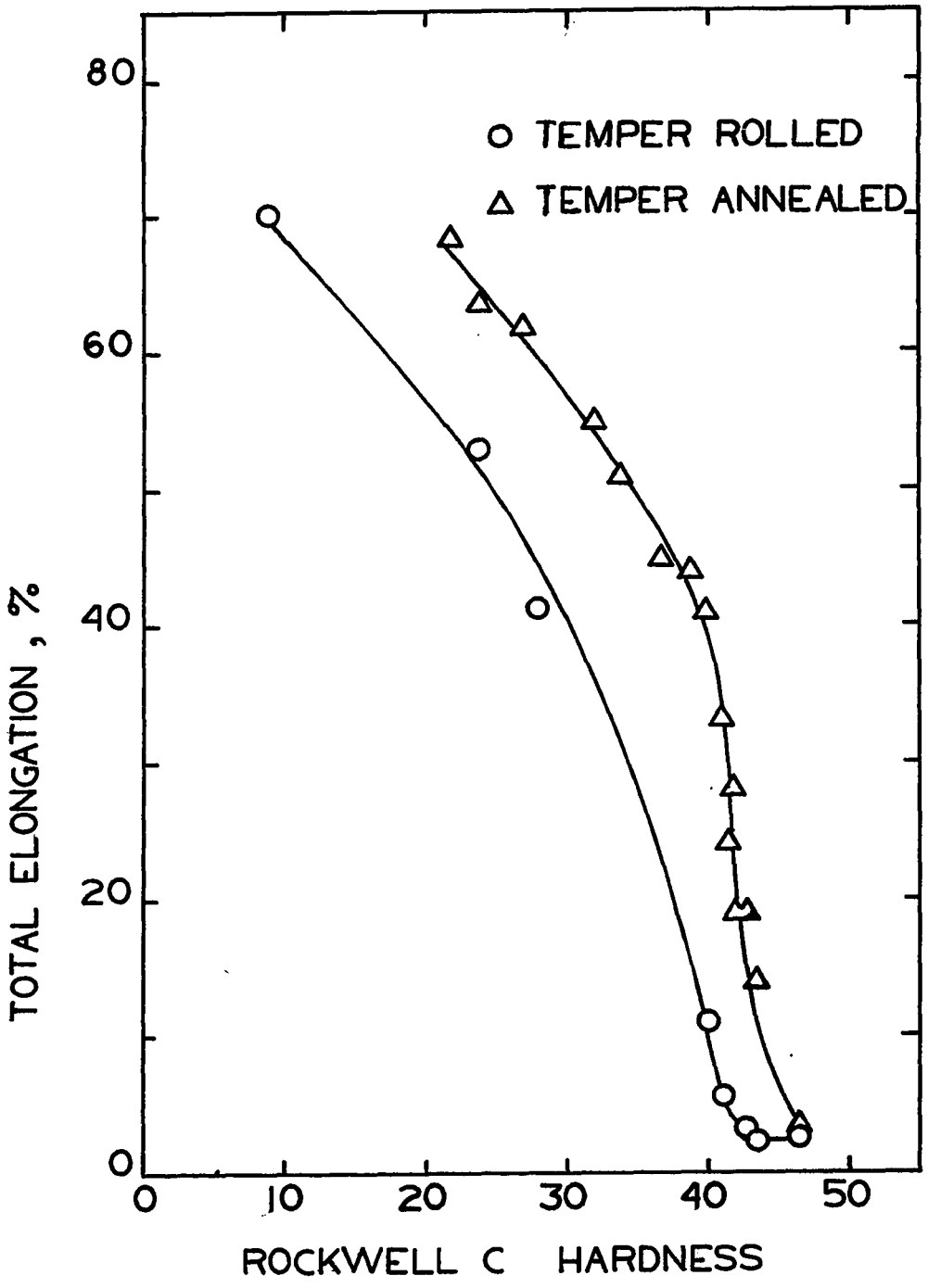

Fig. 47b. Percentage total elongation versus hardness for temper rolled and temper annealed AISI 301 steel

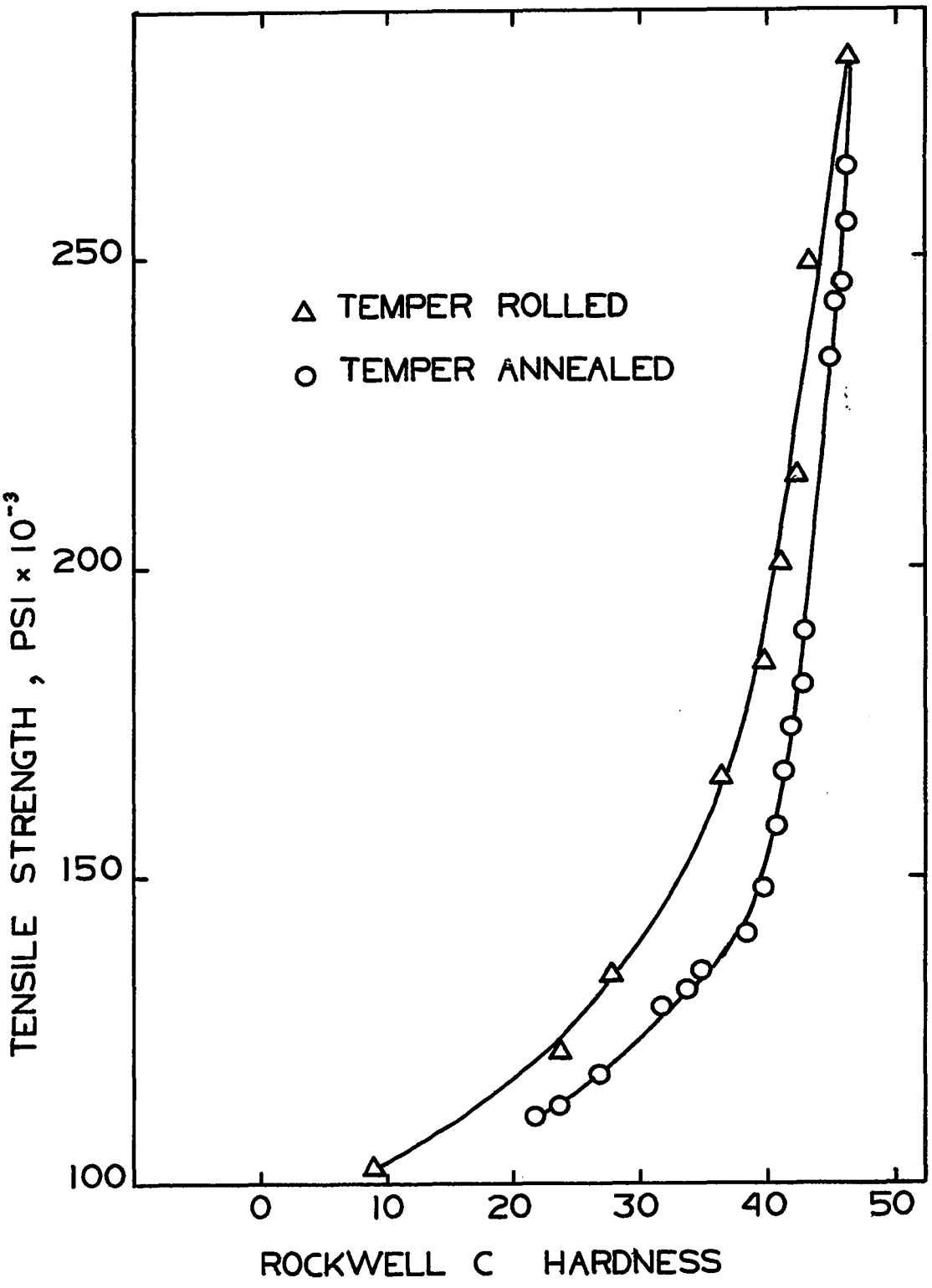

Fig. 48. Comparison of hardness vs tensile strength in temper rolled and temper annealed 301 stainless steel.

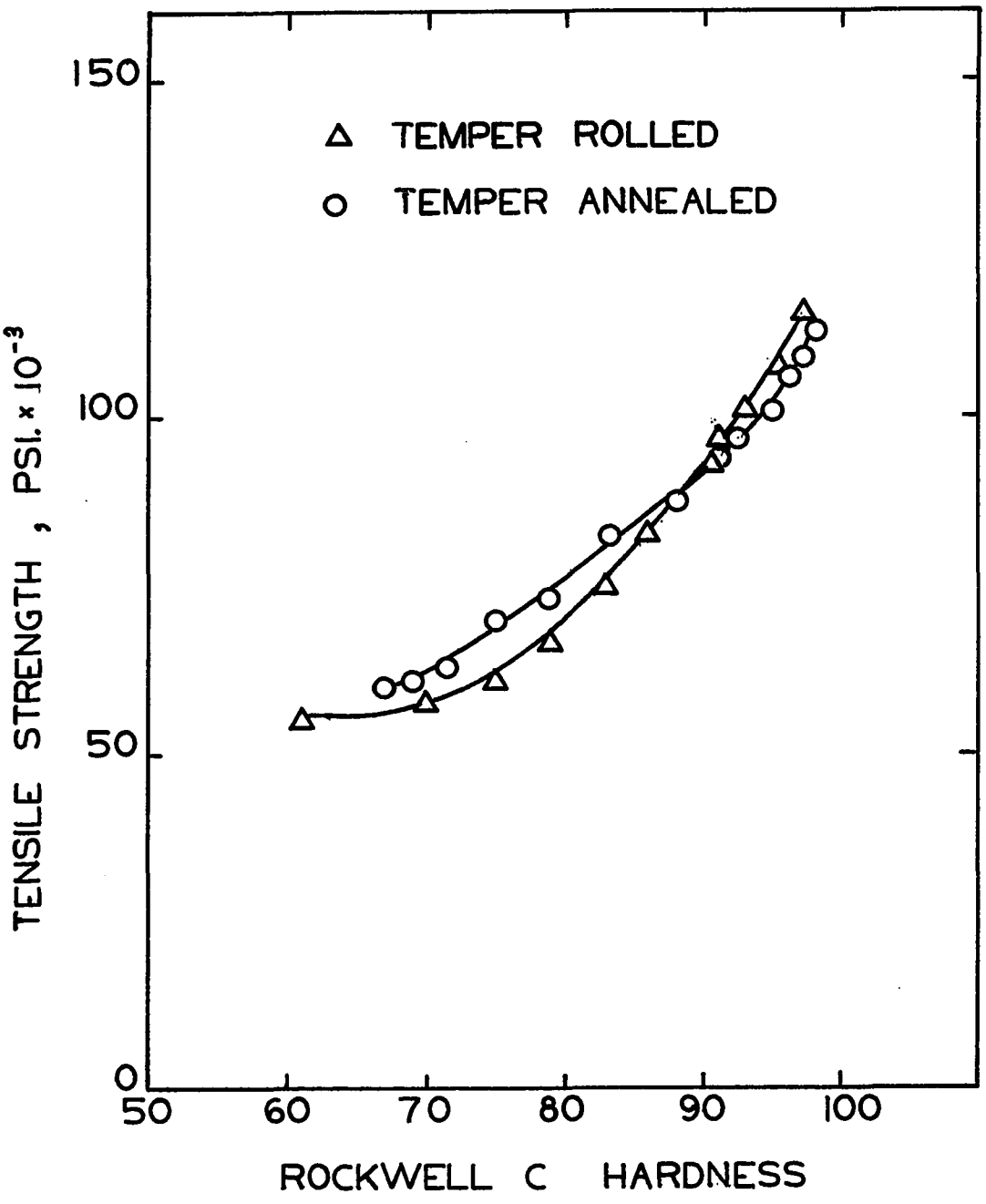

Fig. 49. Comparison of hardness vs. tensile strength in temper rolled and temper annealed mild steel (3).

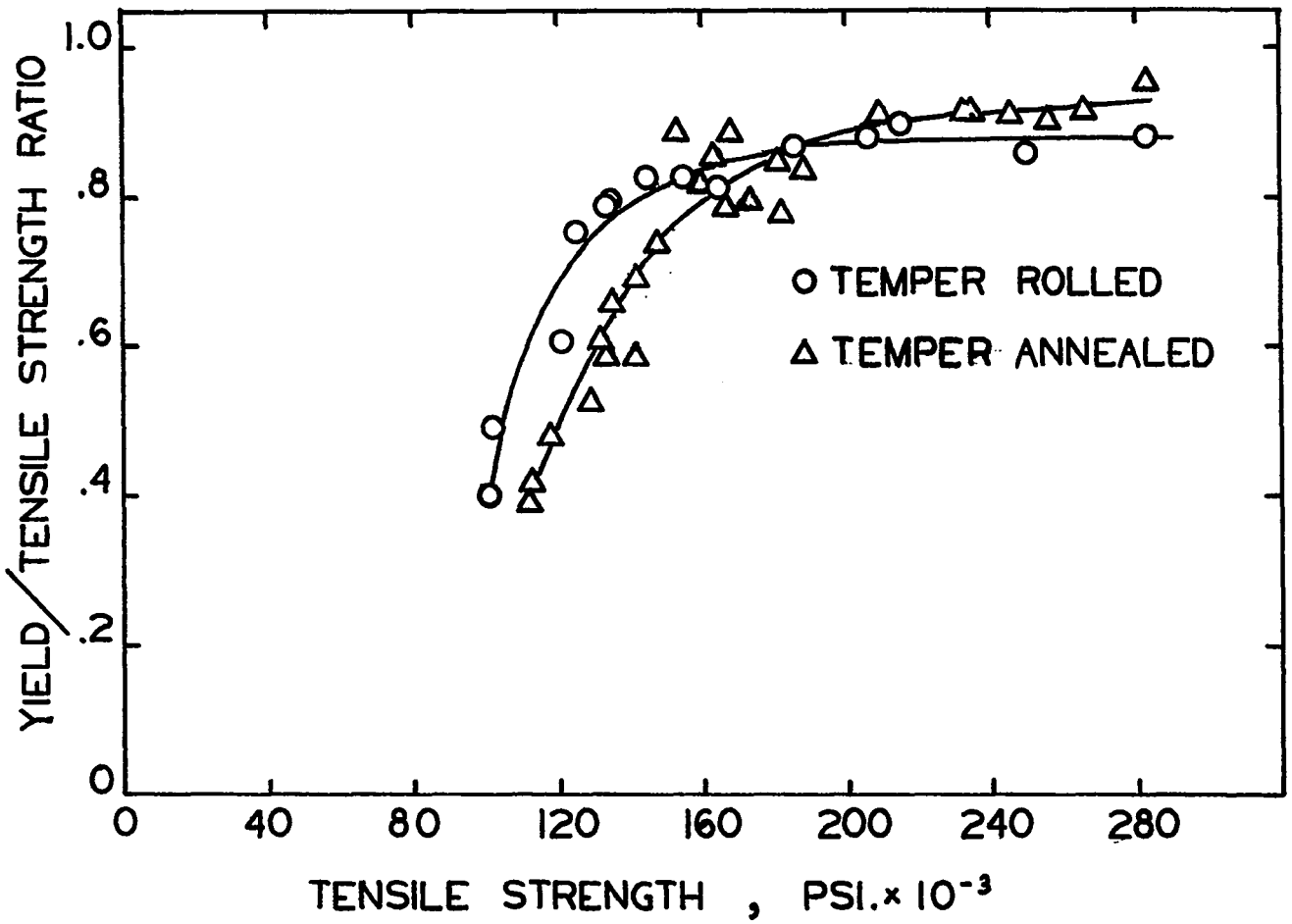

Fig. 50. Comparison of yield/tensile strength ratios for Temper Annealed and Temper Rolled sheet of AISI 301 stainless steel.

E. Erichsen Testing

Representative samples of temper rolled and temper annealed material were chosen for ductility testing, using the Erichsen Testing apparatus discussed in Section IV-D-3. The results are recorded in Table IX . The highly cold worked material failed by cracking parallel to the rolling direction, with only a minor depth of impression, as expected for heavily cold worked austenitic stainless steel (60). On the other hand, it was not possible to fracture the softer material, as this material work hardened sufficiently during deformation to prevent failure at the maximum applied load of 5,000 lbs.

Because of the machine limitations and also because earlier workers in this field (1) found that Erichsen results conveyed little information of value, it was decided not to proceed with further Erichsen tests.

TABLE IX

Erichsen Test Results

Cold Reduction %	Depth of Impression in.	Applied Load lb.
0	0.290	5,000*
	0.300	5,000*
36.0	0.196	5,000*
	0.195	5,000*
	0.195	5,000*
68.2	0.160	5,000*
	0.161	5,000*
73.5	0.800	2,250
	0.105	3,100
	0.105	3,075
79.5	0.105	2,950
	0.110	3,250
	0.107	3,250

* Did not fracture

F. Metallography

Representative photomicrographs were obtained from both temper rolled (Fig.51 to Fig. 55) and temper annealed (Fig. 56 to Fig. 60) specimens. Two magnifications were used, 220 X for general examination and 330 X for better resolution of the martensite phase.

1) Temper Rolled Material

In examining the temper rolled material, the electrolytic etching time was 30 seconds, using a current density of one ampere per square centimeter.

As annealed metastable austenitic stainless steel was temper rolled, an increasing number of martensite plates were seen to form (Fig. 51 to Fig. 53). These plates strongly resembled deformation twins or slip planes, but X-ray results in the present work as well as the results of many other workers (23,34,35,37,38,39,40) indicated that this structure was in fact martensite. Beyond a tensile strength of about 165,000 psi., i.e. over 40% cold reduction, the metallographic structure became indistinquishable (Fig. 54). Up to maximum cold reduction of 80%, i.e. 283,600 psi., the structure appeared to change very little. Elongated bands, parallel to the rolling direction, were all that could be observed (Fig. 55). As will be seen from the X-ray results presented in the next section, considerable austenite was still present, but it could not be detected metallographically.

2) Temper Annealed Material

When examining the temper annealed material, electroyltic etching was only maintained for 5 seconds, except were otherwise indicated. Any further etching completely obliterated the microstructure of most specimens. As oxalic acid etching is also a test of corrosion susceptibility (51), this severe metal attack indicated a loss of corrosion resistance in these specimens.

In austenitic stainless steel, this probably corresponded to chromium carbide(Cr_{23} C_6) precipitation (34,35).

Selected micrographs of temper annealed material are illustrated in Fig. 56 to Fig. 60. The banded microstructure, characteristic of cold worked steel, was observed in all the micrographs of the temper annealed materials. It was believed that this structure was observed only due to the limitations of the etching technique and was brought out at a consequence of rapid carbide precipitation along slip lanes and grain boundaries. This idea was tested by using a modified etching technique. The specimen shown in Fig. 59c was heavily etched, reground slightly on 600 grit carbide paper, and then repolished. Examination of the structure after this procedure revealed, under 220X magnification, only the most heavily etched regions. It was clear that the cold worked grain boundaries, i.e. the elongated bands, and the slip planes, were the most severely attacked. This rapid etching, i.e. chemical attack, around the precipitated carbides would have completely obscured any more "delicate " structures, such as recrystallized grains and annealing twins.

The micrographs of an almost completely annealed material showed much less chemical attack when exposed to the normal etching procedure for temper annealed material,(Fig.60a and Fig. 60b). Most of the carbides had already been redissolved. Optical examination also indicated that the samples shown in Fig. 56 and Fig.57 were also less severely attacked than the material which was annealed further, but this is perhaps not very obvious from the photomicrograph presented here. It is probable that at the short annealing times used for these two samples, eg. 1 sec. or 3 sec., the material only had a very short residence time in the sensitization region, thus permitting only minor precipitation.

Mechanical testing and X-ray diffraction results indicated that the temper annealed material was already partially recrystallized when 150,000 psi. tensile strength was reached and should have been completely recrystallized at 111,650 psi.

This was far from obvious, however, when the present etching techniques were used, and caused confusion during much of the experimental work. In order to reveal the recrystallized grain structure, the metallographic technique was slightly altered. The specimen seen in Fig. 60 (111,650 psi. tensile strength) was etched for a slightly longer than normal time, 20 seconds, and the photomicrographs were obtained with the surface slighly defocused. This revealed a fully recrystallized structure, superimposed on the carbide-streaked background, (Fig. 60 c and Fig. 60 d). The grains size observed was slightly smaller than the grain size of the original annealed material prior to cold work. Similar techniques were attempted with other specimens in the temper annealed series, but it was impossible to reveal any strain free nuclei of recrystallized austenite, as the chemical attack around the carbides completely obliterated any grain boundaries.

From the final sample it can be seen however, that conventional recrystallization did occur but, at the annealing temperatures used, carbide precipitation was very severe, obscuring the metallographic examination. This recrystallization could only be revealed by X-ray analysis as described in the next section.

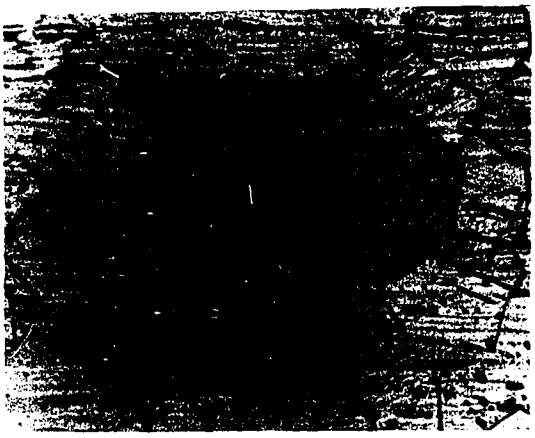

a

b

Fig. 51 Temper Rolled 301 steel — 2.87 Reduction
Tensile Strength — 102,500 psi.
Yield Strength — 50,800 psi.
Uniform Elongation — 55%
Total Elongation — 70%

a

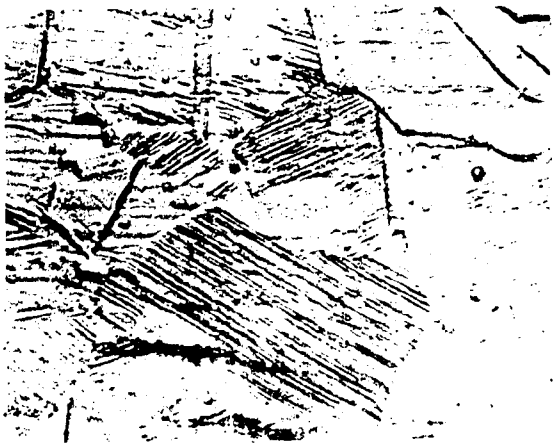

b

Fig. 52 Temper Rolled 301 steel — 11.4% Reduction
Tensile Strength — 121,800 psi.
Yield Strength — 74,400 psi.
Uniform Elongation — 44%
Total Elongation — 53%

a

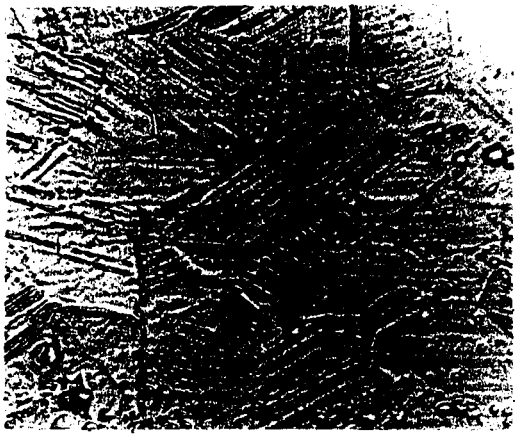

b

Fig. 53 Temper Rolled 301 steel 20.0% Reduction
Tensile Strength 134,600 psi.
Yield Strength 108,700 psi.
Uniform Elongation 31%
Total Elongation 41%

a

b

Fig. 54 Temper Rolled 301 steel 36.0% Reduction
Tensile Strength 165,800 psi.
Yield Strength 135,000 psi.
Uniform Elongation 1.2%
Total Elongation 20%

a

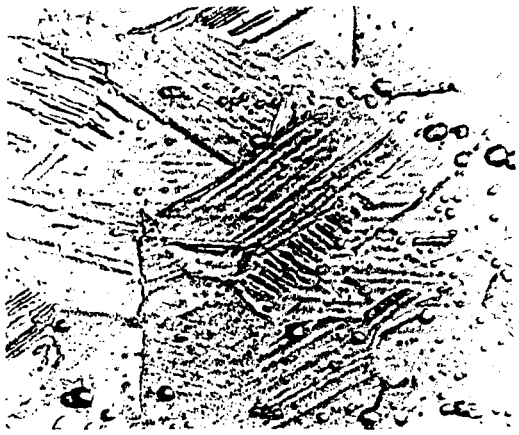

b

Fig. 53 Temper Rolled 301 steel — 20.0% Reduction
Tensile Strength — 134,600 psi.
Yield Strength — 108,700 psi.
Uniform Elongation — 31%
Total Elongation — 41%

a

b

Fig. 54 Temper Rolled 301 steel — 36.0% Reduction
Tensile Strength — 165,800 psi.
Yield Strength — 135,000 psi.
Uniform Elongation — 1.2%
Total Elongation — 20%

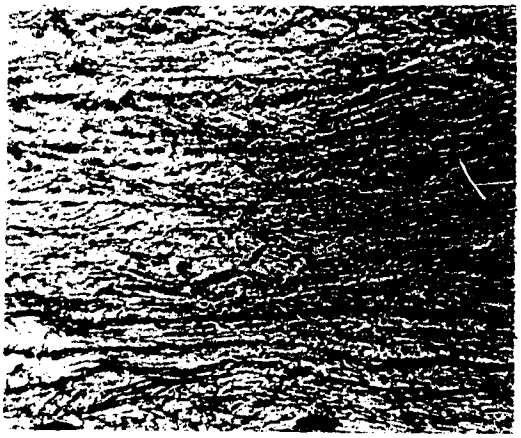

a b

Fig. 55 Temper Rolled 301 steel 79.5% Reduction
Tensile Strength 283,500 psi.
Yield Strength 250,200 psi.
Uniform Elongation 1.1%
Total Elongation 2.6%

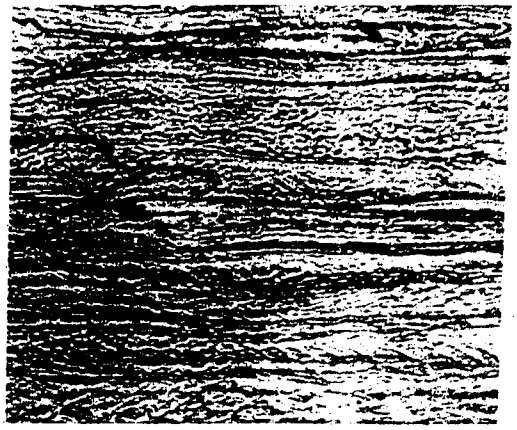

a b

Fig. 56 Temper Annealed 301 Steel 1 sec. at 850°C
Tensile Strength 266,600 psi.
Yield Strength 245,600 psi.
Uniform Elongation 1.5%
Total Elongation 3.6%

a

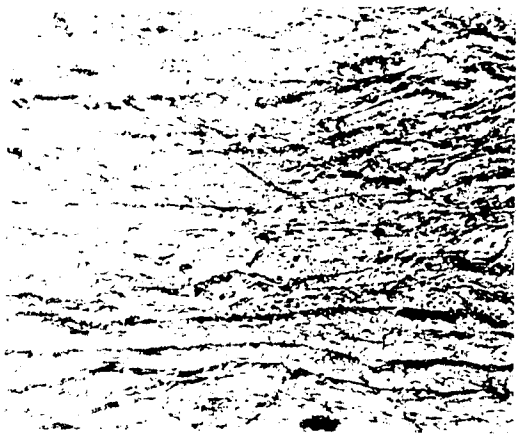

b

Fig. 55 Temper Rolled 301 steel — 79.5% Reduction
Tensile Strength — 283,500 psi.
Yield Strength — 250,200 psi.
Uniform Elongation — 1.1%
Total Elongation — 2.6%

a

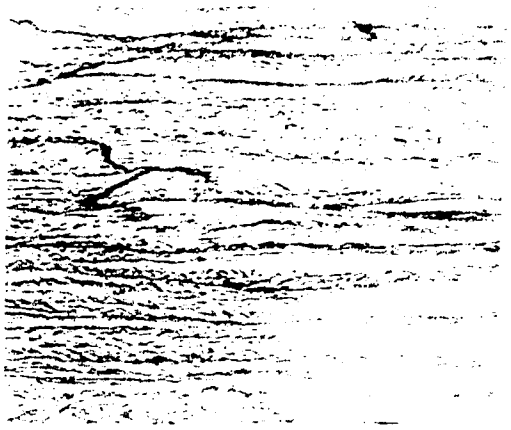

b

Fig. 56 Temper Annealed 301 Steel — 1 sec. at 850°C
Tensile Strength — 266,600 psi.
Yield Strength — 245,600 psi.
Uniform Elongation — 1.5%
Total Elongation — 3.6%

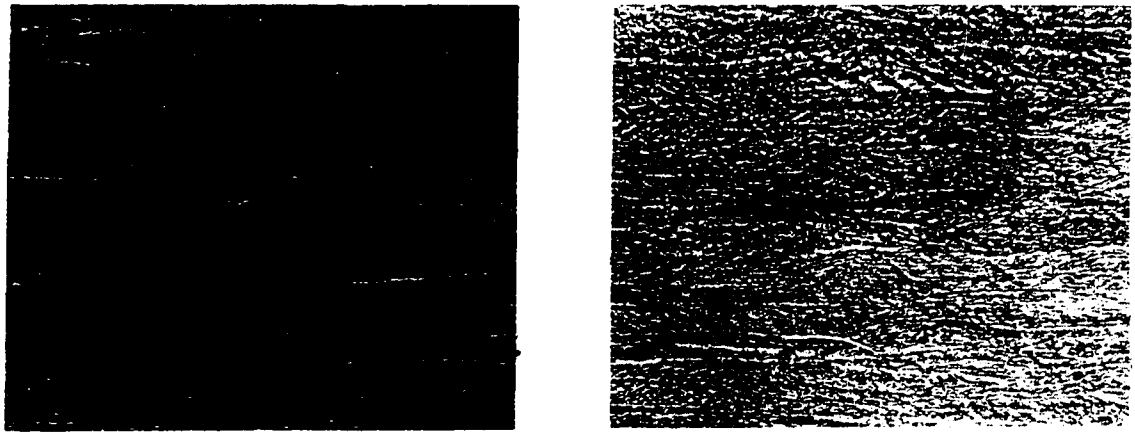

a b

Fig. 57 Temper Annealed 301 Steel 5 sec. at 850°C.

Tensile Strength	233,800 psi.
Yield Strength	215,400 psi.
Uniform Elongation	1.5%
Total Elongation	4.0%

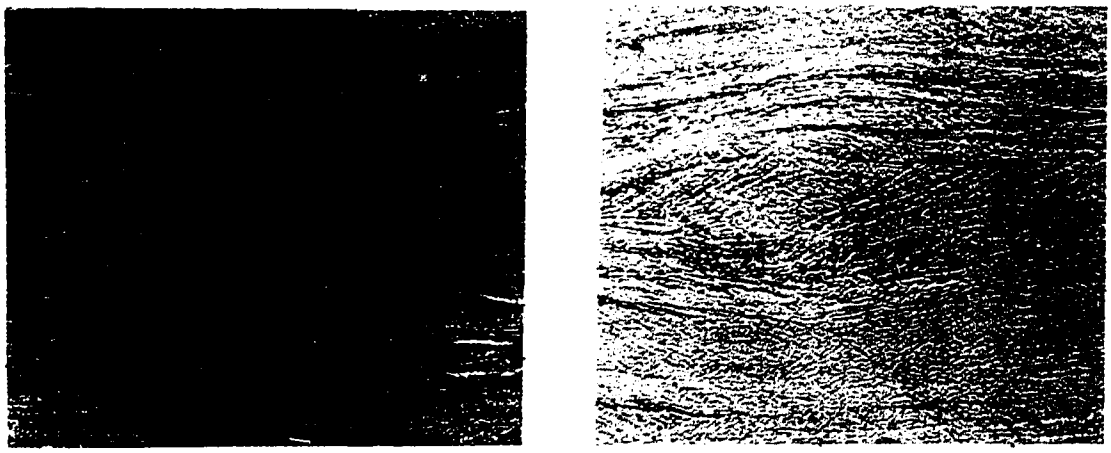

a b

Fig.58 Temper Annealed 301 Steel 12 sec. at 850°C.

Tensile Strength	173,500 psi.
Yield Strength	138,600 psi.
Uniform Elongation	1.5%
Total Elongation	19.0%

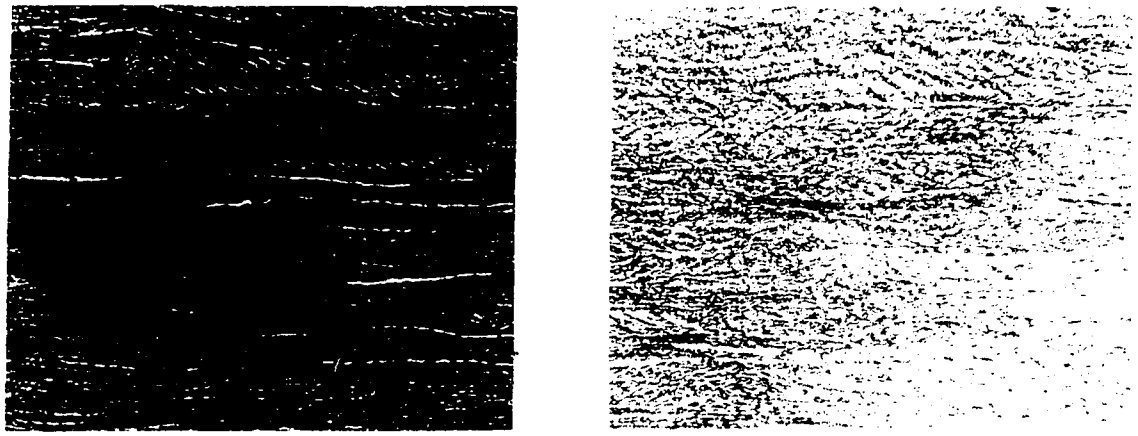

a b

Fig. 57 Temper Annealed 301 Steel 5 sec. at 850°C.

Tensile Strength	233,800 psi.
Yield Strength	215,400 psi.
Uniform Elongation	1.5%
Total Elongation	4.0%

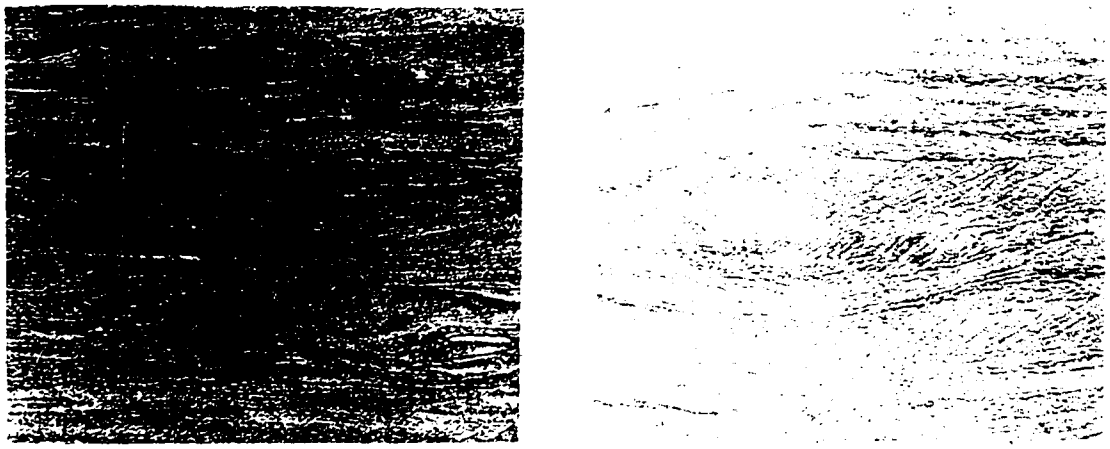

a b

Fig.58 Temper Annealed 301 Steel 12 sec. at 850°C.

Tensile Strength	173,500 psi.
Yield Strength	138,600 psi.
Uniform Elongation	1.5%
Total Elongation	19.0%

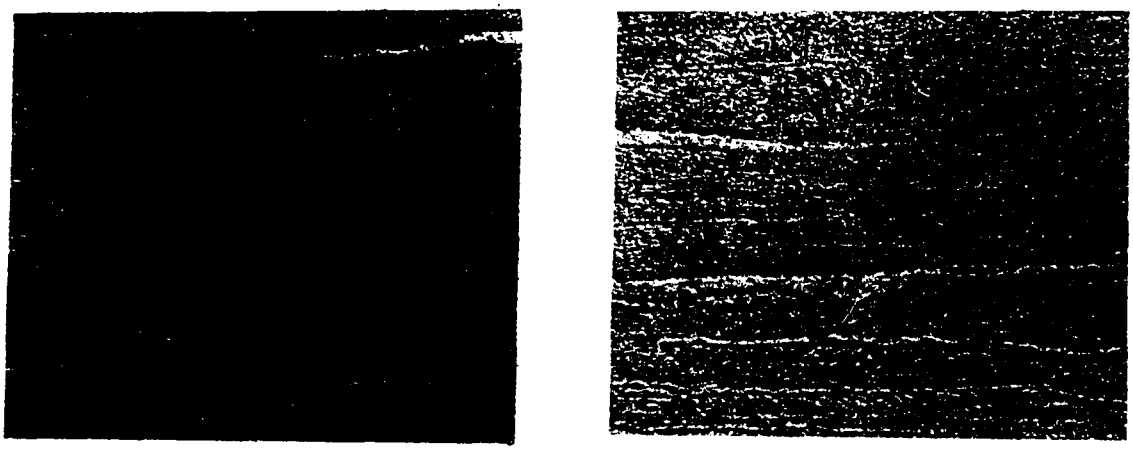

a b

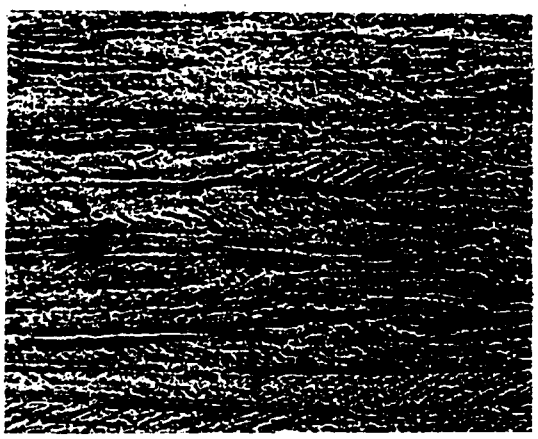

c

Fig. 59 Temper Annealed 301 Steel 45 sec. at 850°C.

Tensile Strength	134,700 psi.
Yield Strength	89,000 psi.
Uniform Elongation	41.0%
Total Elongation	45.0%

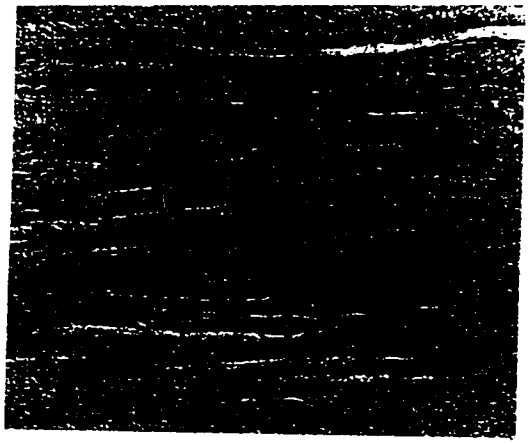

a

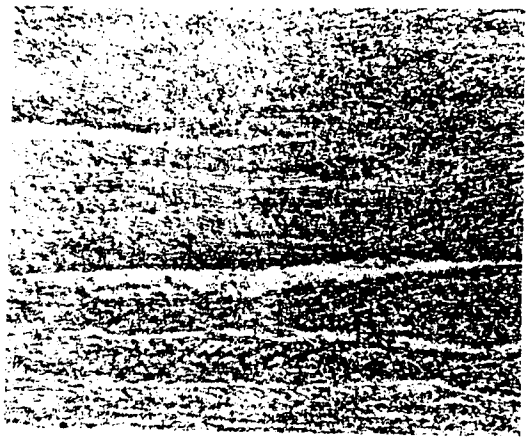

b

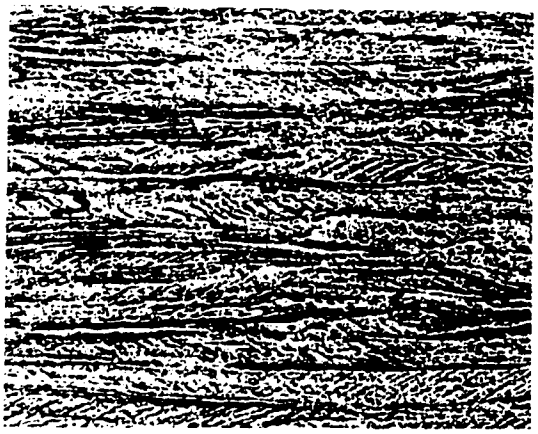

c

Fig. 59 Temper Annealed 301 Steel 45 sec. at 850°C.

Tensile Strength	134,700 psi.
Yield Strength	80,000 psi.
Uniform Elongation	41.0%
Total Elongation	45.0%

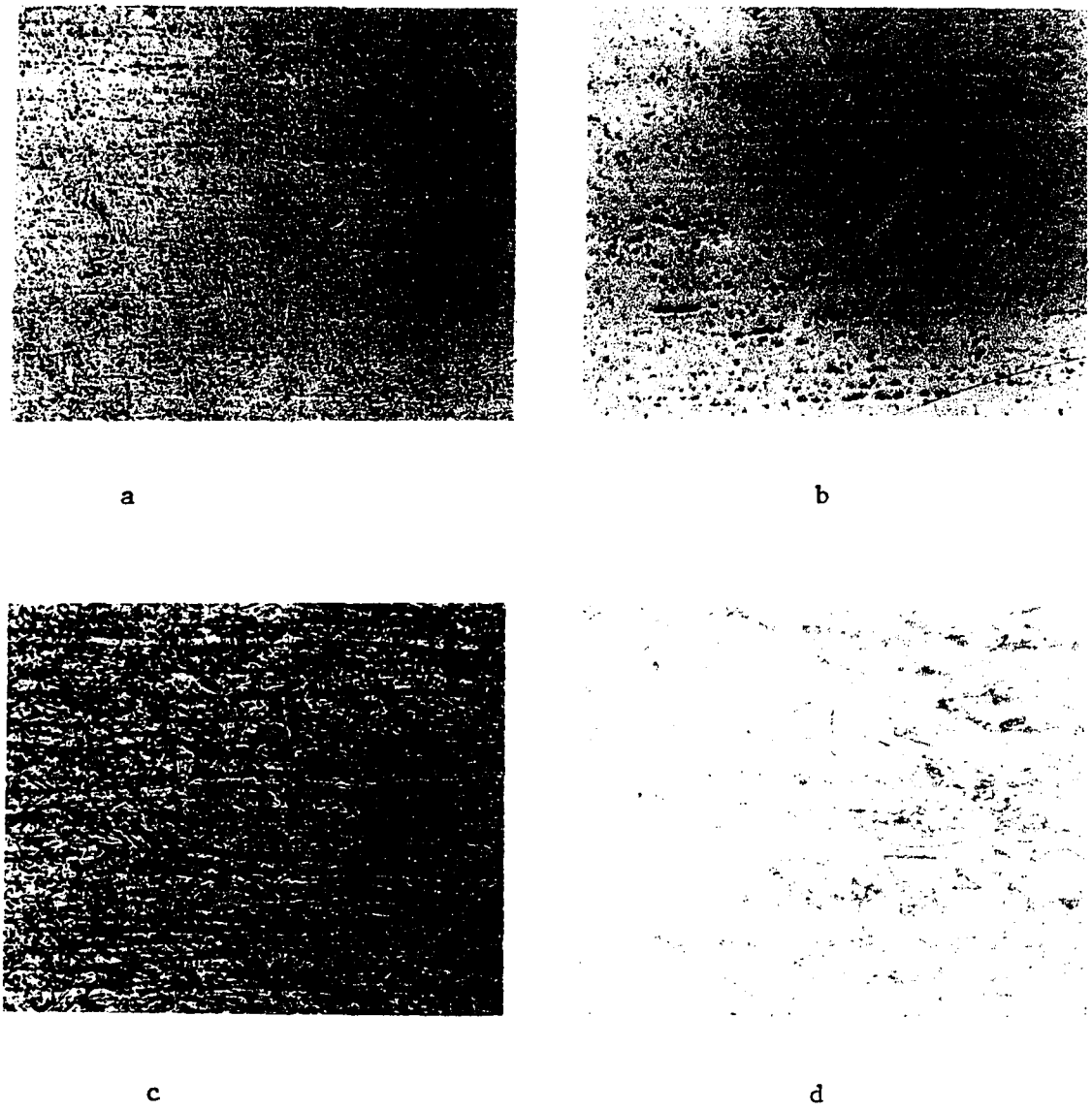

a b

c d

Fig. 60 Temper Annealed 301 Steel 900 sec. at 900°C
Modified Etching Technique

Tensile Strength	111,600 psi.
Yield Strength	44,100 psi.
Uniform Elongation	58.0%
Total Elongation	68.3%

a

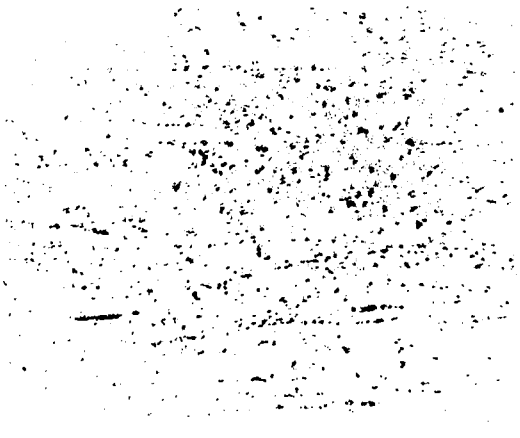

b

c

d

Fig. 60 Temper Annealed 301 Steel 900 sec. at 900°C
Modified Etching Technique

Tensile Strength	111,600 psi.
Yield Strength	44,100 psi.
Uniform Elongation	58.0%
Total Elongation	68.3%

G. X-Ray Analysis Results

The 2θ values found for the peak position of the austenite and martensite phases are given here for easy reference.

111 γ	110 α	200 γ	200 α	220 γ	211 α	311 γ	222 γ	220 α
55.7°	56.5°	65.2°	84.6°	99.3°	111.2°	126.7°	138.0°	145.3°

From these positions, the lattice parameters of the two phases were determined to be the following:

Austenite (γ) $a = 3.594$ Å

Martensite $a = 2.868$ Å

(ferrite equivalent α)

These values were used in the calculation of volume percents of the austenite and martensite as discussed in Sect. IV-6.

1) Temper Rolled Material:

The relative peak intensities of the reflections at different amounts of cold reduction are presented in Table X. The volume percent austenite (V_γ %), of these same materials, calculated from different peak comparisons, is presented in Table XI. In Fig. 61, these calculated volume percents of austenite are plotted against cold reduction. In order to more conveniently compare the properties of temper rolled and temper annealed materials,in Fig. 62, the same results were plotted against the tensile strengths of the specimens.

What is immediately apparent from the figures is that the results fell into two groups, the values using the 220 γ peak as the austenite indicator giving considerably higher readings for volume percent austenite. Results calculated on the basis of 200 γ and 311 γ peaks were very consistent, up to about 35% cold reduction (160,000 psi. tensile strength); further cold reduction produced considerable divergence of results, eg. at 63% cold reduction (200,000 psi. tensile strength), the volume percent austenite could have varied from 15% to 48%. Beyond about 70% reduction (240,000 psi. tensile strength), the results again converged, maintaining the same reading of about 1% austenite to full cold reduction of 80%.

One explanation for this wide divergence of results could have been the effect of crystallographic texture on peak intensities. As was indicated in Sec. IV-6, the rolling texture of austenitic stainless steel at room temperature had (110) parallel to the rolling plane (22,38,39). The (220 γ) plane, thus, also became parallel to the rolling plane when this material was cold rolled. A disproportionately high number of planes would have had this orientation. Since the x-ray beam was directed on this rolling plane, a high austenite analysis was expected if the (220 γ) reflection was used as an indicator of austenite content (52). For this reason the (220 γ) reflection was eliminated from consideration as a basis for austenite calculation.

It will be recalled for Sec. IV-6 that the annealing texture of austenite stainless steel was of the " Brass Type", i.e. (113 γ) parallel to the rolling plane (57). The intermediate anneal prior to final cold reduction could have produced this texture, so that any undistorted austenite grains would still have had this texture and thus the use of this reflection would have given a high austenite phase analysis. Durnin and Ridal maintained that the austenite analysis, using the (113 γ) gave results that agreed with magnetic analysis and that these higher index planes were expected to be less affected by texture. Their materials, however, did not have intermediate anneals after heavy cold reduction. The material was hot rolled to the gauge desired prior to cold reduction and the superimposed annealing texture would not have been observed.

The (200 γ) peak has not been reported to have been greatly affected by the presence of rolling texture. For austenitic stainless steel, cold rolled at room temperature, prior annealing texture should not affect the (200 γ) reflection.

Durnin and Ridal observed that if the 211 α peak was used for phase analysis, the austenite content was always reported higher than if the 200 peak was used for analysis. The same situation was also observed in the present work. Another texture effect considered was the rolling texture that could have been developed in the transformed martensite phase.

As stated in Sect. IV-6 , body centred cubic metals have the (100) plane oriented parallel to the rolling plane. Calculations involving this plane might have given disproportionately high ferrite (martensite) readings and therefore an incorrectly low austenite reading. The effect, however, was expected to be minimal (22).

From the shapes of the curves in Fig. 61 and 62 it can be seen that if attention is confined to those results obtained from using the (200 γ) reflections, an S-shaped curve is obtained. As tensile strength was increased to about 140,000 psi. by cold reduction, there was only a slight drop in austenite analysis. This corresponded to the region where the stress-elongation curve was smooth, without a sharp yield point, and characteristic of annealed FCC material. The martensite needles were a minor component in the soft austenite matrix. Beyond this strength, the rate of austenite content decrease increased sharply (an indirect autocatalytic effect (61)) and the austenite content decreased almost linearly to about 10% austenite at 220,000 psi. At this point the uniform elongation effectively disappeared, as can be seen from Fig. 40 and Fig. 44. If the (311 γ) peak had been used for analysis there would still have been 30% austenite indicated at 220,000 psi. tensile strength. The material would surely have had some ductility.

It was concluded from the previous discussion that the best combination of peaks to give true austenite content was 211 α vs 200 γ , at least for temper rolled materials.

TABLE X

Temper Rolled Material

Average Intensity Measurements (Arbitrary Units)

Versus Per Cent Cold Reduction

Cold Reduction %	311 γ	211 α	220 γ	200 α	200 γ
2.8	25.8	0.2	27.2	0.1	11.7
15.0	21.1	0.5	13.5	0.3	13.3
19.0	19.1	1.0	20.9	0.7	15.0
20.0	22.7	1.0	22.0	0.5	13.1
26.0	15.8	2.0	22.8	1.0	9.7
32.0	13.0	4.5	28.0	2.5	10.3
63.1	23.2	21.4	68.7	14.5	6.3
68.2	19.3	26.7	78.9	16.1	5.8
73.5	1	95.0	73.0	40.0	1
79.5	1	97.8	74.4	43.2	1

TABLE XI

Temper Rolled Material

Volume Per Cent Austenite Determined by

Direct Comparison of X-Ray Diffraction Peaks

of Austenite and Martensite Phases

Versus Per Cent Cold Reduction

$P = I_\alpha / I_\gamma$	$211_\alpha/311_\gamma$	$211_\alpha/220_\gamma$	$211_\alpha/200_\gamma$	$211_\alpha/311_\gamma$	$200_\alpha/220_\gamma$	$200_\alpha/220_\gamma$
$G = R_\gamma/R_\alpha$	1.18	0.549	0.862	3.28	1.529	2.400
$V_\gamma\% = \frac{100}{1+GxP}$	Volume Per Cent Austenite using different peak comparisons					
Reduction %						
2.8	99.0	99.5	99.0	99.0	99.5	98.5
15.0	97.5	98.0	97.0	95.5	97.0	95.0
19.0	94.0	97.5	94.5	89.0	95.0	90.0
20.0	95.0	97.5	94.0	93.0	96.5	91.5
26.0	85.5	95.5	85.0	81.0	93.5	80.0
32.0	71.0	92.0	72.5	61.5	88.0	63.0
63.1	48.0	85.5	25.5	33.0	75.5	15.0
68.2	38.0	84.5	20.0	27.0	76.0	13.0
73.5	1.0	58.5	1.0	1.0	54.5	1.0
79.5	1.0	58.0	1.0	1.0	53.0	1.0

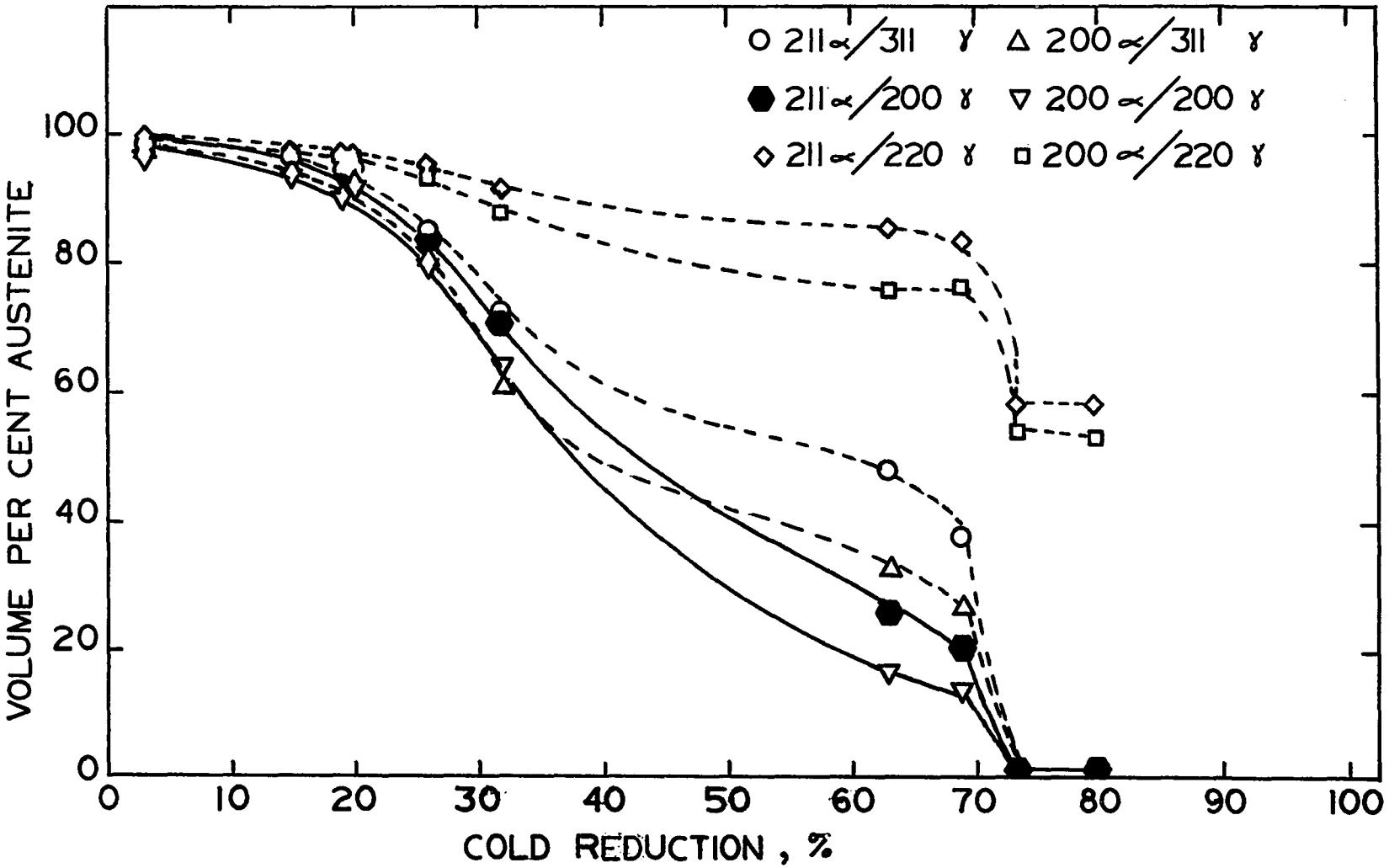

Fig. 61. Volume Percentage Austenite vs. Cold Reduction of AISI 301 steel.

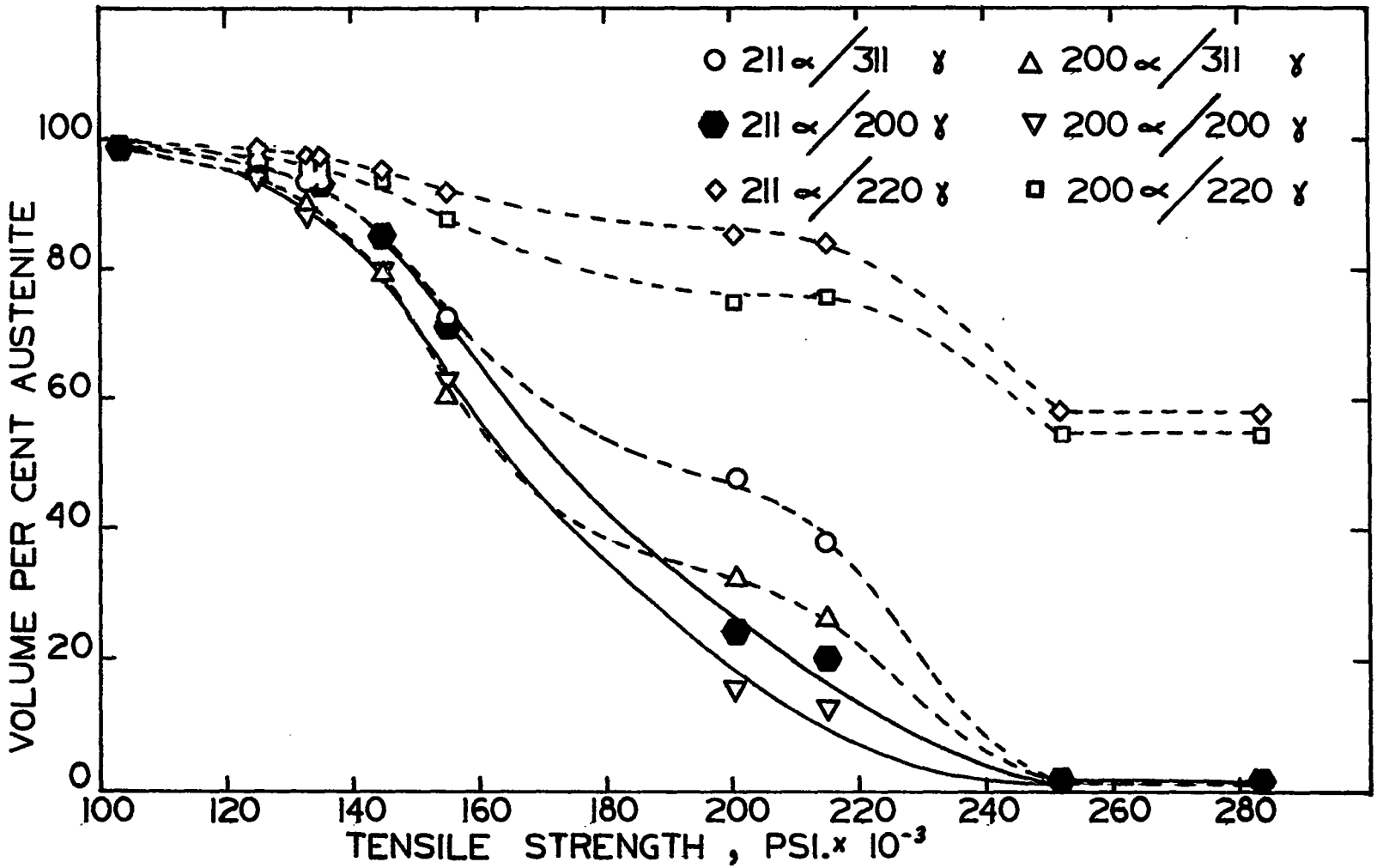

Fig. 62. Volume Percentage Austenite vs. Tensile Strength of Temper Rolled AISI 301 steel

2) Temper Annealed Material:

When analysing the austenite content of temper annealed material by x-ray diffraction, great divergence of results was again observed, depending on the combination of peaks used for analysis (Fig. 63). Of the six peak comparison choices which existed for the interpretation of austenite content, the following one was chosen as being the closest to the truth: 211 α vs 200 γ as shown by the solid symbols in Fig. 63. This was the same combination of peaks found most useful in the calculation of austenite analysis in the temper rolled material. The reasons for this choice may be summarized as follows.

a) The (220 γ) peak is heavily affected by rolling texture and it was thus rejected (22, 52, 57).
b) The (113 γ) peak is heavily affected by annealing texture and was thus also rejected (22, 57).
c) The (200α) peak is eliminated from consideration as it was affected by both rolling and annealind texture much more than the (211α) peak, although the effect was expected to be minor (22).
d) The (200 γ) peak of austenitic stainless steel, cold worked at room temperature, is not greatly affected by rolling or annealing texture. This peak was, thus , used as the austenite content indicator.

All the above arguements emphasized the effect of crystallographic texture, i.e. preferred orientation, on the measured peak intensities and the appropriate peak combination, 211α/200 γ, was chosen on this basis. It is proper to point out, however, that there was one factor in favour of using the 311 γ peak for austenite analysis. The austenite content results, found by using this peak, corresponded closely to the temper rolled data and since the mechanical properties of temper rolled and temper annealed materials were similar, it would have been expected that their phase analysis also be similar.

The data from which the above curves were derived are presented in Table XII and Table XIII .

TABLE XII

Temper Annealed Material

Average Intensity Measurments (Arbitrary Units)

Versus Annealing Time

Annealing Time In Sec.	311 γ	211 α	220 γ	200 α	200 γ
at 850°C					
Run No. 2					
3	0.1	14.0	3.5	7.0	0.1
5	0.1	12.5	5.6	6.2	0.1
10	3.3	4.5	11.0	4.2	0.2
15	4.5	1.7	14.5	1.0	0.2
30	3.6	1.4	16.9	0.8	0.4
45	5.1	0.8	19.4	0.4	0.8
60	9.9	1.5	7.8	0.3	2.7
Run No. 4					
300	-	-	-	-	-
at 900°C					
Run No.5					
300	26.2	0.0	28.2	0.0	12.2
900	29.0	0.0	31.1	0.0	14.2

TABLE XIII

Temper Annealed Material

Volume Per Cent Austenite Determined by Direct Comparison on X-Ray Diffraction Peaks of Austenite and Martensite Phases versus Annealing Time

Annealing	$P = \frac{I\alpha}{I\gamma}$					
Time in sec. at 850°C	$211_\alpha/311_\gamma$	$211_\alpha/220_\gamma$	$211_\alpha/200_\gamma$	$200_\alpha/311_\gamma$	$200_\alpha/220_\gamma$	$200_\alpha/200_\gamma$
$G = R\gamma/R\alpha$	1.18	0.549	0.862	3.28	1.529	2.400
Run No. 2	Volume Percent Austenite using different peak comparisons - $V\gamma\%$					
3	0.5	31.0	0.5	0.5	24.5	0.5
5	1.0	45.0	1.0	0.5	37.0	1.0
10	38.0	82.0	5.0	19.0	63.5	2.0
15	68.0	94.0	15.0	56.0	90.0	9.5
30	69.0	96.0	25.0	59.0	93.5	17.5
45	84.5	98.0	55.0	79.5	97.0	46.5
60	84.5	90.5	67.0	90.0	94.0	77.0
Run No.4						
300	93.0	98.0	81.5	97.0	99.5	97.0
at 900°C						
Run No. 5						
300	100	100	100	100	100	100
900	100	100	100	100	100	100

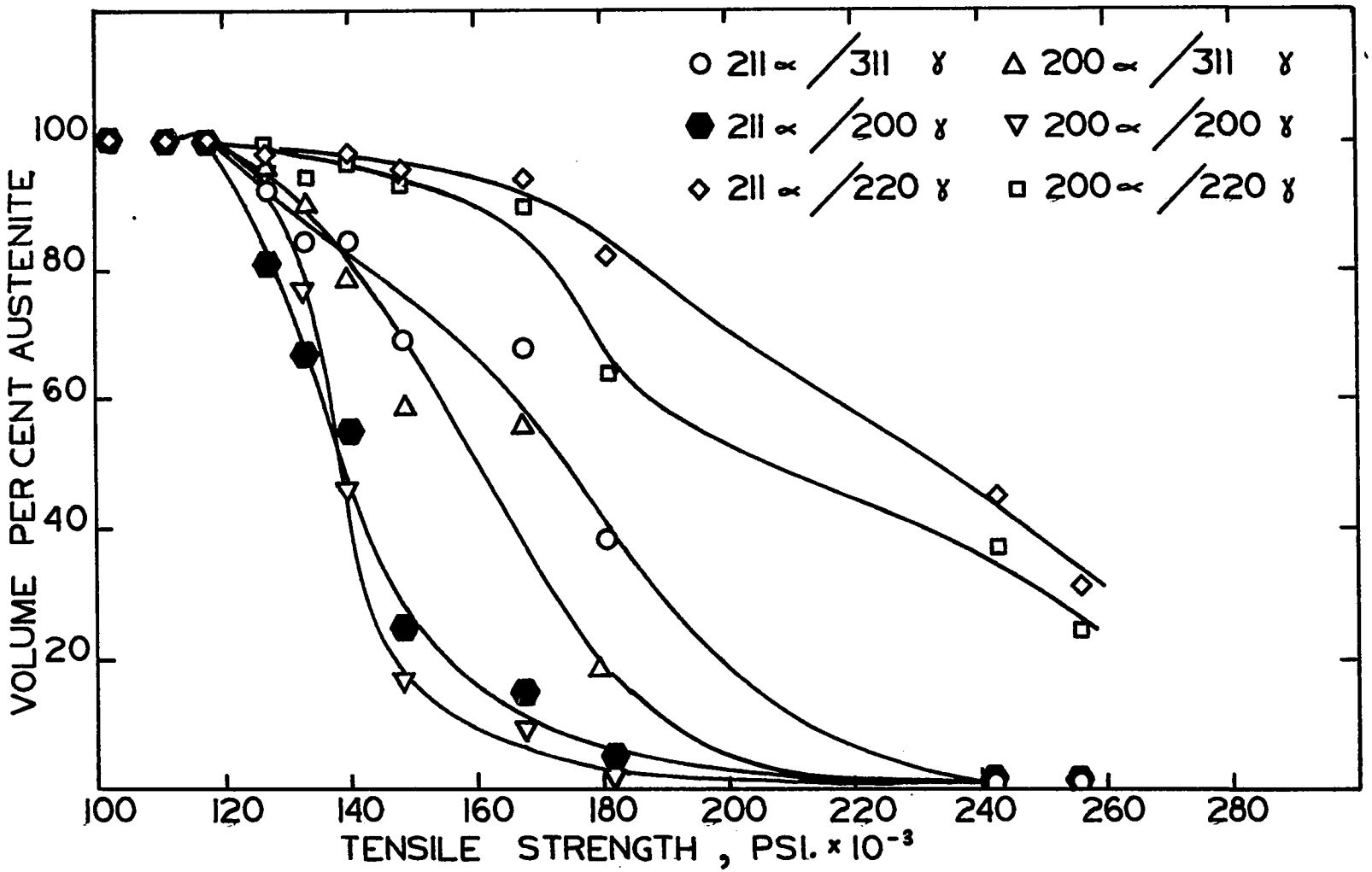

Fig. 63. Volume Percentage Austenite vs Tensile Strength of Temper Annealed AISI 301 steel

3) Back Reflection X-Ray Diffraction Analysis

In order to observe the degree of recrystallization in the various specimens, back reflection X-ray analysis was performed. The results of this analysis, in certain significant cases, were as follows:

Fig. 64 - shows the features of a fully cold worked structure, (80% reduction). Both austenite and martensite phase diffraction rings disappeared into the background which was largely due to fluorescence and scattered radiation.

Fig. 65 - shows an extensively cold worked structure, (68% reduction). Two diffuse austenite rings (311 γ and 222 γ) and one diffuse martensite ring (220α) were observed.

Fig. 66 - shows a specimen partially annealed to 149,000 psi. tensile strength. Two continuous austenite rings (311 γ and 222 γ), considerably sharper than found in Fig. 66, were observed. This sharpening was presumably due to recovery in the cold worked structure. No martensite ring was observed, but the (220 α) reflection was weak even in the hardened condition.

Fig. 67 - shows a specimen partially annealed to 133,600 psi. tensile strength. Two predominantly spotted austenite rings were observed. This was characteristic of an almost completely recrystallized austenite structure.

These x-ray films aided in the interpretation of the metallographic findings. A material of 133,000 psi. tensile strength appeared as cold worked under the microscope, due to the heavy carbide precipitation. In reality, considerable recrystallization had already occurred as could be seen in Fig. 67 (also seen later in Fig. 69).

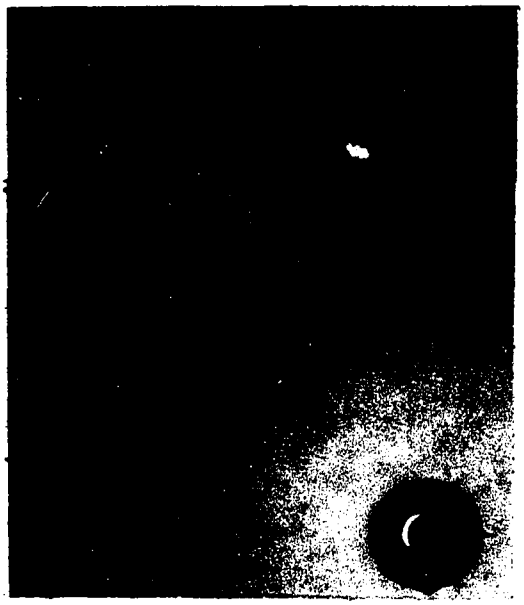

Fig. 64 Back Reflection X-Ray Analysis

Temper Rolled 79.5%
301 Steel

Tensile Strength	283,600 psi.
Yield Strength	274,000 psi.
Uniform Elongation	0.5%
Total Elongation	0.9%

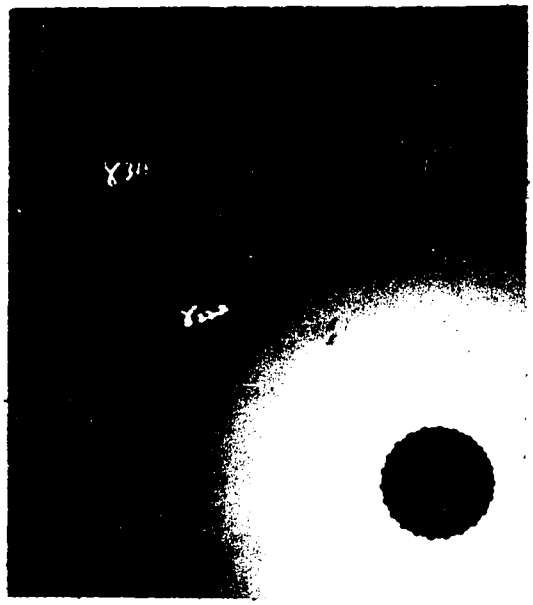

Fig. 65 Back Reflection X-Ray Analysis

Temper Rolled 68.2%
301 Steel

Tensile Strength	214,900 psi.
Yield Strength	195,600 psi.
Uniform Elongation	1.0%
Total Elongation	3.2%

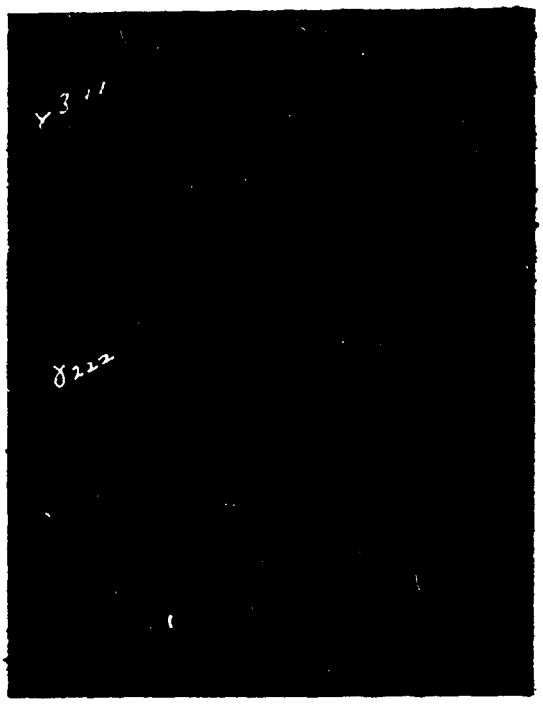

Fig. 66 Back Reflection X-Ray Analysis
Temper Annealed 301 Steel
30 sec. at 850°C.

Tensile Strength	148,600 psi.
Yield Strength	110,100 psi.
Uniform Elongation	30.0%
Total Elongation	41.0%

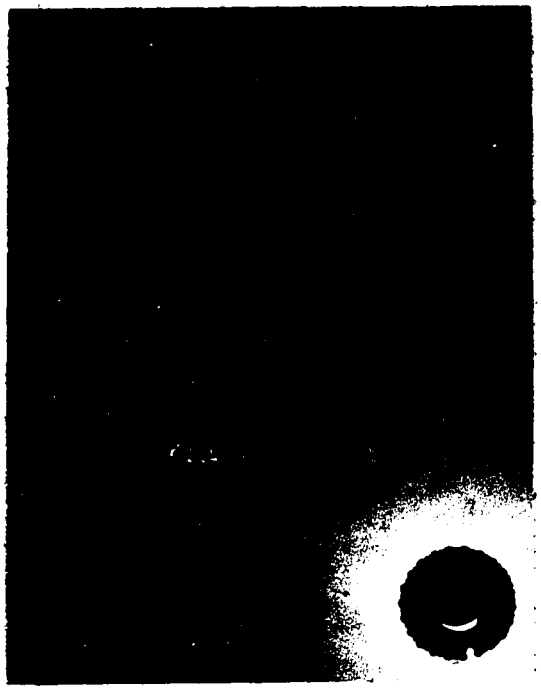

Fig. 67 Back Reflection X-Ray Analysis
Temper Annealed 301 Steel
60 sec. at 850°C.

Tensile Strength	133,600 psi.
Yield Strength	79,500 psi.
Uniform Elongation	41.0%
Total Elongation	48.0%

4) Transmission X-Ray Diffraction Analysis:

In an attempt to determine the extent of preferred orientation in some of the specimens, transmission X-ray analysis was conducted using the same samples that were used for the back reflection pictures illustrated in Fig. 66 and Fig. 67.

Fig. 68 - shows a specimen partially annealed to 149,000 psi. tensile strength. The specimen was observed with the x-ray beam perpendicular to the rolling plane. One continuous austenite ring was observed (111 γ). One ferrite ring (110 α) should have existed within the (111 γ) circle, but it was not observed.

Fig. 69a - showed a specimen partially annealed to 133,600 psi. tensile strength. The specimen was observed with the x-ray beam again perpendicular to the rolling plane. One spotted austenite ring was observed (111 γ), indicating recrystallization, but no obvious preferred orientation.

Fig. 69b - Shows the same specimen partially annealed to 133,600 psi. tensile strength, but this time the specimen was rotated 15^{o} about the vertical axis prior to being exposed to the x-ray beam. One spotted austenite ring was observed (111 γ), but again no preferred orientation.

Virtually no texture was observed in any of the above samples. Only very slight variations in intensity were observed around the diffraction circle. This apparent lack of texture is surprising, since a material annealed from a fully cold worked condition of 80%, should exhibit considerable annealing texture (22 p.568). Perhaps this observation was due to some inadequacy of the technique employed. Structural changes could have occurred during the specimen thinning process or perhaps the extreme interior layers of the samples, thoses exposed by specimen thinning, were the least affected by coldwork as well as subsequent annealing.

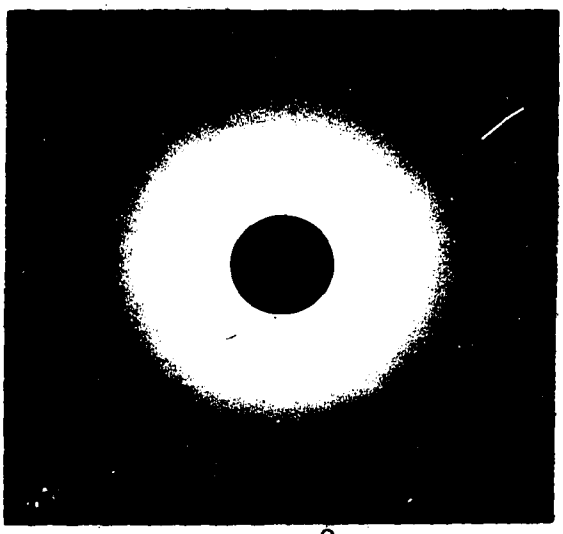

0° Rotation

Fig. 68 Transmission X-Ray Analysis

Temper Annealed 301 Steel

30 sec. at 850°C.

Tensile Strength	148,600 psi.
Yield Strength	110,100 psi.
Uniform Elongation	30.0%
Total Elongation	41.0%

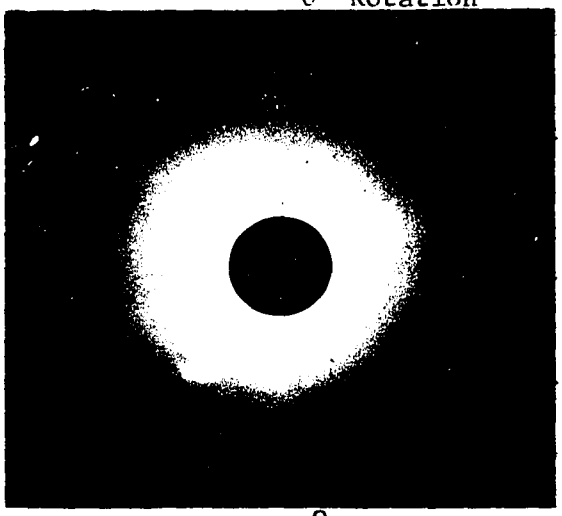

0° Rotation

Fig. 69 Transmission X-Ray Analysis

Temper Annealed 301 Steel

a. 60 sec. at 850°C.

Tensile Strength	133,600 psi.
Yield Strength	79,500 psi.
Uniform Elongation	41.0%
Total Elongation	48.0%

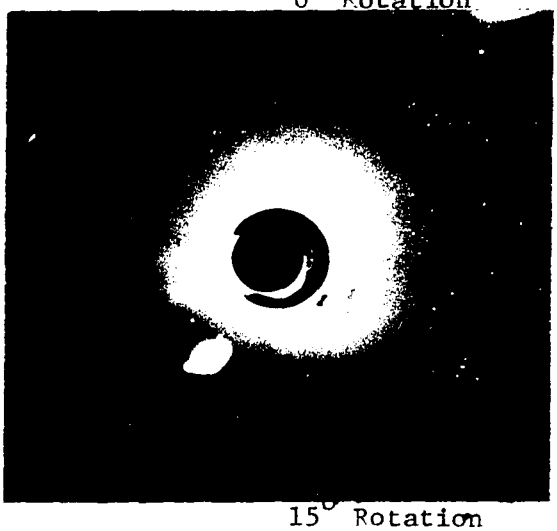

15° Rotation

b.

5) Summary of X-Ray Analysis Results:

The film results suggested that the use of (200 γ) peak for austenite indication was the correct choice (Fig. 63). At 149,000 psi. tensile strength no recrystallization was observed. The 25% austenite present at this strength level was less likely to be visible in the x-ray films than the 75% or 95% austenite content indicated by the other comparisons. At 133,600 psi., a recrystallized structure was observed (Fig. 64), as would have been expected from an indicated 70% austenite content. The solid symbol curve in Fig. 63 also reflected the rapid increase in recrystallized austenite as the material was annealed from 149,000 psi. to 133,000 psi. tensile strength.

The volume percent austenite of temper rolled and temper annealed material (calculated using the 211 α to 200 γ peak comparison in both cases) is indicated in Fig. 70. The difference between the two curves is unexpected when it is considered that the more ductile material (temper annealed) should have had more of the more ductile phase (austenite) at a given strength level. The reverse is indicated in Fig. 70. This might have been a factor in the previously mentioned anomalous hardness effect (Sect. V-d). Perhaps the stronger phase, when in a stress relieved condition, is more ductile than the more plastic phase when cold worked.

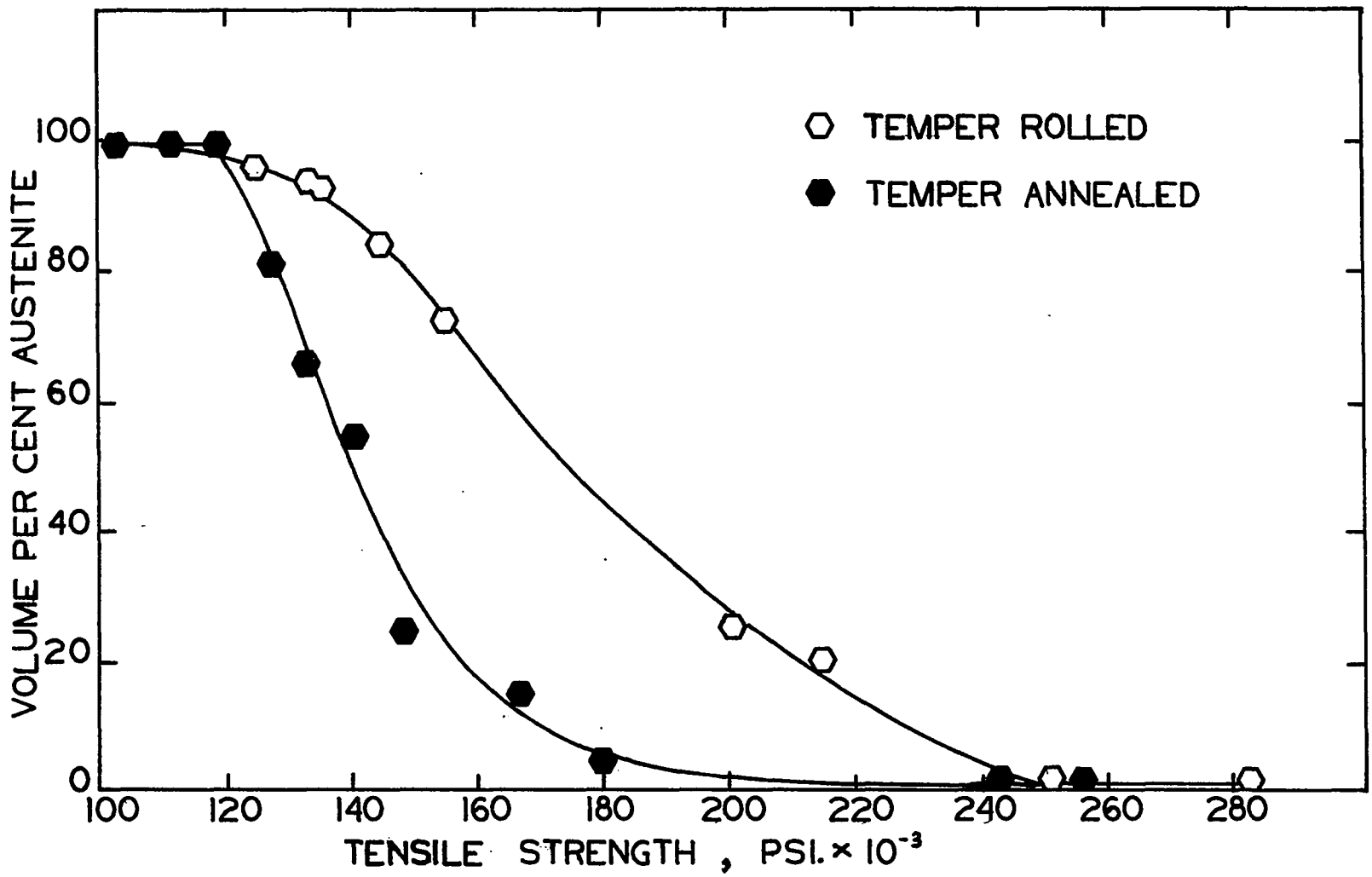

Fig. 70. Volume Percentage Austenite vs. Tensile Strength of Temper Rolled and Temper Annealed AISI 301 steel - Determined by Direct Comparison of 211α/200γ peaks.

H. Discussion of S. Adams' Model for Annealing in Light of the Present Work.

A model describing the relationship between mechanical properties of metals and the degree of cold work or annealing was developed by S. Adams concurrently with the present work. Adams' treatment is reproduced in Appendix A and the findings were summarized in Sect. I-C.

Adams attempted to estimate the mechanical properties of metal sheet at various stages of temper rolling and at various stages of temper annealing, using only the readily available data of the fully annealed and fully hardened states.

His analysis is that of a two constituent structure, each constituent having markedly different mechanical properties. The data used, referred to, of course, to the annealed and fully cold worked conditions of the same structural phase, i.e. no crystallographic phase change was induced during work hardening. Only normal necking was encountered in his work and thus the total elongation was a predictable function of the uniform elongation.

In order to compare materials with widely varying mechanical properties, the tensile strengths and elongations were expressed in normalized form as discussed previously (Sect. I-C), i.e.

$$1)\quad Fs = \frac{S - So}{St - So} \qquad 2)\quad Fe = \frac{(\epsilon_u) - (\epsilon_u)_T}{(\epsilon_u)_o - (\epsilon_u)_T}$$

When normalized tensile strength, Fs was plotted against normalized elongation, Fe, the temper annealing data was very similar for a wide variety of materials (Fig. 16). What did vary considerably, however, was the temper rolling data.

The key parameter was found to be Fs*, the normalized tensile strength at which uniform elongation effectively disappeared i.e. Fe = 0. The tensile strength is expressed as 4) $Fs^* = (\epsilon_u)o \frac{So}{St-So}$. The lower the value of Fs*, the greater was the divergence between the temper rolled and temper annealed curves and therefore the greater the benefits of temper annealing. From equation (4) it can be seen that Fs* is reduced if:

1. $(\epsilon_u)o$ is small, i.e. annealed uniform elongation is small.
2. So/St is small, i.e. rapid strain hardening
3. St is large, i.e. the effect is greater if the material is heavily cold worked.

The material used in the present work, 301 stainless steel, is characterized by:

a. Very large $(\epsilon_u)o$ and $(\epsilon_T)o$: 0.57 and 0.73 respectively
b. Small So/St : 0.36
c. Large St : 283,500 psi.

These mechanical properties would have opposing effects on Fs*. Two of the factors are "favorable" for significantly increasing ductility through temper annealing (b and c). One factor is expected to have a " detrimental" effect (a).

A comparison of the pertinent mechanical properties of the 301 stainless steel, mild steel (3), copper (1), brass (62) and Al-Mg Alloys (2) is given in Table XIV .

Mild steel is a material which shows good elongation improvement after temper annealing and this is reflected in a low value of Fs*, eg. about 0.25 when using $(\epsilon_u)o$ and about 0.30 when using $(\epsilon_T)o$. On the other hand, tough pitch copper is a material which shows very little ductility improvement with temper annealing and this is reflected in a high value of Fs*, eg. about 0.60 when using $(\epsilon_T)o$.

The Fs* value of Brass (Fs* = 0.59) would predict a similar small improvement in ductility with temper annealing. Judging from the Fs* value of about 0.50, the improvement in properties for aluminum alloys 57S and 54S produced by temper annealing is expected to be better than for Brass - probably significantly so, but certainly not approaching that of mild steel. The experimental result of these materials, as indicated in Fig. 1,2,3,4, confirm to the above conditions.

In the case of 301 stainless steel, the experimental and Theoretical Fs* values agreed very closely when $(\epsilon_u)o$ was used in the calculation. The low Fs* value of 0.30 would predict good temper annealing properties. This, however, was found not to be the case, as was seen in Fig. 44 and 45. There were only modest ductility improvements brought about by temper annealing. It must be recalled, however, that at the tensile strength where uniform elongation effectively disappeared, i.e. Fs*, discontinuous necking began. If the Fs* is recalculated with the maximum tensile strength, St, being the strength at the start of discontinuous necking, i.e. about 160,000 psi:

$$Fs^* = (\epsilon_u)o \frac{So}{St-So} = 0.57 \times \frac{101,000}{64,000} = 0.91$$

The expected ductility improvement would thus be even less than observed.

The theoretical and experimental values of Fs* calculated with the use of $(\epsilon_T)o$ values do not agree very well. The theoretical value of Fs* = 0.40 would indicate considerable possible improvement in ductility with temper annealing. The experimental value of Fs* = 0.60 seems to reflect the actual modest improvement in mechanical properties.

In examining the Tensile Strength vs Eu% curve in Fig. 44, it is seen that this partial annealing curve is shaped slightly different from those shown in Figs. 1,2,3,4. The drastic softening from 283,000 psi. to 215,000 psi., (about 1/3 of the strain hardening produced during temper rolling) produced no increase in elongation at all.

This would indicate that, at these high strengths, another softening process, other than recovery or recrystallization was taking place. Carbide precipitation was probably occurring, so that the strain in the martensite was removed but no improvement in ductility was observed because of the presence of the precipitated carbides. Total elongation did not improve until discontinuous yielding started to occur below 215,000 psi. Uniform elongation was not improved until about 160,000 psi. was reached. It can be visualized from Fig. 44 that if a normal annealing curve started at 283,500 psi, instead of 215,000 psi., a considerable improvement in ductility would have occurred, as reflected in the Fs* value of 0.40.

It is impossible to assess the value of S. Adams' annealing model from the present experimental material. Here, in addition to the processes of simple strain hardening, recovery, recrystallization, and grain growth encountered in previous work (1,2,3), following factors were added:

1. Crystallographic phase changes occurred during cold reduction and annealing of cold worked material.
2. Carbide precipitation occurred during annealing.
3. Discontinuous yielding occurred during mechanical testing in a range of tensile strengths.

The material used in the present work was thus a complex alloy, yielding results which were difficult to accomodate to a theoretical model. Stainless steels which would, perhaps, be easier to deal with, from the theoretical point of view, would be AISI 304 or a low carbon AISI 305, alloys which are stable at room temperature to austenite decomposition and are less susceptible to carbide precipitation.

TABLE XIV

Comparison of Critical Mechanical Properties of the Materials Discussed in Adams' Model for Temper Rolling and Temper Annealing

Mechanical Property	301 Steel	Mild Steel	Copper	Brass	Al-Mg Alloys	
$(\epsilon_u)_o$	0.57	0.29	0.30	*	*	*
$(\epsilon_u)_T$	0.01	0.01	0.01	*	*	*
$(\epsilon_T)_o$	0.73	0.35	0.40	0.54	0.23	0.23
$(\epsilon_T)_T$	0.02	0.02	0.02	0.03	0.05	0.05
S_o, psi	101,000	55,000	35,000	49,000	28,000	37,500
S_T, psi	283,500	116,500	60,000	101,000	42,000	54,000
S_o/S_T	0.36	0.47	.58	.49	.66	.69
S^*, psi $\epsilon_T \doteq 0$	210,000	73,000	50,000	80,000	35,000	49,000
F_s^* TH. $(\epsilon_u)_o$	0.32	0.26	0.42	*	*	*
F_s^* EXP. $(\epsilon_u)_o$	0.30	0.24	0.40	*	*	*
F_s^* TH. $(\epsilon_T)_o$	0.40	0.31	0.56	0.51	0.46	0.53
F_s^* EXP. $(\epsilon_T)_o$	0.60	0.30	0.60	0.59	0.50	0.57

* Not Available.

I. Some Comments in Retrospect

It was discovered during the course of this work that carbide precipitation could not be avoided during temper annealing no matter how quickly the sensitization range was traversed in reaching the experimental temperature. Lower annealing temperatures, even in the severely sensitization temperature range, could have been used. The experimental conditions could thus have been more easily controlled; the annealing times would have been in minutes, not in seconds as necessitated by the high annealing temperatures in the present work.

An alternative annealing technique could have been used. Specimens could have been held at the desired temperatures for, say, one hour, the annealing temperatures being progressively increased from about 500°C to 1000°C. Carbide precipitation would have occurred, of course, but only the mechanical properties would have been of interest. If these properties were found to be commercially useful, corrosion resistance could be maintained by stabilizers like Columbium, in any steel developed to make use of these properties.

Carbide precipitation probably severely restricts grain growth. As annealing temperature were raised from 850°C to 900°C, marked softening was obtained, due, presumably, to greater austenite content as well as a larger recrystallized grain size. If the annealing temperature had been lowered to below 850°C, the effect of carbides on grain growth and phase transformation would have been expected to be even more marked.

Austenite/martensite phase analysis by x-ray diffraction techniques proved very complex due to the great degree of preferred orientation produced in the experimental specimens.

Magnetic analysis might have been usefully employed in analysing specimens in the middle of the analysis range.

The extent of discontinuous yielding, as experienced in this type of stainless steel, is greatly affected by strain rate. A more rapid strain rate could have, perhaps, completely eliminated discontinuous yielding, thus producing normal necking. The data could have thus been directly comparable over the full testing range. Necking is also affected by the shape of the specimen, but in the present work, the material was limited to flat strip, shaped to ASTM specification E-8.

Any of the above suggestions might have made the experimental technique easier, but it is doubtful if the results would have been any more suitable for theoretical analysis, due to the complex metallurgy of AISI 301 Stainless Steel. The examination of a more stable steel would have been more useful.

Section VI

SUMMARY AND CONCLUSIONS

VI SUMMARY AND CONCLUSIONS

AISI 301 stainless steel was cold reduced various amounts up to 80%, in order to obtain a full range of tempers for temper rolled material. Material, which had been cold reduced 80%, was annealed at 850°C and 900°C for varying lengths of time to obtain a similar range of tempers; this was termed temper annealing. The mechanical properties of temper rolled and temper annealed materials were compared and the results may be summarized as follows:

1. AISI 301 steel is characterized by very rapid strain hardening, eg. 80% cold reduction increases tensile strength from 101,000 psi. to 283,600 psi. and increases yield strength even more spectacularly, from 40,000 psi. to over 260,000 psi.

2. The rapid rate of strain hardening was due to the formation of strain induced martensite during cold work.

3. Heavily rolled (80% reduction) material was temper annealed at 850°C, a very high annealing temperature. Good reproducibility of results was achieved over four separate runs. A few specimens were annealed at 900°C for comparatively long holding times in order to achieve more rapid grain growth, so that a grain size, approaching that of the pre-cold worked state, could be achieved.

4. The rapid loss of strength, without a corresponding increase in ductility, obtained by temper annealing of heavily worked material, was believed to be due to carbide precipitation from the martensite phase. This martensite subsequently changed to the more ductile phase, austenite.

5. When testing both the temper rolled and temper annealed materials, three distinct stress- elongation curves were obtained:

   a) A smooth curve, without yield point, characteristic of annealed FCC material was observed up to about 140,000 psi. tensile strength (Fig. 36).

   b) Discontinuous yielding was observed in the range of tensile strengths of about 140,000 to 200,000 psi.(Fig. 37).

   c) A curve characteristic of brittle failure was observed above 200,000 psi. (Fig. 38).

6. Due to the occurrence of discontinuous yielding, the total elongation was considered a misleading indicator of formability, eg. at a tensile strength of 155,000 psi., the total elongation was 33%, while the uniform elongation was only about 1%. The material could not be considered ductile.

7. The temper annealed material showed a modest but useful improvement in both total and uniform elongations when compared to temper rolled material of the same tensile strength up to about 210,000 psi. Although the absolute improvement achieved was only 15% of uniform elongation, the relative improvement was from 10% to 25% uniform elongation, representing an increase of 150%. Beyond 210,000 psi. tensile strength, no improvement was found.

8. Hardness is not a good indicator of ductility or formability. It is however, a closer measure of tensile strength. In the present work, an anomalous hardness effect was observed. The more ductile material (temper annealed) was harder than the less ductile material (temper rolled) at the same tensile strength (Fig. 48).

9. The yield strength to tensile strength ratio (ys/ts) was believed to be a good indicator of formability (3), a low ratio indicating a large amount of uniform plastic flow available for fabrication. The temper annealed material showed a lower ys/ts ratio up to about 180,000/200,000 psi. tensile strength.

10. Metallographic observations may be summarized as follows: The martensite formed by cold work had the appearance of deformation twins. Beyond 40% cold reduction, the structure became indistinct and appeared as bands, parallel to the rolling direction. The temper annealed material retained the banded structure. This appearance was believed to be due to severe etching attack surrounding the chromium carbide precipitates formed at grain boundaries and slip planes during annealing. This severe attack obliterated the more delicate structures, such as the boundaries of recrystallized grains or annealing twins. Special etching techniques revealed recrystallized grains, superimposed on the precipitate structure. But even this observation was only achieved after the majority of the carbides were redissolved.

11. The analysis of austenite volume percent was achieved by using a direct comparison x-ray diffraction technique. The intensities of the diffraction peaks were greatly affected by both rolling and annealing textures, and this could not be completely overcome by spinning of the sample. The 211 α /200 γ peak comparison was decided upon as being suitable for the analysis of both temper rolled and temper annealed material.

12. Using this peak comparison, it was observed that temper annealed material contained less of the more ductile austenite phase than temper rolled material of the same tensile strength. This condition is unexpected since the temper annealed material was more ductile at these same strengths.

13. Recrystallization of strain free grains was revealed using back reflection x-ray diffraction and transmission x-ray diffraction techniques. Optical metallographic techniques did not reveal these new grains, except a highly advanced states of recrystallization.

14. S. Adams predicted that temper annealing curves, when expressed in normalized form, should be almost the same for a wide variety of materials. The key parameter was said to be Fs*, the normalized tensile strength at which uniform elongation disappears with increasing cold work. A low value of Fs* for a material would indicate significantly greater ductility in temper annealed material. The most significant mechanical properties affecting Fs* were found to be $(\epsilon_u)o$, So/St, St. His analysis would permit the **forecasting** of the mechanical properties of the full range of temper rolled and temper annealed material from only the properties of their fully annealed and fully hardened states. One property cannot fully predict mechanical behavior, but a combination of properties expressed in the formulas presented by Adams (noteably $Fs^* = (\epsilon_u)o \frac{So}{St-So}$, can successfully predict temper rolled or temper annealed tensile strengths and elongations.

15. It was difficult, however, to evaluate the accuracy of Adams' model for mechanical properties from the data of the present work.

The material was too complex for meaningful comparisons with theory. Crystallographic phase changes, carbide precipitation, and discontinuous yielding were observed in addition to the recovery, recrystallization, grain growth, and strain hardening processes investigated by Adams. A more simple system, such as AISI 304 L or low carbon AISI 305 steel, would perhaps have been more useful in investigating the effect of temper annealing on austenitic stainless steel and consequently, the validity of Adams' model.

Section VII

SUGGESTIONS FOR FUTURE WORK

VII SUGGESTIONS FOR FUTURE WORK

1. It would be useful to evaluate S. Adams' model more thoroughly. The influences of the critical parameters, i.e. $(\epsilon_u)_o$, So/St, St, on mechanical properties of temper rolled and temper annealed material could be isolated. A simple system should be tested in order to avoid the problems encountered in the present work. A potentially useful austenitic stainless steel for this investigation would be 304L, perhaps cold worked at slightly above room temperature.

2. It is believed that Ferritic Stainless Steel (AISI 446 or muffler Alloys) (31 p.50) could be usefully partially annealed (17). In these steels the total elongation in the annealed state $(\epsilon_T)_o$ is about 25%. S. Adams predicted that this elongation could be usefully improved. If ductility could be improved significantly, the applications of this comparatively cheaper stainless steel could perhaps be increased. There are, however, very few data on the mechanical properties of cold worked ferritic stainless steel (31, 36) but fabrication is known to be difficult. The metal is brittle at room temperature. Its use has ,thus, been limited.

APPENDIX A

THE ESTIMATION OF PROPERTIES OF PARTIALLY ANNEALED MATERIALS

Introduction

In many applications of sheet metal a balance between strength and elongation or formability is required. The traditional method of obtaining this is to partly work the annealed strip by temper rolling to a degree that adequately strengthens without destroying too much tensile ductility. A newer approach is to partially anneal fully hardened sheet. Investigations of such methods have been made at McGill for Mild Steel(2), Copper(3). Aluminum alloys (4) and in association with Noranda for Brass (5). It is always found that, for any attainable UTS partial annealing gives greater elongations. The extent of the improvement depends on the amount of rolling strain given before annealing and on the material used. It is useful to be able to understand this and to be able to make an estimate of the improvement likely before undertaking extensive experimental work.

An attempt is made to do this in the present work. The problem is essentially one of interpolation. The UTS, yield strength and elongation are known for the annealed and fully work hardened sheet and an attempt is made to estimate the properties for sheet that has been less heavily worked or for sheet that been partially annealed back from the fully hardened state. The latter is more important since the properties at the various rolling tempers should be available.

Specifications in the sheet-metal industry are generally written in terms of the Ultimate Tensile Strength (UTS) and the total elongation. A clear idea of the physical meaning of these terms is important for a discussion of the relationship between them.

During the plastic extension of a tensile specimen the area contracts since the total volume remains constant. The load on the specimen continues to increase as long as the rate of work hardening is sufficient to compensate for the decrease in cross section. However a stage is eventually reached when the work-hardening is not sufficient. Any slightly thinner section of the specimen will continue to thin-- uniform straining is restricted and deformation is confined to the necked region. The value of the nominal stress at maximum load is the "UTS" and the strain to that point is the " uniform strain". With flat strip specimens a diffuse neck can form at first and some further uniform strain occurs, as the load decreases slightly (1), but eventually a sharp neck angled across the specimen forms, and fracture occurs. At this stage the metal is still ductile in the sense that it can be deformed in compression; what is lost is the ability to strain uniformly in tension. The strain to reach the UTS increases with the rate of work-hardening i.e. with a decrease in the ratio of the proof stress to the UTS. The uniform elongation, and also the total elongation, in fact, measure the capacity to work-harden. A very ductile metal like lead shows negligible elongation when tested in tension at normal strain rates. However for most metals the formability, particularly in processes involving stretching operations like deep drawing, correlates well with the elongation. The total elongation is often measured, including the necking strain; this is meaningful only if it correlates with the uniform strain.

2 RELATION BETWEEN UTS. AND ELONGATION

2.1 Temper Rolling

During the deformation, the true stress, δ, and the natural stress are related by

$$\delta = f(\epsilon) \qquad \ldots 1$$

The natural strain can be derived from the engineering strain, ϵ by $\varepsilon = \log_e (1 + \epsilon)$

It is readily shown that -- eg. (8) -- the maximum in the load on a tensile specimen occurs when

$$\frac{d\delta}{d\varepsilon} = \delta \qquad \ldots 2$$

The point on equ. 1 defined by equ. 2. defines the true stress and strain, δ_u and ε_u , at the U.T.S,'S': see fig. 1

Now $S A_o = A \delta_u$

where A_o and A are the original and current cross-sectional area;

i.e. $S = \delta_u \exp(-\varepsilon_u) = \delta_u / (1+\varepsilon_u)$ ...3

The necking point defined by equ.2 is marked on fig.1 by 'A'. If a specimen of annealed metal is prestrained by ε_p to point 'B', before A, unloaded, remeasured and retested the new elongation is now.

$$\varepsilon_u' = (\varepsilon_u)_o - \varepsilon_p$$

The value of the stress at the necking point is unchanged but the U.T.S. rises: see fig. 1

$$S' = \delta_u \exp(-\varepsilon_u')$$

Once the prestrain, ε_p is larger than the annealed uniform strain, $(\varepsilon_u)_o$, there is no uniform strain. It is convenient to identify the U.T.S at the point where the uniform strain vanishes.

When $(\varepsilon_u)_o = \varepsilon_p$ ie $\varepsilon_u = 0$

$S = S^* = \delta_u = S_o (1+(\varepsilon_u)_o)$

Where S_o is the annealed U.T.S.

It is reasonable to suppose that rolling an annealed sample prior to testing is equivalent to offsetting the stress-strain curve by an amount, ε_p, that is some function of the rolling strain.

e.g. $\varepsilon_p = c\,\varepsilon_T$

where $\varepsilon_T = \log_e \left(\frac{1}{1-R}\right)$

where R is the fractional reduction in rolling.

As long as this equivalent ε_p is less than the annealed uniform strain, the temper rolled material shows some uniform strain and the true stress at the UTS is constant:-

$$\sigma_u = S(1+\epsilon_u) = S\exp(\varepsilon_u) = \text{constant}$$

$$\varepsilon_u = (\varepsilon_u)_o - c\cdot\varepsilon_T$$

These relations provide a check on temper-rolling data. Such a check is useful because it can be difficult to measure precisely the uniform elongation at the necking point, particularly for flat strip specimens where a sharp neck forms somewhat later than the diffuse one representing the fulfillment of equation 1. Real materials, also, continue to show a small amount of uniform strain even after heavy prior deformation, presumably because of small amounts of low temperature recovery.

In comparing a variety of materials it is useful to use normalized UTS and elongation parameters, defined by:-

$$F_S = \frac{S - So}{St - So}$$

where S, So, S_T, are the UTS for the metal under test, the annealed and fully hardened states respectively. Similarly

$$F_E = \frac{\epsilon_u - (\epsilon_u)_T}{(\epsilon_u)_o - (\epsilon_u)_T}$$

The relationship between UTS and elongation is best displayed by plotting UTS against elongation, or in terms of the normalized parameters, F_S vs F_E. The use of F_E somewhat extends the analysis because, if the total elongation is some constant linear function of the uniform elongation, the total elongations can be used to find F_E.

After temper rolling

once $F_E = 0$

$$F_S \geq F_S^* = (\epsilon_u)_o \cdot \frac{So}{St - So}$$

...(4)

Up to that point $F_s = F_s^* \times \frac{1-F_e}{1-(\epsilon_u)_o F_E}$ by manipulation ...(5)

The value of F_S at which $F_E = 0$ can be seen to be reduced for decreasing So/S_T and $(\epsilon_u)_o$. However low values of So/S_T for a given reduction correspond to rapid strain-hardening i.e. to a large value of $(\epsilon_u)_o$. Generally the uniform elongation vanishes at lower values of F_S if the total reduction is large and if the rate of strain hardening factor, (So/St), or the annealed uniform elongation, is small.

Divergences between the ideal and experimental curves can be attributed to difficulties in measuring the uniform elongation and to small amounts of recovery which lead to a more gradual approach to $F_E = 0$.

The relation between the rolling strain and the equivalent prior strain must be determined experimentally. A useful general form for the stress-strain relation is

$$\sigma = k_1 (k_2 + (\epsilon + b + c \times \epsilon_T)^n) \quad \ldots 6$$

The constants can be found from the annealed properties and from the temper rolled data. When K_2, b and ϵ_T are zero this equation reduces to the well known power law.

2.2. Partially Annealed Materials

If it is supposed that softening during annealing takes place by recrystallization, a partially annealed metal is composed of a mixture of work-hardened and soft recrystallized regions.

It is mechanically duplex and analogous to a duplex alloy. An attempt can be made to estimate the properties of such a material.

At some stage during a tensile test, after an overall strain of ε has been applied the load is the product of the cross-sectional area and the average stress , $\bar{\delta}$, on it.

Accordingly the nominal stress = $\bar{\delta} \times \exp(-\varepsilon)$ ...7

The problem is to relate $\bar{\delta}$ to the stresses in the components as a function of their relative amounts and of the strain applied. Several assumptions must be made.

1. Individual regions of the soft and hard regions, called α and β , have the mechanical properties of bulk materials. In this case, using the stress-strain relation equ.6, the average stress in the material is related to the average strain

   by $$\bar{\delta}_\alpha = k_1(k_2 + (\bar{\varepsilon}_\alpha + b)^n)$$

and for the material β

$$\delta_\beta = k_1(k_2 + (\bar{\varepsilon}_\beta + c\varepsilon_T + b)^n)$$

2. The areal and linear fractions of the components remain unchanged during deformation, with no preferred orientation. On any cross-section then the average stress is given by

$$\bar{\delta} = V\bar{\delta}_\alpha + (1-V)\bar{\delta}_\beta$$

where V is the volume fraction of the annealed material.

3. A small increment in the overall strain is related to the increments in the average strain in the α and β by (cf.(6)) $d\varepsilon = V d\bar{\varepsilon}_\alpha + (1-V) d\bar{\varepsilon}_\beta$

4. Finally some relation between $\bar{\varepsilon}_\alpha$ and $\bar{\varepsilon}_\beta$ must be assumed. Two suggestions have been made(6):
   (a) equi-strain hypothesis: the strain in both components is the same and differences in the hardness of the components is ignored.

(b) equi-stress hypothesis: the stress is the same so that deformation occurs only in the soft component until it work-hardens sufficiently. Continuity is ignored and also the influence of neighboring regions on one another.

(c) A form intermediate between (a) and (b) can be suggested. The work done per unit volume is supposed to remain constant so that hard regions deform less than soft ones according to

$$d\varepsilon_\alpha \cdot \delta_\alpha = d\varepsilon_\beta \cdot \delta_\beta$$

(d) Experimental studies of duplex brass and Ag-Mg alloys

(7) have shown that for more than 30% by volume of the hard component the equi-strain law, (a) applies. For less than 30% the strain in the hard phase is linearly related to the total strain;

i.e. $$d\varepsilon_\beta = d\varepsilon \frac{1-V}{0.30} \qquad \text{for } V \geq 0.70$$

Where V is the volume fraction of the soft component. Using assumptions 1,2,3, and one of the forms of 4, the nominal stress at increasing applies strains can be calculated and the maxium, i.e. the U.T.S., found.

Computer methods were used to find the UTS. and uniform elongation for different values of the material constants in Equ. 6. In this way the expected behavior of hypothetical materials could be studied. Fig. 2 shows the effect of modifying the strain assumption (iv). Apart from the equi-stress law can in fact be rejected as later comparison with experiment will show. For one thing, the rapid drop of the ratio of the proof stress to the UTS with only a small amount of recrystallization is not observed, experimentally.

Fig. 3 shows the partial annealing curves for two different possible materials with two different initial reductions. The various strain assumptions agree closely and these are not distinguished. It is noteworthy that there is little difference in the partial annealing curves for widely differing reductions and annealed elongations. This

has been confirmed for a wide range of assumed values of the constants in the stress strain law.

2.3 Comparison with Experiment

The UTS - elongation curves for some of the results of (2), (3), (4), (5), together with additional data of the present writer for copper, are shown on Fig. 4. Fig. 5 shows these results and others superimposed on a F_s F_e graph. They all lie closely together confirming this aspect of the theory. On Fig. 6 a detailed comparison is given for steel, using (2). The constants in the stress strain laws were chosen to fit the annealed and fully hard results. It can be seen that the analysis underestimates the elongation at any given value of F_s. By making quite arbitrary assumptions concerning the relations between strain in the hard and soft regions, the agreement can be improved, but some of the divergence is doubtless due to the influence of recovery as a softening mechanism.

A great deal of data has been obtained for the annealing properties of metals and alloys, but most of it is not suitable for the present purposes since hardness values were found. The use of UTS - Elongation diagrams, rather than individual graphs of UTS and elongation against time represents a very useful way of following the course of annealing. The earliest use seems to have been in (2). The normalized diagrams have the advantage of being more compact.

3. Discussion

Although the theoretical and experimental partial annealing curves do not agree well, they both show that there is not a great difference between the properties of different materials when they are expressed in normalized form. The improvement given by partial annealing is largest if the F_e figures for partial annealing and temper rolling differ most for a given F_s. Over a range of materials this difference will be most marked when the temper rolling curves fall most rapidly, since the partial annealing curves are roughly the same. The greatest improvement to be obtained by partial

annealing should be found when the elongation of the annealed material is low and when there is a large amount of cold working before partial annealing.

The partial annealing curves, for two extreme conditions do differ to some extent -- Fig. 3. The computer studies indicate the higher values of strain hardening, or annealed elongation, make the bend in the partial annealing curve sharper and the effects of the extent of rolling before partial annealing is most apparent at these high elongations. This tends to make even more certain the conclusions of the preceeding paragraph.

As an example: it is possible that stainless steel may be useful partially annealed. Leaving aside metallurgical difficulties concerned with carbide precipitation etc., it can be seen that since the annealed elongation are very large (up to 75%) the cold worked material is still ductile up to high reductions. Very high reductions to produce material to use for partial annealing will be necessary, if a significant improvement in ductility is to be achieved, -- this may involve practical difficulties.

On the other hand if the annealed elongation is low, although a considerable relative improvement in the ductility is possible by partial annealing, the absolute improvement may not be large or significant -- 2% elongation is four times ½% but 2% elongation is probably not significant or useful. Between these extremes the materials that may be usefully partially annealed can be found. It can readily be seen why partial annealing is more effective for mild-steel, with a relatively low annealed elongation, than for brass, with a high annealed elongation. It is to be expected that the most impressive improvements will be found in materials with annealed elongations in the range 15-25% e.g. Al alloys and possibly ferritic stainless steels.

Fig. 7 shows the success of the prediction of temper-rolled and partially annealed properties for steel. The temper rolling curve was constructed using the annealed and fully hardened

values of U.T.S. and elongation, and the formula given in Section 2.1. Using the annealed and fully hardened values and the results of Section 2.2 an estimated partial annealing curve can be drawn. Alternatively a more empirical approach may be used. A mean curve for all known materials can be drawn from Fig.5 and this curve used to construct the partial annealing curve. In all these calculations the relations

$$S = Fs\ (\ St-So) \ -\ So$$

$$\epsilon_u = Fe\ ((\ \epsilon_u)o - (\ \epsilon_u)T) - (\ \epsilon_u)T$$

are used.

CONCLUSIONS

It is possible to predict the properties of temper-rolled and partially annealed materials using only the properties of the fully hardened and fully annealed material. The agreement with experiment is quite good. The results may also be used to estimate which materials may be most usefully partially annealed.

References:

1. R. Hill J. Mech. Phys. Solids (1952) 1:19
2. C.J. Adams M.Sc. Thesis McGill 1969
3. H.Fritz & W.M.Williams, J.E.M.(1964 - 65) 93; 578
4. D.V.Parsons M.E. Thesis McGill 1966
5. Noranda Research Centre. Internal Report No. 119
6. J.E. Dorn and C.D. Starr pp 71-94
   " Relation of Properties to Microstructure" A.S.M. (1954)
7. L.M. Clarebrough and G.R.Perger Aust. J. Sci Res. 5 (1): 14
8. Deiter "Mechanical Metallurgy".

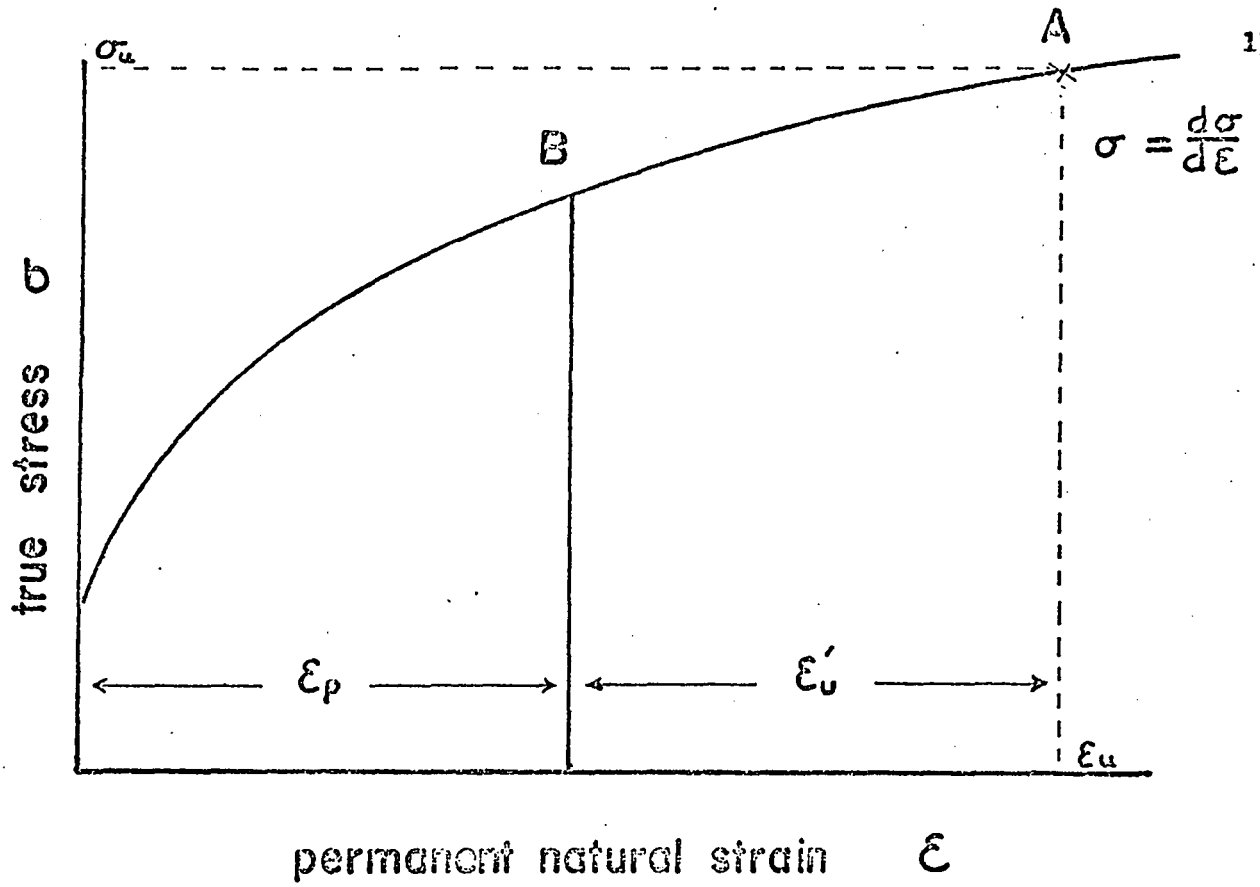
A
σ_u
B
$\sigma = \frac{d\sigma}{d\varepsilon}$
true stress σ
ε_p
ε'_u
ε_u
permanent natural strain ε

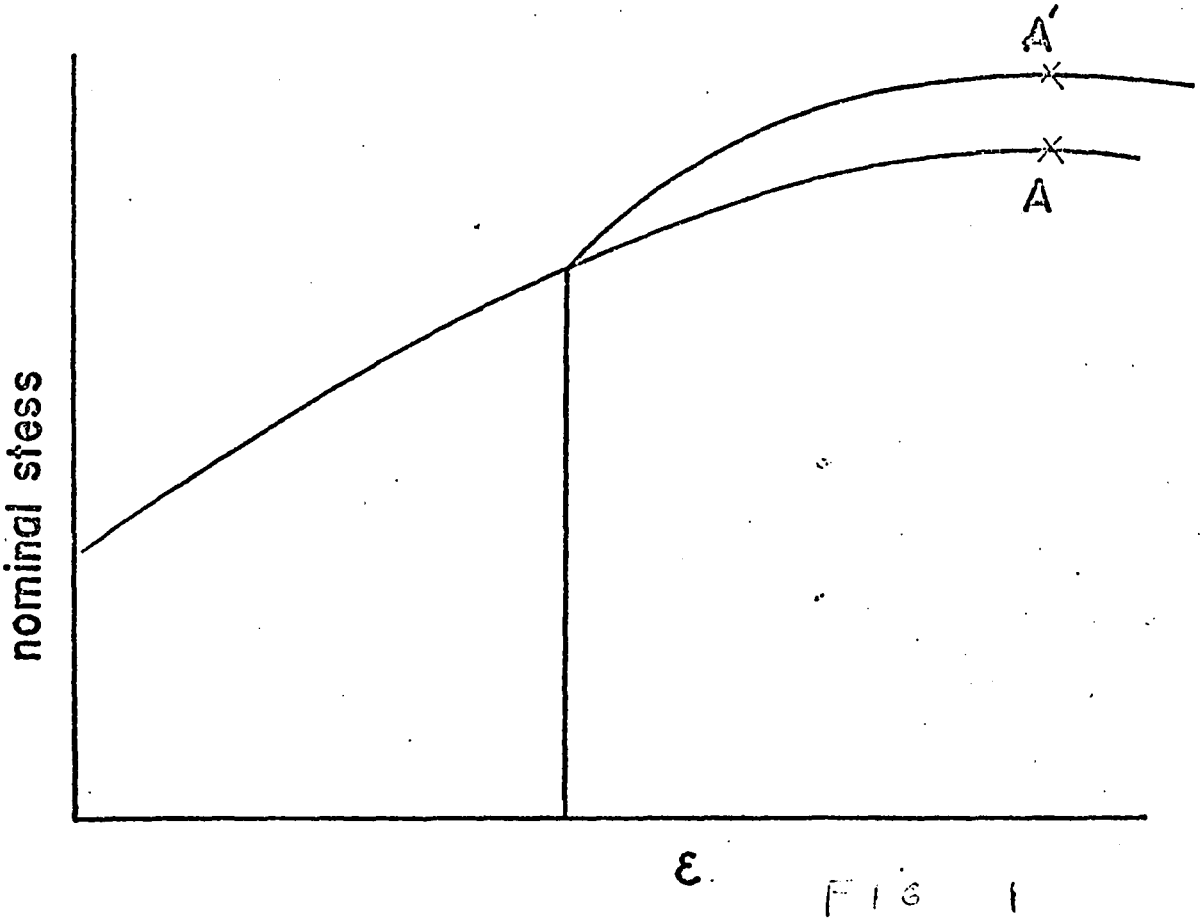
A'
A
nominal stess
ε

FIG 1

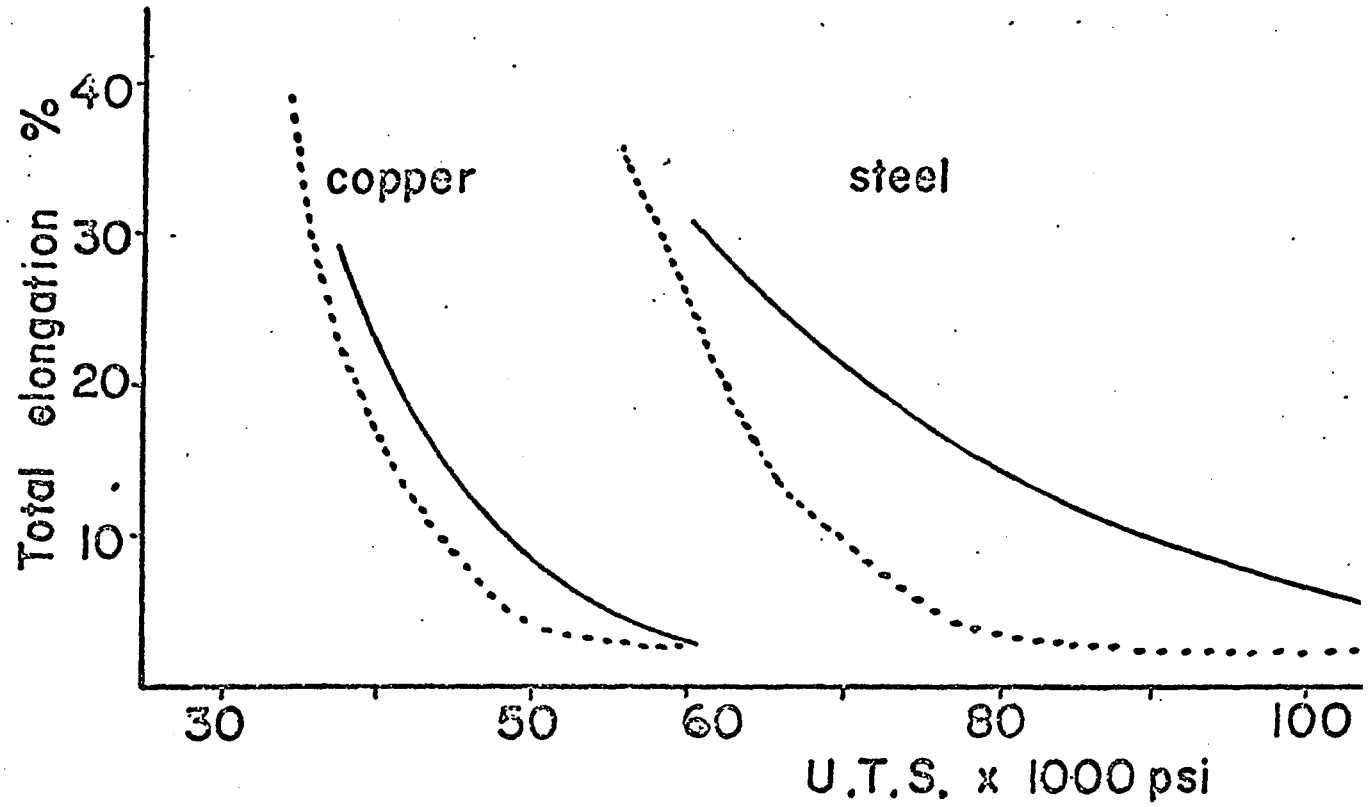
Total elongation %
40
30
20
10
copper
steel
30
50
60
80
100
U.T.S. x 1000 psi

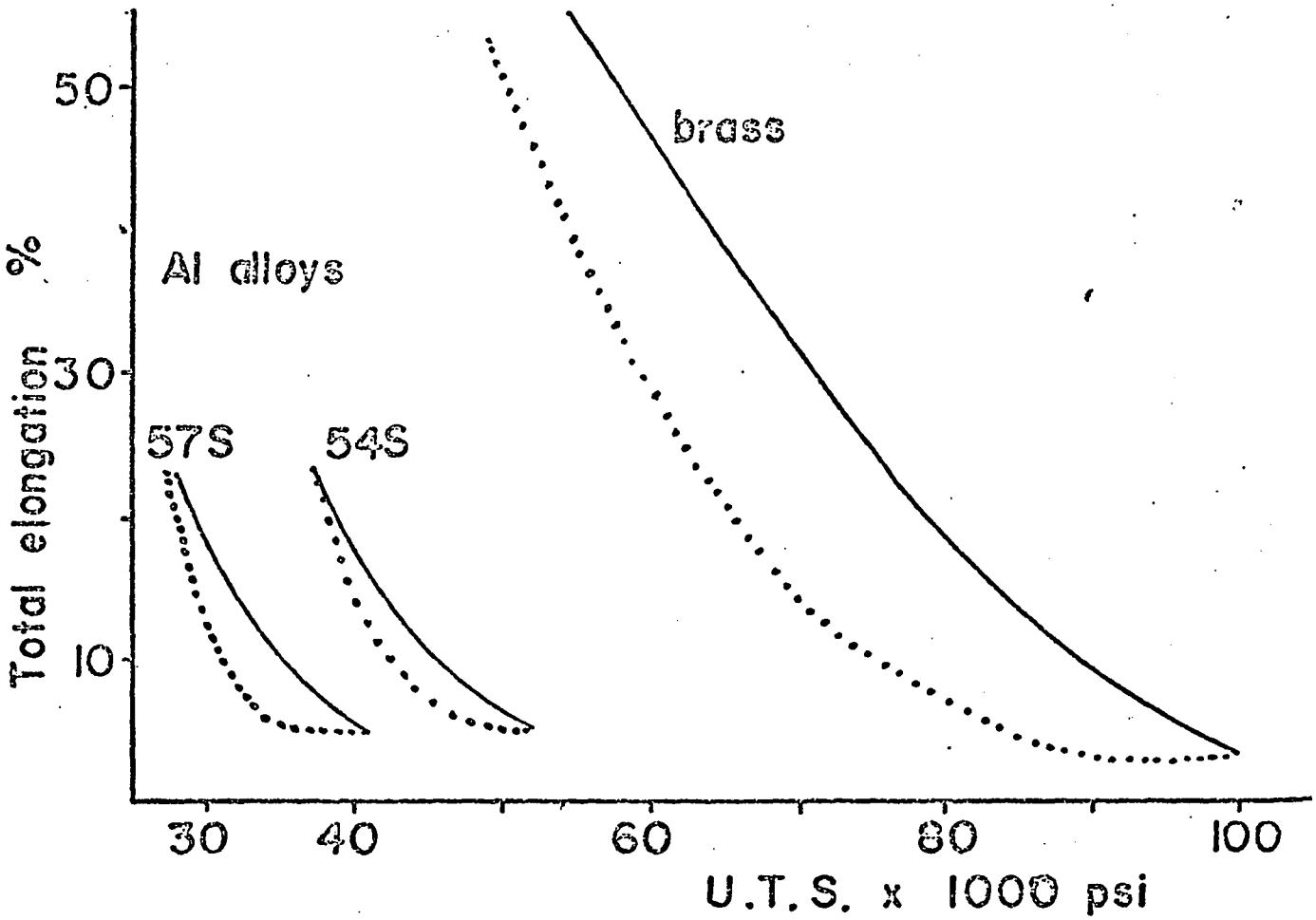
Total elongation %
50
30
10
brass
Al alloys
57S
54S
30
40
60
80
100
U.T.S. x 1000 psi

FIG 4

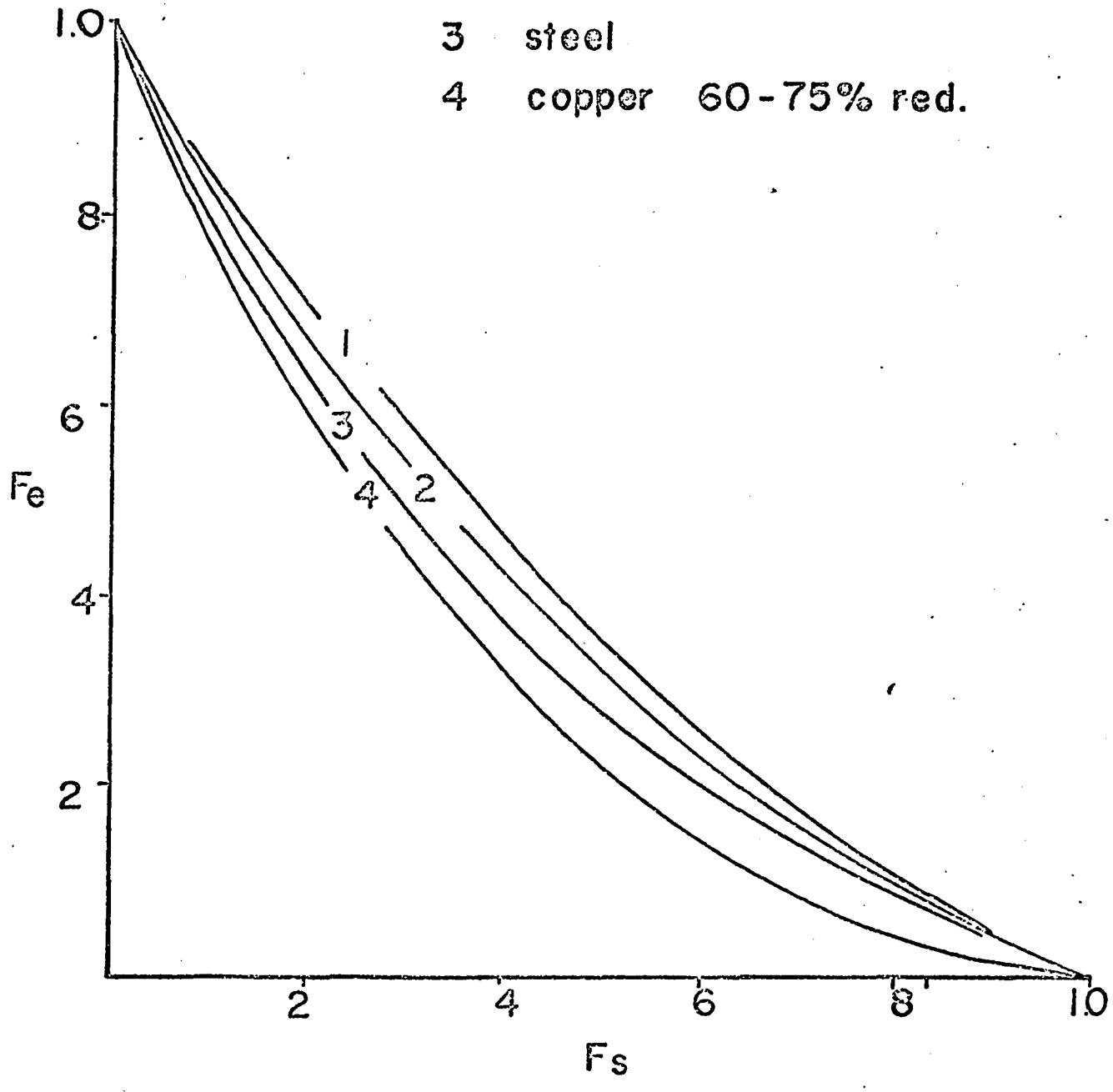
1 brass
2 Al alloys 57S 54S
3 steel
4 copper 60-75% red.
1.0
8
6
4
2
Fe
1
3
4
2
2
4
6
8
1.0
Fs

FIG. 5

H/Steel.

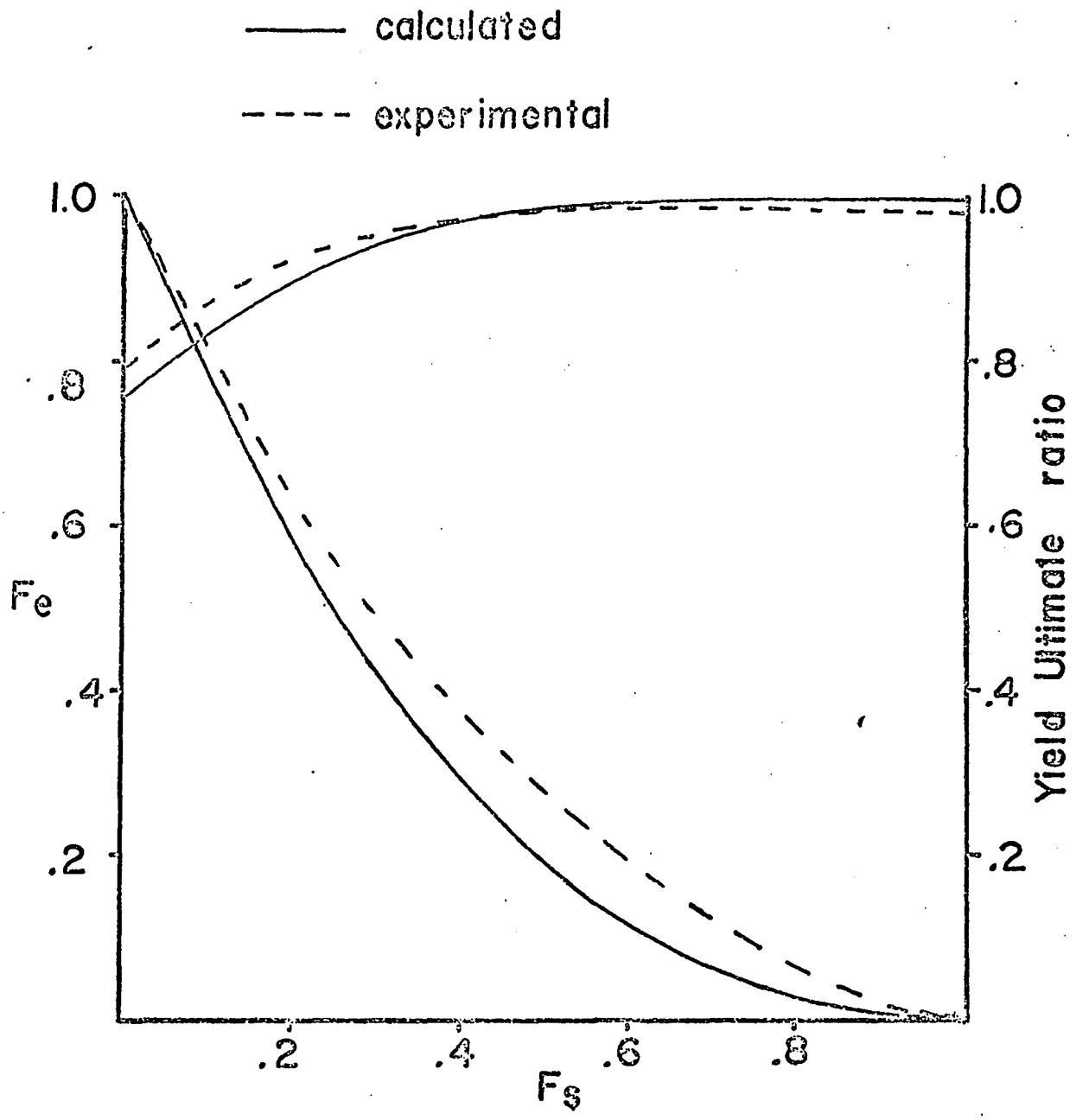
calculated
experimental
1.0
.8
.6
.4
.2
Fe
.2
.4
.6
.8
Fs
Yield Ultimate ratio

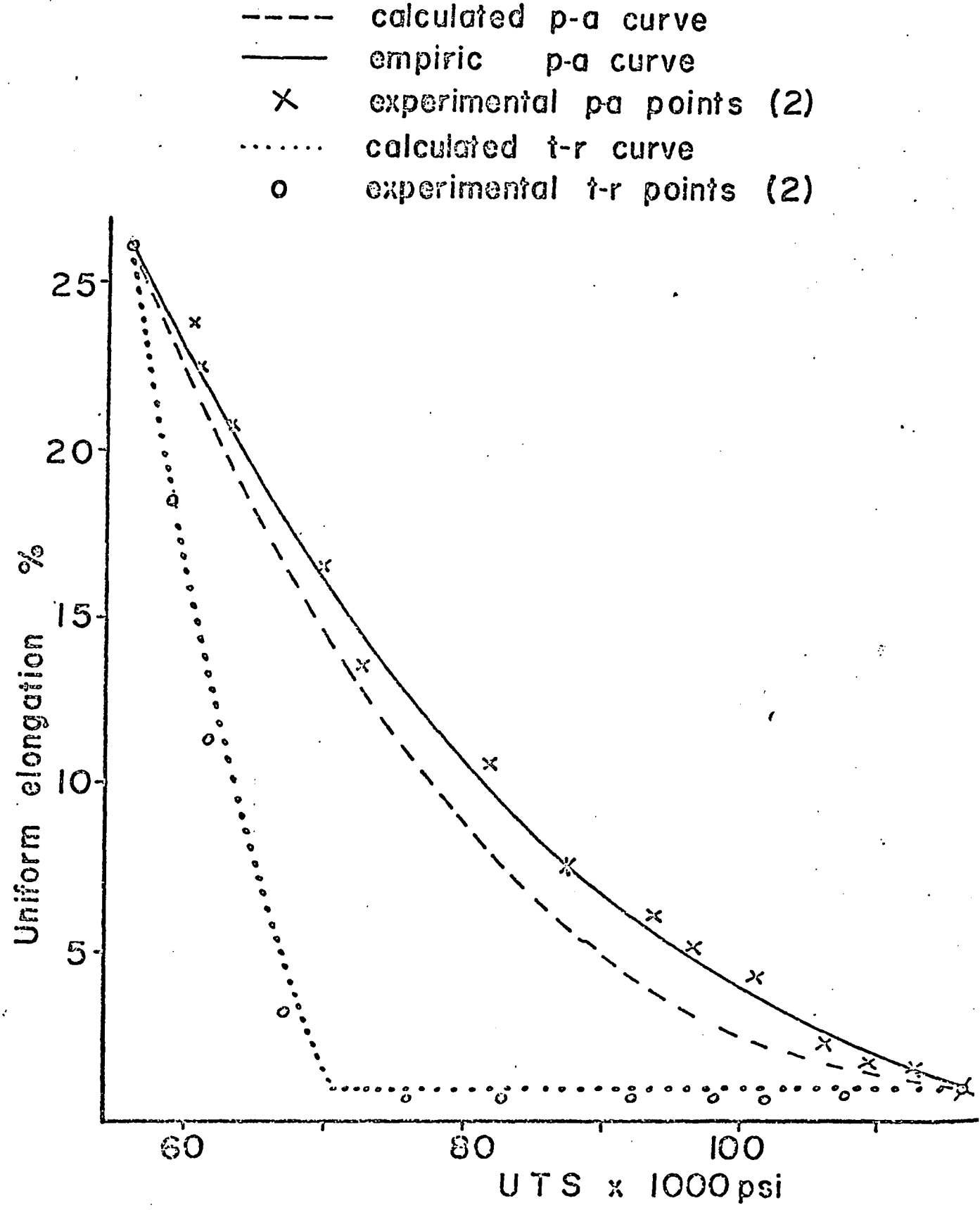
calculated p-a curve
empiric p-a curve
experimental pa points (2)
calculated t-r curve
experimental t-r points (2)
Uniform elongation %
25
20
15
10
5
60
80
100
UTS x 1000 psi

REFERENCES

List of References

1. H.M. Fritz; " The Partial Annealing of Copper", M.Eng. Thesis, 1964, McGill Univ.
2. D.V. Parsons; " The Partial Annealing of Aluminum-Magnesium Alloys", M.Eng. Thesis, 1967, McGill Univ.
3. C.J. Adams; " The Partial Annealing of Low-Carbon Steel Strip", M.Sc. Thesis, 1969, McGill Univ.
4. American Society for Metals; Metals Handbook, Novelty, Ohio, 1948.
5. H.M. Fritz and W.M. Williams; " A Comparison of Temper Rolled and Annealed-to-Temper Copper", J. Inst. Metals, 1964-65, 93, 578.
6. C.P. Paton; " Batch Thermal Treatment of Light Alloys, " J.Inst. Metals, 1951-52, 80, 311.
7. Mechanical and Physical Properties of Austenitic Chromium-Nickel Stainless Steels at Ambient Temperatures, The International Nickel Company, Inc., 67 Wall Street, New York, N.Y. 1963.
8. A.G. Guy; Elements of Physical Metallurgy, Addison-Wesley Reading, Mass., 1959.
9. R.E. Reed-Hill; Physical Metallurgy Principles,Van Nostrand, Princeton, 1964.
10. R.W. Cahn; Physical Metallurgy, North-Holland Publishing Co., Amsterdam, 1965.
11. H. Wiedersich; " Hardening Mechanisms and the Theory of Deformation," Journal of Metals, May 1964, 425.
12. N.J. Petch; " The Cleavage Strength of Polycrystals", J. Iron Steel Inst., 1953, 174 , 25.
13. H. Hu; " Annealing of Silicon-Iron Single Crystals," Recovery and Recrystallization of Metals, L. Himmel, ed, Gordon and Breach, New York, 1963, 311.
14. R.A. Vandermeer & P. Gordon; " The Influence of Recovery on Recrystallization in Aluminum, " ibid", 211.
15. Recrystallization, Grain Growth and Textures, Seminar 1965, American Society for Metals, Metals Park, Ohio, 1966.
16. J.E. Burke & D. Turnbull; " Recrystallization and Grain Growth", Progress in Metal Physics, 3, 1952, 220.

17. S. Adams; " The Estimation of Properties of Partially Annealed Materials", Private communications (Appendix A) .

18. W. Hume-Rothery; The Structures of Alloys of Iron, Pergamon Press London, 1966.

19. E.S. Machlin; " Diffusionless (Martensitic) Transformation to Strengthen Metals", The Strengthening of Metals, D. Peckner, ed., Reinhold Publishing Corp., New York, 1964.

20. J.W. Christian; " Military Transformation: an Introductory Survey", Physical Properties of Martensite and Bainite, Sp. Report No. 93, Iron and Steel Institute, London, 1965.

21. J. Burke; The Kinetics of Phase Transformations in Metals, Pergamon Press, London, 1965.

22. C.S. Barrett & T.B. Massalski: Structure of Metals, McGraw-Hill New York, 1966.

23. W. Rostoker and J.R. Dvorak; Interpretation of Metallographic Structures, Academic Press, New York, 1965.

24. E.C. Bain; " The Nature of Martensite", Trans AIME, 1924, 70, 25-46.

25. J.S. Bowles and J.K. Mackenzie; " The Crystallography of Martensite Transformations", Acta Met., 1954, 2, 129-137.

26. M.S. Wechsler eal; " On the Theory of The Formation of Martensite," Trans AIME, 1953, 197, 1503.

27. J.W. Christian; " Martensitic Transformation: a Current Assessment", Int. Symp. on the Mechanisms of Phase Transformation in Crystalline Solids, Inst. of Metals, Manchester, July 1968.

28. C.M. Wayman; " Ferrous Martensite," Physical Properties of Martensite and Bainite, Sp. Peport No. 93, Iron and Steel Inst., London, 1965.

29. Republic Enduro Stainless Steels, Republic Steel Corporation, Massillion, Ohio, 1951.

30. L. Aitchison and W.I. Pumphrey: Engineering Steels, Macdonald & Evans, Ltd., London, 1953.

31. J.G. Parr and A. Hanson; An Introduction to Stainless Steel, American Society for Metals, Metals Park, Ohio.

32. L. Colombier and J. Hochmann; Stainless Steel and Heat Resisting Steels, St. Martin's Press, New York, 1968.

33. The Making, Shaping and Treating of Steel, H.F. McGannon, ed., United States Steel Corp., Pittsburgh, Pa., 1964.

34. B. Cina; " Metastability of Austenite in 18/8 Cr-Ni Alloy", JISI, 1955, 179, 230.

35. S.R. Thomas and G.Krauss; " Cyclic Martensitic Transformation and the Structure of a Commercial 18 Cr-8 Ni Stainless Steel", Trans, Met. Soc. AIME, Aug. 1967, 239, 240.

36. R. Barker; " High Strength Stainless Steel", Metallurgia, Aug. 1967, 76, 49.

37. D.C. Ludwigson and J.A. Berger; " Plastic Behavior of Metastable Austenitic Stainless Steels", JISI, January 1969, 207, 63.

38. Y. Fukase et al; " On the Anomalous Behavior of Mechanical Properties of Metastable Cr-Ni Austenitic Stainless Steels around Ambient Temperature, " Trans. ISIJ, 1968, 8, 311.

39. W.F. Barclay; " The Mechanisms at Deformation and Work Hardening In AISI Type 301 Stainless Steel", Advances in the Technology of Stainless Steels and Related Alloys, ASTM Special Technical Publication No. 369, 1963.

40.P.G. Bastien and J.M.B. Dedieu; " Formation and Tempering of Martensite in 18/8 Steels", J.I.S.I., July 1956, 183, 254.

41. R. Lagneborg; " The Martensite Transformation in 18% Cr-8% Ni Steels", Acta. Met., 1964, 12, 823.

42. R.P. Reed; " The Spontenous Martensitic Transformations in 18% Cr, 8% Ni Steels", Acta Met., 1962, 10, 865.

43. C.J. Guntner and R.P. Reed; " The Effect of Experimental Variables Including the Martensitic Transformation on the Low-Temperature Mechanical Properties of Austenitic Stainless Steel", Trans. ASM, 1962, 55, 399.

44. R.P. Reed & C.J. Guntner; " Stress - Induced Martensite Transformation in 18 Cr- 8 Ni Steel," Trans. TMS-AIME, Dec. 1964, 230, 1713.

45. B. Cina; " Effect of Cold Work on the Transformation in Some Fe-Ni-Cr Alloys," J.I.S.I., 1954, 177, 406.

46. J.P. Bressanelli and A. Moskowitz; " Effects of Strain Rate, Temperature, and Composition on Tensile Properties of Metastable Austenitic Stainless Steels," Trans, ASM, 1966, 59, 223.

47. Z.S. Basinski; " The Instability of Plastic Flow of Metals at Very Low Temperatures," Proc. Roy. Soc. London, A240, 1957, 229.

48. J.F. Watson and J.L. Christian; " Serrations in the Stress/Strain Curve of Cold-Worked 301 Stainless Steel at 20°K," J.I.S.I., 1960, 195, 439.

49. K.M. Carlsen and K.C. Thomas; " Effect of Compostion, Heat Treatment and Cold Rolling on Mechanical Properties of Cr-Ni Stainless Steel," Trans.ASM, 1962, 55, 462.

50. ASTM Standards, 1968, Part 31, General Testing Methods, Tension Testing of Metallic Materials, E 8, 202.

51. ASTM Standards, 1964, Part 3, Steel Sheet, Strip, Bar, Rod, Wire; Metallic Coated Products: Electrolytic Oxalic acid Etching Test, A-262, 230.

52. J.Durnin and K.A. Ridal;" Determination of Retained Austenite in steel by X-Ray Diffraction," JISI, January 1968, 206, 60.

53. B.D. Cullity; Elements of X-Ray Diffraction, Addison- Wesley, Reading, Mass., 1956.

54. ibid p.263-269.

55. ibid p.12.

56. R.W.K. Honeycombe; The Plastic Deformation of Metals, Edward Arnold, Great Britian, 1968.

57. S.R. Goodman and H. Hsum; " Texture Transition in Austenitic Stainless Steel", Trans. AIME, 230, 1413.

58. O.J. Blickwede;" Sheet Steel-Micrometallurgy by the Millions", Trans. ASM, 1968, 61, 653.

59. W.B. Morrison; " The Effect of Grain Size on the Stress-Strain Relationship of Low-Carbon Steel," Trans. ASM, 1966, 59, 824.

60. J.D. Jevons; The Metallurgy of Deep Drawing and Pressing, John Wiley, New York, 1942, 316.

61. T. Angel; " Formation of Martensite in Austenitic Stainless Steel", J.I.S.I. 1954, 177, 165.

62. J. Valic, J.C.T. Farge, W.M. Williams: " Temper Annealing of 70/30 Brass", Noranda Research Centre Internal Report No. 119, 1967.